Ore Geology Reviews 64 (2015) 667–719

Contents lists available at ScienceDirect

Ore Geology Reviews

journal homepage: www.elsevier.com/locate/oregeorev

Tantalum–(niobium–tin) mineralisation in African pegmatites and rare metal granites: Constraints from Ta–Nb oxide mineralogy, geochemistry and U–Pb geochronology

Frank Melcher [a,*], Torsten Graupner [a], Hans-Eike Gäbler [a], Maria Sitnikova [a], Friedhelm Henjes-Kunst [a], Thomas Oberthür [a], Axel Gerdes [b], Stijn Dewaele [c]

[a] Bundesanstalt für Geowissenschaften und Rohstoffe, Stilleweg 2, D-30655 Hannover, Germany
[b] Institut für Geowissenschaften, Petrologie und Geochemie, Universität Frankfurt, Altenhöferallee 1, D-60438 Frankfurt am Main, Germany
[c] Department of Geology and Mineralogy, Royal Museum for Central Africa, Leuvensesteenweg 13, 3080 Tervuren, Belgium

ARTICLE INFO

Article history:
Received 20 December 2012
Received in revised form 22 August 2013
Accepted 2 September 2013
Available online 12 September 2013

Keywords:
Tantalum
Tantalum–niobium oxide
Columbite-group minerals
Rare-element pegmatite
Rare-metal granite
Africa
Mineral chemistry

ABSTRACT

Tantalum, an important metal for high-technology applications, is recovered from oxide minerals that are present as minor constituents in rare-metal granites and granitic rare-element pegmatites. Columbite-group minerals (CGM) account for the majority of the current tantalum production; other Ta–Nb oxides (TNO) such as tapiolite, wodginite, ixiolite, rutile and pyrochlore-supergroup minerals may also be used.

In this paper mineralogical and geochemical data with a focus on opaque minerals as well as age determinations on CGM using the U–Pb method are presented for 13 rare-element granite and pegmatite districts in Africa, covering Archean, Paleoproterozoic, Neoproterozoic, Paleozoic and Mesozoic provinces. Geological, economic and geochronological data are reviewed.

Each period of Ta-ore formation is characterised by peculiar mineralogical and geochemical features that assist in discriminating these provinces. Compositions of CGM are extremely variable: Fe-rich types predominate in the Man Shield (Sierra Leone), the Congo Craton (Democratic Republic of the Congo), the Kamativi Belt (Zimbabwe) and the Jos Plateau (Nigeria). Mn-rich columbite–tantalite is typical of the Alto Ligonha Province (Mozambique), the Arabian–Nubian Shield and the Tantalite Valley pegmatites (southern Namibia). Large compositional variations through Fe–Mn fractionation, followed by Nb–Ta fractionation are typical for pegmatites of the Kibara Belt of Central Africa, pegmatites associated with the Older Granites of Nigeria and some pegmatites in the Damara Belt of Namibia. CGM, tapiolite, wodginite and ixiolite accommodate minor and trace elements at the sub-ppm to weight-percent level. Trace elements are incorporated in TNO in a systematic fashion, e.g. wodginite and ixiolite carry higher Ti, Zr, Hf, Sn and Li concentrations than CGM and tapiolite. Compared to tapiolite, CGM have higher concentrations of all trace elements except Hf and occasionally Zr, Ti, Sn and Mg. The composition of TNO related to rare-element pegmatites is rather different from rare-metal granites: the latter have high REE and Th concentrations, and low Li and Mg. Pegmatite-hosted TNO are highly variable in composition, with types poor in REE, typical of LCT-family pegmatites, and types rich in REE — showing affinity for NYF-family or mixed LCT–NYF pegmatites. Major and trace elements show regional characteristics that are conspicuous in normalised trace element and REE diagrams. In general, CGM from Ta-ore provinces are characterised by the predominance of one type of REE distribution pattern characterised by ratios between individual groups of REE (light, middle, heavy REE) and the presence and intensity of anomalies (e.g. Eu/Eu*).

Despite textural complexities such as complex zoning patterns and multiple mineralisation stages, the chemical compositions of CGM, tapiolite and wodginite–ixiolite from rare-metal granite and rare-element pegmatite provinces indicate that they are cogenetic and reflect specific source characteristics that may be used to discriminate among rocks of different origin.

Geochronological data produced for CGM from ore districts are discussed together with the respective ore mineralogy and minor and trace element geochemistry of TNO to reconsider the geodynamics of pegmatite formation. In Africa, formation of rare element-bearing pegmatites and granites is related to syn- to late-orogenic (e.g., West African Craton, Zimbabwe Craton), post-orogenic (Kibara Belt, Damara Belt, Older Granites of Nigeria, Adola Belt of Ethiopia) and anorogenic (Younger Granites of Nigeria) tectonic and magmatic episodes.

* Corresponding author at: Chair of Geology and Economic Geology, University of Leoben, Peter-Tunnerstraße 5, 8700 Leoben, Austria. Tel.: +43 3842 402 6100.
E-mail address: frank.melcher@unileoben.ac.at (F. Melcher).

0169-1368/$ – see front matter
http://dx.doi.org/10.1016/j.oregeorev.2013.09.003

The late-orogenic TNO mineralisation associated with A-type granites in the Eastern Desert of Egypt shares geochemical features with the anorogenic Younger Granites of Nigeria.

1. Introduction

Tantalum usage has developed significantly over recent years and is now extensive in electronic applications, in super alloys, in specialty metal products for the medical and chemical industries and in metal carbide for the metal working tools industry. Tantalum is recovered from oxide minerals that are present as minor constituents in rare-metal granites and granitic rare-element pegmatites (Černý et al., 2005). Columbite-group minerals (columbite–tantalite solid solution series; CGM) account for the majority of the current tantalum production. However, a large number of Ta–Nb oxides (TNO) are known to occur in such rocks (Černý and Ercit, 1989). Despite considerable research on the chemistry of TNO from well known individual localities of pegmatite and rare-metal granites worldwide (e.g., Greer Lake and Tanco pegmatites, Manitoba, Canada, Černý et al., 1986; Van Lichtervelde et al., 2007; Kenticha pegmatite, Ethiopia, Küster et al., 2009; Greenbushes and Wodgina pegmatites, Western Australia, Partington et al., 1995; rare-metal granites of the Yichun complex, SE China, Belkasmi et al., 2000), as well as regional studies (e.g., granitic pegmatites of the Pampean Ranges, Argentina, Galliski and Černý, 2006; rare-metal granitoids of the Eastern Desert, Egypt, Abdalla et al., 1998; rare-element pegmatites of the Serido Belt, Brazil, Baumgartner et al., 2006), little is known about their compositional variation, especially when focussing on the mineralogically and genetically important trace elements. Previous data sets were generally derived from electron microprobe work, which mainly covers the major (Ta, Nb, Fe and Mn) and some of the minor elements (e.g., Ti, Sn, W, Zr and U), due to the limitations of the method. The paucity of information on trace element abundances and isotopic data (e.g., the U–Pb system) for CGM and other TNO formed an obstacle for a systematic comparison of tantalum-bearing deposits occurring within tantalum ore provinces. Therefore, a systematic approach under special consideration of high-quality age information for the tantalum minerals themselves will provide a major contribution for a better understanding of the genesis of rare-metal granites and rare-element pegmatites within their major periods of formation in Earth history.

A project on mineralogical and geochemical fingerprinting of Ta–Nb mineral concentrates (coltan) was initiated in 2006 (Melcher et al., 2008a,b). A vast dataset has emerged comprising mineralogical, geochemical and textural information, as well as age determinations using the U–Pb method (Gäbler et al., 2011; Graupner et al., 2010; Melcher et al., 2009). Samples from more than 30 rare-element granite and pegmatite districts worldwide were analysed. The focus was originally on occurrences in Africa, resulting in a very large data set of African coltan samples. This justifies a detailed presentation of the tantalum districts from this continent. A description of Ta mineralisation from important mining districts and occurrences in other parts of the world will be presented in a separate paper.

Mineralogical and geochemical data for the most important Ta–Nb–Sn phases derive from ca. 15,000 electron microprobe and 9000 LA-ICP-MS analyses of major, minor and trace elements in Ta–Nb minerals. In addition, U–Pb dating has been performed on numerous columbite–tantalite samples. The combined mineralogical and geochemical data reflect and define regional and local differences ("signatures"; Melcher et al., 2009; Savu-Krohn et al., 2011).

2. Distribution of rare-element pegmatites and rare-metal granites in Africa, classification and mineralogy

The African continent is richly endowed with rare metal mineralised pegmatites (Fetherston, 2004; Landes, 1935; Schneiderhöhn, 1961; von Knorring, 1970; von Knorring and Condliffe, 1987; von Knorring and Fadipe, 1981). Central African countries (Democratic Republic of the Congo, Rwanda, Burundi, and Uganda) have an almost 100-year-long history of Sn and Ta production. Further Ta–Nb–Sn provinces are found in Egypt, Ethiopia, Somalia, Mozambique, Madagascar, Namibia, Nigeria, Zimbabwe, South Africa and some countries in West Africa. A map and database compiling more than 1500 locations of known deposits of Ta and Nb in Africa has been published by Deschamps et al. (2006).

The early attempts to classify granitic pegmatites, dating back to Jahns (1955), Ginsburg et al. (1979) and Černý (1989, 1990, 1992), have seen many modifications (e.g., Černý and Ercit, 2005; Černý et al., 2012; London, 2008; Simmons and Webber, 2008). The divisions and subdivisions into classes, subclasses and subtypes are primarily based on an estimation of the depth of crystallisation, combined with textural (e.g., miarolitic), geochemical and mineralogical attributes. The latter include major and minor minerals present in pegmatites, such as TNO and other minerals concentrating high-field-strength elements (HFSE). Five classes of granitic pegmatites are distinguished that may contain discrete Ta–Nb–Sn minerals: (1) abyssal, (2) muscovite, (3) muscovite-rare-element, (4) rare-element and (5) miarolitic classes (Černý and Ercit, 2005; Černý et al., 2012; London, 2008; Simmons and Webber, 2008). However, only the rare-element class is of economic interest with respect to Ta mineralisation. Within this class, a REE (= rare earth elements) subclass with Be, REE + Y, U, Th, F and Nb > Ta as typical minor elements is distinguished from a Li subclass with Li, Rb, Cs, Be, Ga, Sn, Hf, Nb–Ta, B, P and F. Further subdivision of subclasses into types and subtypes is based on typical Li, REE, Be and Nb–Ta mineral phases; for example in the rare-element-Li subclass four types and seven subtypes have been identified (Černý and Ercit, 2005). In contrast to the more descriptive class–subclass–type–subtype classification, the "family concept" (Černý, 1990, 1991a; London, 1995) also considers genetic aspects of pegmatites and related granites, such as their crustal environment, protolith and processes. Here, a lithium–caesium–tantalum (LCT) family is distinguished from a niobium–yttrium–fluorine (NYF) family. LCT-family pegmatites are more common and economically more important; the family consists of members of the rare-element-Li and miarolitic-Li subclasses, whereas the NYF family comprises the rare-element-REE and miarolitic-REE subclasses. In addition, mixed LCT–NYF types do exist (Černý and Ercit, 2005; Novák et al., 2012).

TNO are present in both granitic pegmatites and rare-metal granites. The most important minerals considered in this study and their formulae are summarised in Appendix 1. For further details on the mineralogy and mineral chemistry of the TNO, the reader is referred to Foord (1982), Černý and Ercit (1985, 1989), Ercit (1994, 2005a, 2010), Ercit et al. (1995), Novák and Černý (2001), Novák et al. (2000, 2003), Wise et al. (1985) and Wise and Černý (1990).

Solid solution members of the orthorhombic *columbite–tantalite group* (*CGM*) with the general formula AB_2O_6 ($A = Fe^{2+}$, Mn^{2+} and $B = Nb^{5+}$, Ta^{5+}) are the most important source of Ta, commonly making up the major proportion of TNO in a given deposit. The end-members of the CGM are columbite-(Fe), columbite-(Mn), tantalite-(Mn) and tantalite-(Fe). Their composition is traditionally expressed as molar ratios $\#Mn = 100 * Mn/(Mn + Fe)$ and $\#Ta = 100 * Ta/(Ta + Nb)$, and plotted in the "columbite quadrilateral". The structures of both ordered and disordered CGM accommodate minor quantities of Ti, Sn, Zr, Hf, Sc, REE and other elements. *Columbite-(Mg)*, [$Mg(Ta, Nb)_2O_6$] is rare and was described from pegmatites crystallising in a Mg-rich environment (Mathias et al., 1963).

Tapiolite is a tetragonal modification of AB_2O_6, with tapiolite-(Fe) being much more abundant than tapiolite-(Mn). A miscibility gap exists

between these phases and CGM, but its extent has been studied only rudimentarily (Černý et al., 1992; Ercit, 2010; Wegorzewski, 2009). Tapiolite is quite common in many pegmatite deposits and may even form a major phase. It is structurally related to rutile and cassiterite, which explains elevated Ti and Sn concentrations commonly observed in this mineral.

Wodginite (Ercit et al., 1992a,b,c) and *ixiolite* are compositionally related complex phases that usually contain Sn in the weight-percent range and often also Li, Ti, Zr, Hf, Sc, W and U. Their chemical composition is frequently illustrated with the "columbite quadrilateral". Ixiolite has an orthorhombic unit cell corresponding to a disordered structure derived from that of CGM. Heating of ixiolite induces ordering into a wodginite-type structure, which has a monoclinic unit cell. The general wodginite formula (ACB_2O_8) implies the following distribution of cations at the three crystallographic sites: A = Mn and Fe^{2+}; C = Sn, Ti, Fe^{3+} and Ta; and B = Ta and Nb. Chemical analyses are insufficient to distinguish monoclinic wodginite from orthorhombic ixiolite and, in the absence of structural data, these minerals are simply referred to as wodginite–ixiolite in the present paper.

Minerals of the *pyrochlore supergroup* with a cubic structure are second in abundance only to the CGM in many Ta–Nb deposits. In some deposits, including NYF-family pegmatites, alkaline granites and especially carbonatites, they are more abundant than CGM. Their general formula is $A_{2-m}B_2X_{6-w}Y_{1-n}$, where: $A^{[8]}$ = Ca, Na, Ag, Mn, Sr, Ba, Fe^{2+}, Pb^{2+}, Sn^{2+}, Sb^{3+}, Bi^{3+}, Sc, U, Th, REE + Y, vacancy and H_2O; $B^{[6]}$ = Nb, Ta, Ti, V^{5+}, Sb^{5+}, W, Fe^{3+}, Sn^{4+}, Zr, Hf, Mg, Al and Si; X = O, subordinate OH and F, and Y = O, OH, F, vacancy, H_2O, K, Cs and Rb (Atencio et al., 2010; Hogarth, 1977; Lumpkin et al., 1986). Traditionally, three subgroups have been distinguished based on the relative proportions of B-site cations: the betafite subgroup with 2Ti > (Ta + Nb); the pyrochlore subgroup with (Nb + Ta) > 2 Ti and Nb > Ta, and the microlite subgroup with (Nb + Ta) > 2 Ti and Nb < Ta. The new nomenclature approved by the CNMNC-IMA (Atencio et al., 2010) is now based on the ions in the A, B and Y sites, and five groups are recommended based on the B-site occupancy: pyrochlore (Nb), microlite (Ta), roméite (Sb), betafite (Ti), and elsmoreite (W). The new names are composed of two prefixes and a root name (identical to the name of the group). The first prefix indicates the dominant anion/cation of the dominant valence at the Y-site, and the second prefix refers to the dominant cation of the dominant valence at the A-site.

In pegmatites, the most important minerals are members of the *microlite group* [$(Ca,Na)_{2-x}Ta_2O_6(OH,F,H_2O)_{1-y}$]. They are either present as a primary phase or more commonly replace CGM and other primary TNO. Microlite may accommodate appreciable concentrations of U or Pb ("uranmicrolite", "plumbomicrolite", both now discredited; Atencio et al., 2010), Th, and REE. In many deposits, U-rich microlite is the major source of radioactivity.

A number of somewhat poorly defined, often metamict and altered, REE + Y- and often U–Th-bearing TNO are known mainly in NYF-family pegmatites and granites, but also as accessories in assemblages of the LCT family. These include members of the *aeschynite group* (e.g., aeschynite, nioboaeschynite, tantalaeschynite, with suffixes indicating the preferred A cation, e.g., Ce, Nd, Y), *euxenite group* (euxenite, tanteuxenite, polycrase, uranpolycrase), *samarskite group* and *fergusonite group*. Ercit (2005b) has developed a method to identify these minerals using a statistical approach based on electron microprobe analyses. Chemically, minerals of the *aeschynite* and *euxenite* groups differ from pyrochlore-supergroup members by their 1:2 ratio between the number of A- and B-site cations, compared to a typically higher ratio in the latter. *Aeschynite*- and *euxenite*-group minerals have the general formula $AB_2(O,OH)_6$, with A = Ca, REE + Y, U, Pb; B = Ti, Nb, Ta (Bermanec et al., 2008). The aeschynite structure shows a preference for larger A cations than the euxenite structure, and hence, aeschynite-group minerals typically have higher LREE/HREE ratios than euxenite-group minerals. *Samarskite*-group minerals have the general formula ABO_4, where A = REE + Y, Ca, U and Fe and B = Ta, Nb and Ti (Hanson et al, 1999; Warner and Ewing, 1993). All members are monoclinic, and Fe is a ubiquitous A-site cation. *Fergusonite*-group minerals also have the general formula ABO_4 (Guastoni et al., 2010), where A stands for REE + Y, and B for Nb and Ta; e.g., fergusonite-(Y) [$YNbO_4$] and formanite-(Y) [$YTaO_4$]. Both tetragonal and monoclinic members are known.

Tantalian rutile ("*strüverite*") and *niobian rutile* ("*ilmenorutile*") are regarded as solid solutions of rutile and "mono-tapiolite" (Černý and Ercit, 1985). These phases are usually heterogeneous with exsolved columbite or ilmenite.

Stibiotantalite [$SbTaO_4$] and *bismutotantalite* [$Bi(Ta,Nb)O_4$] are minor phases known from only a few pegmatites (Galliski et al., 2001).

Rare TNO include members of the solid solution series *foordite–thoreaulite* (Černý et al., 1988; Uher et al., 2008), *simpsonite* (Ercit, 1986), *rankamaite*, *cesplumtantite*, *fersmite*, *rynersonite*, *liandradite*, *petscheckite* (Mücke and Strunz, 1978) and others. These minerals were also identified in the present study. Their formulae and crystal structures are listed in Appendix 1. Details on their chemical composition will be given in Section 6.

3. Methods

Concentrate samples from different mine sites in many African countries have been investigated (Fig. 1). The ore concentrates were either sampled during the study or obtained from mining companies and museum collections. In addition, single crystals of Ta–Nb minerals were selected from locations where concentrates were not available. For details on the geographical coordinates of the sample locations and sample characteristics, the reader is referred to a table in the electronic supplementary material (Appendix 2) and an additional map showing the location of samples collected in east-central Africa (Fig. 2). More than 500 samples have been collected from rare-metal granite and rare-element pegmatite provinces to document chemical changes in Ta–Nb–Sn minerals. Polished sections were prepared from concentrate, single-crystal and hard rock samples. The mineralogical composition of concentrates was quantitatively determined using scanning electron microscope/mineral liberation analysis techniques (SEM/MLA). In each concentrate, up to several thousand grains were identified depending on the grain size, using energy-dispersive spectrometry (EDS) combined with back-scattered electron (BSE) imaging (Fandrich et al., 2007; Gu, 2003; Melcher et al., 2008a,b). In Table 1, results of these measurements are presented in a condensed form and some examples of classified concentrates are presented in Fig. 3. Due to different beneficiation techniques used in the field (e.g., simple panning, gravity separation, magnetic separation, flotation), the quality of the concentrates varied enormously.

Selected mineral grains were subsequently analysed using electron microprobe (also known as electron-probe microanalysis, EPMA) and laser ablation inductively coupled plasma mass spectrometry techniques (LA-ICP-MS). A CAMECA SX 100 electron microprobe equipped with five wavelength-dispersive spectrometers and an energy-dispersive system (Princeton Gamma Technologies) was used to determine major and minor element concentrations. The instrument was operated at a 30 kV acceleration voltage, 40 nA sample current and appropriate counting times to reach a detection limit of 200 ppm for minor and trace elements. Pure metals and natural minerals, including tapiolite and columbite-(Fe), were used as standards. In this work, La to Sm are referred to as light REE (LREE), Gd to Ho + Y as middle REE (MREE), and Er to Lu as heavy REE (HREE).

Two types of laser ablation systems were applied for in-situ determination of trace elements: (1) a 266 nm Nd:YAG laser (New Wave) coupled to an Agilent 7500i quadrupole mass spectrometer at the University of Erlangen. Electron-microprobe analyses on preselected spots were used for external calibration; and (2) a 193 nm excimer laser (New Wave UP193-FX) coupled to a Thermo Scientific ELEMENT

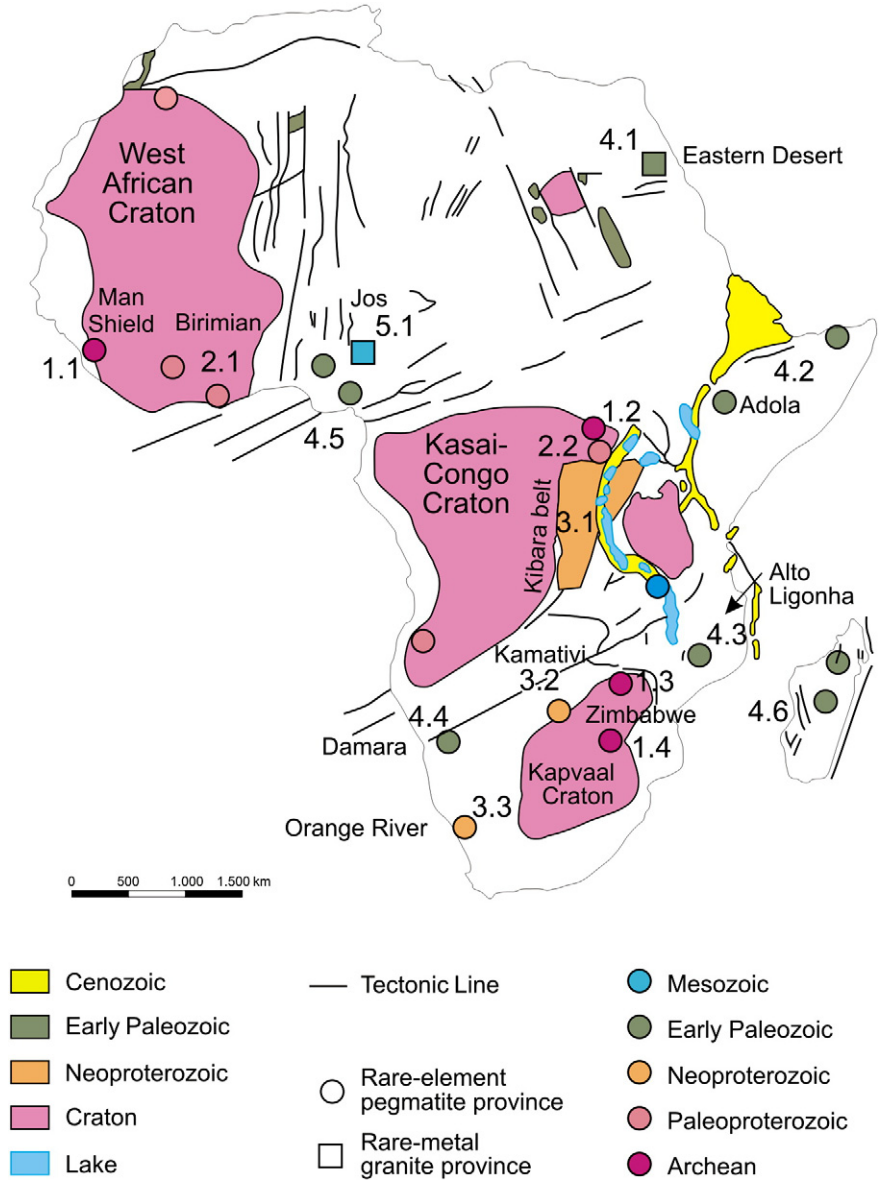

Fig. 1. Map of African rare-element pegmatite and rare-metal granite provinces (different symbols). Colours indicate age provinces. The following numbered provinces are dealt with in the text: 1.1 Man Shield, 1.2 Congo Craton, 1.3 Zimbabwe Craton, 1.4 Kaapvaal Craton, 2.1 Birimian Province, 2.2 Kibalian in north-eastern DRC, 3.1 Kibara Belt, 3.2 Kamativi Schist Belt, 3.3 Orange River Belt, 4.1 Eastern Desert, 4.2 Adola Belt, 4.3 Alto Ligonha Province, 4.4 Damara Belt, 4.5 Older Granites (Nigeria), 4.6 Madagascar, 5.1 Younger Granites (Nigeria). Map base is modified from Schlüter (2006).

XR sector field mass spectrometer, with an additional Faraday cup at the Bundesanstalt für Geowissenschaften und Rohstoffe (BGR). Major elements were measured during the ablation using the Faraday cup. For details of the methodology and standardisation, the reader is referred to Gäbler et al. (2011).

Uranium–lead dating was carried out both (1) on crystal fragments using conventional thermal ionisation mass spectrometry (TIMS) and (2) in-situ using a Thermo-Scientific Element II sector field ICP-MS, coupled to a New Wave UP213 ultraviolet laser system with a low-volume ablation cell (University of Frankfurt). Spot size varied from 30 to 60 μm. Raw data were corrected for background signal, common Pb, laser-induced elemental fractionation, instrumental mass discrimination and time-dependant elemental fractionation (Gerdes and Zeh, 2006). The analytical reproducibility (e.g., GJ-1 reference zircon) of the $^{206}Pb/^{238}U$ and $^{207}Pb/^{206}Pb$ ratios was about 0.8 and 0.5%, respectively. No matrix dependent U/Pb fractionation was observed.

The chemical procedures to separate U and Pb for TIMS analysis were adapted from Romer and Wright (1992) and Romer and Smeds (1994). U and Pb were measured in multi-collector mode on a MM354 TIMS (University of Toronto) and a ThermoFinnigan Triton (BGR). To minimise the effects of disturbance of the U–Pb isotopic system in CGM, strong HF leaching of the grains prior to dissolution has been proposed (Romer and Wright, 1992). At the University of Toronto, individual fragments (<100 μm; ≪1 mg) that are not leached in HF were analysed separately ("single-grain method"). This allows careful inspection of the quality of the fragments to be dated. However, variations in age within a concentrate cannot be detected by this method. At the BGR, fragments from different grains (fragment size 0.08–0.16 mm; mass 1–4 mg) were investigated ("multi-grain method"). The fragments were leached in several steps using warm diluted HF, HCl and HNO_3 prior to dissolution. The radiometric results are summarised in Table 2. The degree of concordance was calculated as follows: $^{206}Pb/^{238}U$ age × $100/^{207}Pb/^{206}Pb$ age. Representative

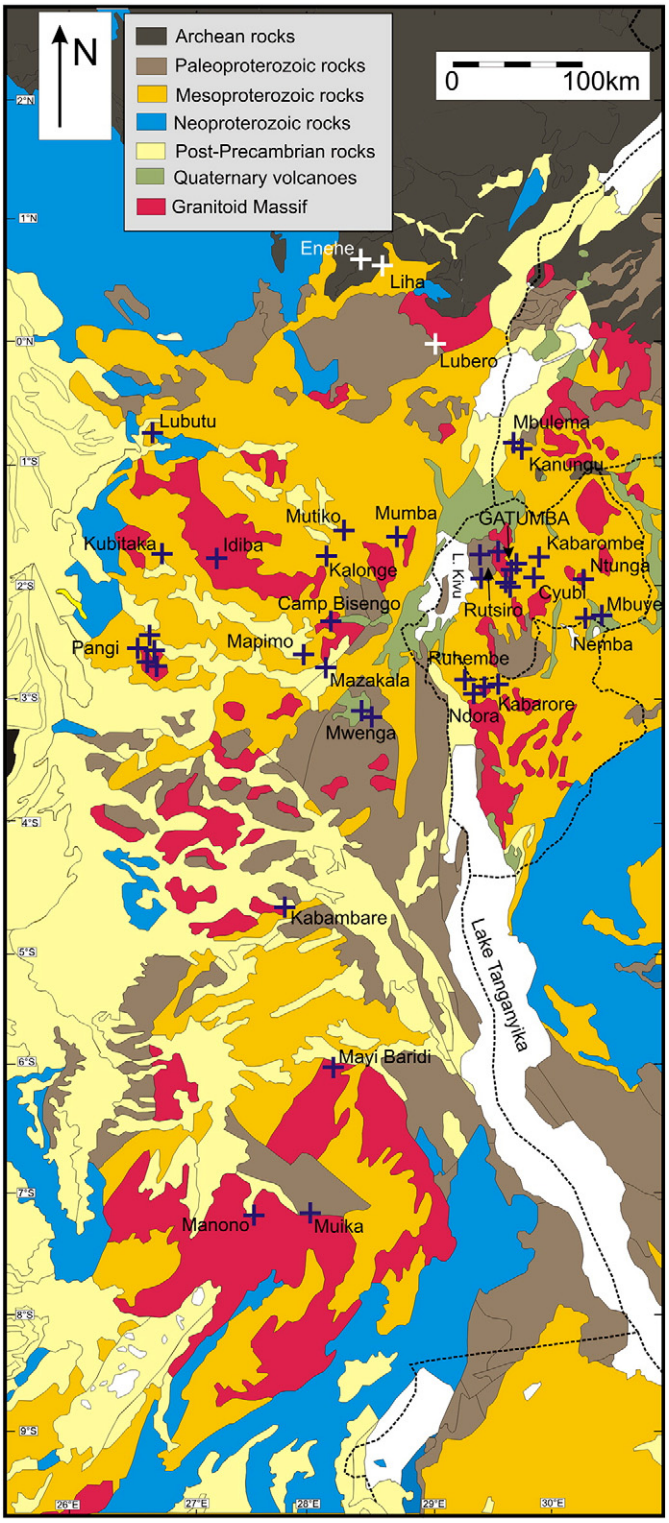

Fig. 2. Simplified geological map of the Great Lakes Region showing the location of samples from the Kibara Belt and the Congo Craton.

U–Pb concordia diagrams are shown in Fig. 4. U–Pb dating of CGM by both, the TIMS and the LA-ICP-MS methods may yield complex and often also reverse discordant ages (Romer and Smeds, 1997 and references therein; Smith et al., 2004). This may be explained by disturbance of the U–Pb isotope system due to small-scale element redistribution or loss initiating from U-rich damaged (metamict) areas in the mineral (Romer, 2003). Loss or redistribution of intermediate daughter isotopes of the U–Pb decay series may also be envisaged as a mechanism for geologically unrealistic U–Pb and/or Pb–Pb ages (Romer, 2008).

In a large number of samples, U–Pb ages were estimated from about 15 to 40 single-spot analyses of CGM in polished sections using the sector field LA-ICP-MS data (Gäbler et al., 2011). Spots with low radiogenic Pb portions (i.e., $^{207}Pb_{rad}$ < 50% of total ^{207}Pb) were excluded from the age estimate. $^{206}Pb_{rad}/^{238}U$ and $^{207}Pb_{rad}/^{235}U$ ratios of the sample were calculated for each single spot and plotted on a concordia diagram. A robust linear regression algorithm (based on the minimisation of the sum of the absolute values of the distances in y-direction) was used to calculate the intersections with the concordia curve. The age of the upper intersection was used as the U–Pb age estimate for discordant samples. For samples which did not show discordance, the age of the intersection with the Concordia curve close to the sample points was used as U–Pb age estimate. Gäbler et al. (2011) demonstrated that the attribution of a coltan sample to a mineral province characterised by a common geological history could be done based on the sector field LA-ICP-MS U–Pb data. The mean of the absolute difference between age estimates and independent age determinations was 55 Ma (minimum: 6 Ma, maximum: 198 Ma). In the following, data obtained using this method are termed "age estimates".

4. African granitic–pegmatitic Ta(–Nb–Sn) provinces: significance, geology, mineralogy and radiometric ages

Tantalum deposits in Africa are associated with rare-metal granites and granitic rare-element pegmatites. Minerals are mostly recovered from weathered pegmatite (Fig. 5) or from eluvial and alluvial placer deposits. Five metallogenetic epochs are distinguished in this paper (Fig. 1): (1) Archean, predating 2500 Ma (e.g., Zimbabwe Craton, Kaapvaal Craton, Man Shield, Congo Craton); (2) Paleoproterozoic, ca. 2000 Ma (e.g., Birimian Province in West Africa; Ubendian Belt in Central Africa); (3) early Neoproterozoic, ca. 1000–900 Ma (e.g., Kibara Belt in Central Africa; Kamativi Belt in Zimbabwe; Namaqua Province in Namibia and South Africa); (4) late Neoproterozoic to early Paleozoic, termed Pan-African in this study, ca. 600 to 450 Ma (e.g., Arabian–Nubian Shield, Mozambique Belt, Damara Belt in Namibia); and (5) Mesozoic (ca. 200 Ma) alkaline ring complexes (e.g., Jos Plateau in Nigeria). Pegmatite and rare-element provinces are described below from the oldest to the youngest. Altogether, new data from 13 African granitic/pegmatitic provinces are presented and discussed. Each section contains basic geological information and production data. This is followed by a discussion of radiometric data and the mineralogy, which is mainly based on ore concentrates and thus focuses on opaque heavy minerals. Back-scatter electron images showing characteristic minerals and textures are shown in Fig. 6. "Columbite quadrilateral" diagrams illustrate the compositional variation of CGM, tapiolite and wodginite–ixiolite and highlight major-element variations in these minerals within each province (Fig. 7). A miscibility gap to Fe–Ta-rich phases collectively attributed to tapiolite is evident. However, TNO phases have been classified by their chemical composition only in this work. The trace element chemistry of the major ore minerals is treated separately in Sections 5 and 6.

4.1. Archean (>2500 Ma)

4.1.1. Man Shield (Sierra Leone)

Alluvial deposits of columbite–tantalite, cassiterite and rutile, related to late-orogenic granites (>2500 Ma), are known from the Man Shield (1.1 in Fig. 1) in Sierra Leone (Morel, 1979; Patrick and Forward, 2005; Wright et al., 1985). Small scale mining of columbite–tantalite takes place in Sierra Leone but the amounts produced are not large (Roskill, 2012). A few prospecting and mining licences have been granted (Geological Survey and Mines Division, 2008). Hutchinson (1955)

Table 1
Mineralogical composition (heavy minerals) of rare-element pegmatites and granites from typical ore mineral concentrates (in area percent).

Locality	Province	District	Country	Age (Ga)	N	total Ta–Nb minerals	CGM total	Relative proportion of end member				Ratio to total Ta–Nb minerals	
								FeC	FeT	MnC	MnT	Tapiolite	Wodginite, ixiolite
Lutenga	Kibara Belt	South Kivu	DRC	1.0	2	43–76	35–71	14–63	15–42	17–22	<0.5	4–18	<0.2
Camp Bisengo	Kibara Belt	South Kivu	DRC	1.0	1	50	41	29	42	27	2	13	0.5
Mapimo Mulungu	Kibara Belt	South Kivu	DRC	1.0	1	55	54	53	12	33	1	2	–
Shabunda, Mazakala	Kibara Belt	South Kivu	DRC	1.0	1	84	83	62	6	32	0.3	0.7	–
Kalonge, Luka	Kibara Belt	South Kivu	DRC	1.0	1	15	13	79	0.5	20	<0.1	–	4.3
Kibeke Pangi	Kibara Belt	Maniema	DRC	1.0	1	97	96	71	5	23	<0.1	0.3	–
Pangi, Camp Makambo	Kibara Belt	Maniema	DRC	1.0	1	84	78	9	30	42	19	3.5	2.4
Idiba, Kalukangala	Kibara Belt	Maniema	DRC	1.0	1	90	90	35	3	62	0.3	–	–
Yubili	Kibara Belt	Maniema	DRC	1.0	1	91	83	5	28	39	28	4.2	2.9
Bassin Obea Lubutu	Kibara Belt	Maniema	DRC	1.0	2	97	96	74–78	4–6	18–20	<0.3	0.7–0.9	–
Abuki, Katanta, Pangi	Kibara Belt	Maniema	DRC	1.0	1	98	98	6	23	58	13	0.1	–
Kabambare, Kaozi	Kibara Belt	Katanga	DRC	1.0	1	76	73	19	9	67	4	0.3	0.1
Manono	Kibara Belt	Katanga	DRC	1.0	14	54–84	52–83	1.1–5.3	0.6–7.3	62–82	9–31	<0.8	<2.5
Mayi Baridi	Kibara Belt	Katanga	DRC	1.0	2	76–87	57–70	35–40	0–1	0–1	58–65	18–24	<1
Gatumba	Kibara Belt	Gatumba	Rwanda	1.0	4	37–95	37–92	11–35	11–37	27–61	13–24	1.2–5.4	<3.3
Gasasa	Kibara Belt	Gatumba	Rwanda	1.0	1	74	40	18	62	20	<1	40	–
Ruhanga	Kibara Belt	Gatumba	Rwanda	1.0	6	24–81	24–81	0.4–35	<12	57–79	<41	<0.2	<0.8
Buranga	Kibara Belt	Gatumba	Rwanda	1.0	2	78–79	10–78	11	1–42	19–81	8–28	<1	<1.3
Nyarigamba	Kibara Belt	Gatumba	Rwanda	1.0	2	62–80	48–71	7–20	<0.2	59–79	1–33	–	<0.2
Shori 3	Kibara Belt	Gatumba	Rwanda	1.0	2	35–49	34–48	36–57	20–25	22–38	<1	0.4–2.8	0.5
Kirwa–Gasovu	Kibara Belt	Gatumba	Rwanda	1.0	1	54	54	39	11	49	1	0.3	0.1
Nyabisindu–Gasovu	Kibara Belt	Gatumba	Rwanda	1.0	1	81	80	57	9	34	0.2	0.6	–
Cyubi	Kibara Belt	Gatumba	Rwanda	1.0	2	83–88	61–79	8–21	5–45	13–30	17–60	10–21	0.1–0.3
Nkegete	Kibara Belt	Gatumba	Rwanda	1.0	1	72	71	46	18	35	1	2	–
Bijyojyo	Kibara Belt	Gatumba	Rwanda	1.0	2	25–30	25–30	50–55	4–5	40–45	0.2–0.4	<0.4	<0.1
Muhanga	Kibara Belt	Gatumba	Rwanda	1.0	1	61	61	23	9	61	7	0.4	0.1
Rukaragata	Kibara Belt	Gatumba	Rwanda	1.0	1	28	25	34	42	24	0.3	8	0.4
Nemba	Kibara Belt	Nemba	Rwanda	1.0	4	21–58	21–57	0.5–7.4	10–24	48–61	20–29	<1.8	<2.7
Ntunga	Kibara Belt	Ntunga	Rwanda	1.0	1	27	20	–	6	45	49	4	2
Rutsiro	Kibara Belt	Rutsiro	Rwanda	1.0	3	32–61	32–61	17–53	1–10	37–82	<1.1	<1.2	<0.5
Nyatubindi	Kibara Belt	Rutsiro	Rwanda	1.0	3	11–58	10–57	59–66	12–28	7–29	<0.8	<2.7	<0.3
Kabarombe	Kibara Belt	Kayanza	Rwanda	1.0	2	27–30	19–29	3–5	2–24	25–37	47–57	1–4	2–20
Munege	Kibara Belt	Kayanza	Burundi	1.0	2	28–37	28–37	13–23	7–39	17–23	30–45	<1	2–3
Kamativi	Kamativi Belt		Zimbabwe	1.0	2	50–53	48–51	50–55	<20	23–24	3–25	2–3	<0.5
Marropino	Alto Ligonha	Lurio Belt	Mozambique	0.5	7	23–61	4–61	<12	<14	29–77	13–71	<0.6	<0.8
Morrua	Alto Ligonha	Lurio Belt	Mozambique	0.5	2	13–50	11–49	<1	<14	<1	85–100	–	–
Moneia	Alto Ligonha	Lurio Belt	Mozambique	0.5	5	60–93	54–85	–	<9	<1	90–100	<6	–
Muiane	Alto Ligonha	Lurio Belt	Mozambique	0.5	1	97	96	4	3	89	4	–	–
Somipe	Alto Ligonha	Lurio Belt	Mozambique	0.5	1	16	16	100	–	–	–	–	–
not specified	Man Shield		Sierra Leone	2.8	1	79	54	71	28	0	1	32	–
Abu Dabbab	Arabian–Nubian Shield	Eastern Desert	Egypt	0.6	1	8	6.2	6	–	8	86	12	21
Kenticha	Arabian–Nubian Shield	Adola Belt	Ethiopia	0.5	2	54–61	48–55	<1	1	16–39	59–82	<0.1	<0.1
Sepeteri	Older Granites	Oyo state	Nigeria	0.5	1	8	8	13	39	43	5	0.1	1.8
Lema	Older Granites	Kwara state	Nigeria	0.5	1	64	24	11	11	49	29	1.5	2.1
Bauchi	Jos Plateau		Nigeria	0.2	6	5–86	5–85	>98	<1	0.2–2.3	–	<0.4	–

FeC, columbite-(Fe); FeT, tantalite-(Fe); MnC, columbite-(Mn); MnT, tantalite-(Mn); BiT, bismutotantalite; SbT, stibiotantalite.

revealed that "ilmenorutile" from the Tonkolili district is in fact an intergrowth of columbite and rutile. Three alluvial concentrates originating from Sierra Leone were investigated. Two of them are dominated by large poikilitic grains of Nb–Fe–Ta-rich rutile, with abundant inclusions of columbite-(Fe) (Fig. 6a), ilmenite, zircon and some rare minerals such as fersmite and a Sc-rich phase (11–16 wt.% Sc_2O_3) approximating $(Sc,Fe)_2(Nb,Ta,Ti,Zr)_3O_{10}$ in composition. Fairly homogeneous grains of columbite-(Fe) characterised by variable #Mn (5–50) and low #Ta values (<30) are subordinate (Fig. 7a). The third concentrate consists of columbite-(Fe)/tantalite-(Fe) (#Mn 15–30, #Ta <60) and tapiolite, besides significant ilmenite, garnet, and some monazite, cassiterite and zircon. Age estimates for columbite according to Gäbler et al. (2011) range from 2600 (sample 750) to 2850 Ma (samples 538, 1231).

4.1.2. Congo Craton (DRC)

No information is available about the relationship between different granite generations and Ta–Nb–Sn mineralisation found in placer deposits on the Archean Congo Craton (1.2 in Fig. 1) in the Democratic Republic of the Congo–Central African Republic, also known as "DRC–ZAR", "Haut–Zaïre" or "West-Nilian" Craton; Milési et al. (2006).

A U–Pb age of 2487 ± 8 Ma obtained for columbite (sample 101; Table 2) collected from the area of Mambasa (north-eastern DRC) corresponds to the late Archean to Paleoproterozoic pegmatite mineralisation in the Kibalian Greenstone Belt. More details on this mineralisation are presented in Section 4.2.2.

4.1.3. Zimbabwe Craton (Zimbabwe)

On the Zimbabwe Craton (1.3 in Fig. 1), historical Ta production is recorded from LCT pegmatites at Bikita in the Masvingo Greenstone Belt (formerly the Victoria Schist Belt). From 1916 to 1950, 160 tons of columbite–tantalite concentrate were produced. These pegmatites host significant Li (petalite, lepidolite, spodumene, eucryptite, amblygonite) and Cs (pollucite) resources (Martin, 1964). Sn–Ta ore occurs in marginal pockets of quartz-rich zones in large masses of lepidolite greisen. Recent mostly artisanal activities, mainly for Sn, have taken place in the north-east of Zimbabwe, at Benson Mine, Sutswe, Rusambo and Shamva.

Microlite-group	BiT, SbT	Samarskite, euxenite, fergusonite	Cassiterite	Wolframite scheelite	Rutile	Ilmenite	Gahnite	Zircon	Monazite	Xenotime	Apatite	Sulphides	Garnet	Exotic phases
0.3–0.7	–	<1.4	5–43	<0.6	<0.6	1	0.1	<0.1	0.5–2.8	<0.6	<0.1	<3	0.2–1.3	
4.6	–	–	39	<0.1	–	1.4	–	0.3	0.4	–	–	–	0.3	
<0.1	–	–	5.3	–	4.5	17		0.6	1	0.4	–	–	–	
0.2	–	–	2	<0.1	2	1	–	<0.1	0.6	<0.1	–	–	1.9	
6.5	–	–	6	–	4.5	55	–	4.4	1.1	–	–	–	0.2	
–	–	–	<0.1	0.9	1	0.2	<0.1	<0.1	0.4	–	–	–	–	
0.2	–	–	1.6	7	<0.1	2	–	<0.1	<0.1	<0.1	–	–	–	
–	–	–	–	–	<0.1	–	–	0.1	–	–	–	–	–	
1.3	–	–	1.3	4.9	<0.1	0.5	–	<0.1	<0.1	<0.1	–	–	–	
<0.2	–	–	–	<0.1	<0.1	0.2	–	<0.1	0.2	0.1	–	–	0.2–0.5	
0.1	–	–	–	–	–	–	–	<0.1	–	–	–	–	–	
3.3	–	–	–	–	–	–	–	<0.1	–	–	–	–	–	
<1.4	–	–	0.7–6.2	<0.1	<0.1	0.6–2.7	<0.1	<0.7	<0.3	<0.6	–	<0.2	0.1–2.1	
<0.5	–	–	<1	–	1	<1	–	–	–	–	–	–	0.3–1.4	
<12	–	–	0.4–4.8	<3.7	<5	<3.5	–	<0.5	<0.1	<0.1	–	–	<0.4	
9	–	–	2	–	0.7	–	0.2	2.5	3	–	–	–	–	
<5.5	–	–	6–23	<0.1	<20	<1	–	<3	<1	–	–	–	<1.4	
0.2–86	–	–	<0.7	–	<0.1	–	–	<1.6	–	–	–	–	<0.1	Complex phosphates
11–22	–	–	1–2	–	<0.4	<0.1	–	9–13	<0.1	–	–	–	<0.1	
0.5	–	–	33–47	–	<0.1	<6.5	–	1	<0.1	–	–	–	<0.1	
0.3	–	–	31	–	<0.1	<0.2	–	1.8	–	<0.1	–	–	0.4	
0.1	–	–	4.3	–	0.4	1	–	0.9	<0.1	<0.1	–	–	<0.1	
<7	–	–	<2	–	–	–	–	0.2–0.4	<0.1	–	–	–	1–4	
0.2	–	–	4	–	1	3.7	–	0.5	0.1	–	–	–	–	
<0.2	–	–	15–17	–	<0.3	1.5	–	1	<0.1	<0.1	–	–	<0.1	
–	–	–	2	–	0.3	3	–	0.1	–	–	–	–	<0.1	
0.9	–	–	69	–	0.8	<0.1	–	0.1	–	–	–	–	–	
<1	–	–	23–45	<0.1	<0.1	<1	–	<2	<0.1	–	–	–	0.1–0.3	Ferronigerite <0.8
19	–	–	67	–	–	–	–	0.1	–	–	–	–	–	
<0.1	–	–	29–46	<3.3	<0.1	1	–	<1	<0.1	–	–	–	<0.1	
<0.2	–	–	35–77	–	<0.3	<0.3	–	0.3–0.7	<0.3	<0.1	–	–	<0.1	
0–6	–	–	68–71	–	–	–	0.3–0.6	–	–	–	–	–	–	
<2	–	–	12–57	–	0.1	0.2–0.3	–	0.5–1	–	–	–	–	–	
<0.3	–	–	12–13	–	0.1	0.7–0.9	0.1	0.3	1.3–1.6	0.3–0.4	1–1.2	0.1	9–16	
0.1–87	<1.2 BiT	<0.2	–	–	<0.2	<0.5	<2.5	<0.9	3–21	1–13	<0.1	<2.6	0.4–38	Bismuth 0.8–2.5
<16	–	–	–	–	<0.1	8–16	–	<0.1	<0.1	<0.1	<1	–	<0.2	Ca–Th phosphate 0.3
2–10	–	–	–	–	<0.5	<15	–	<1	–	<0.1	–	–	<2	
0.5	–	–	–	–	–	–	–	–	–	–	–	–	–	
1	–	–	–	–	<0.1	<0.1	–	0.9	62	17	–	–	2	
0.1	–	–	0.5	–	–	11	–	<0.1	0.6	–	–	–	6	
2	–	–	78	0.2	–	0.2	–	1.2	–	–	0.4	0.1	0.1	
8–11	–	–	<0.1	–	<0.2	1–2	0.8–2.4	0.5	<0.1	–	<0.1	–	1	
0.1		–	9	–	0.8	18	–	14	5	–	–	–	<0.1	
58	5.6 SbT	–	<0.1	–	0.4	37	<0.1	1.5	0.1	–	–	–	<0.1	
<4	–	<0.5	1.4–68	<1	<0.5	0–48	–	0–80	<2.1	<1	<0.1	–	<0.2	Th-silicate <4

Archean ages were obtained for CGM from the Bikita (2617 ± 1 Ma for three grains, on average 93% concordant; sample 056, Fig. 4a) and Benson mine pegmatites (2587 ± 4 Ma; on average 97% concordant; sample 098, Table 2). These ages are in agreement with previous age estimates obtained by independent methods (Bikita: 2650 ± 50 Ma by Rb–Sr dating of lepidolite, Herzog et al., 1960). A zircon U–Pb age of 2601 ±14 Ma was reported for an anorogenic, post-tectonic Chilimanzi-type granite external to the Masvingo Belt (Murehwa granite; Jelsma et al., 1996).

From Bikita, tantalite-(Mn), tapiolite-(Fe), wodginite, simpsonite, microlite, euxenite, fergusonite and cassiterite have been reported (Martin, 1964; von Knorring and Fadipe, 1981). The Benson 3 and 4 pegmatites carry tantalite-(Mn), wodginite, stibiotantalite, simpsonite and microlite (von Knorring and Fadipe, 1981; von Knorring and Hornung, 1963). Due to the lack of suitable concentrates, only single crystals were investigated in this study. These comprise columbite-(Mn) at Bikita, wodginite replaced by CGM, microlite, cassiterite and scheelite at the Benson mine and wodginite replaced by microlite, with inclusions of cassiterite and zircon at Sutswe. Chemical zoning involves variations in #Ta and #Mn of ca. 10 mol% each (Fig. 7b). At the Benson mine, columbite–tantalite of intermediate composition is a reaction product that formed during retrograde alteration of wodginite.

4.1.4. Kaapvaal Craton (South Africa)

Ta and Nb mineralisation on the Kaapvaal Craton is associated with pegmatites located in Limpopo and Mpumalanga. Historical production of 13.5 tons of columbite–tantalite was reported in 1991 (Roskill, 2012). Mineralised pegmatites occur in several areas, e.g. close to Giyani and in the Murchison Greenstone Belt (e.g., Boelema and Hira, 1998; Poujol and Robb, 1999) (Fig. 1). Poujol and Robb (1999) suggested a minimum age of 2.85 Ga for the pegmatites south of the Murchison Belt (U–Pb dating of zircon). In the Leeuwspruit North pegmatite within the Murchison Belt, beryl and emerald, as well as tantalite and columbite, were produced (Vearncombe et al., 1992). Columbite-(Fe,Mn) of low #Ta (12) from Giyani was available for analysis (Fig. 7b).

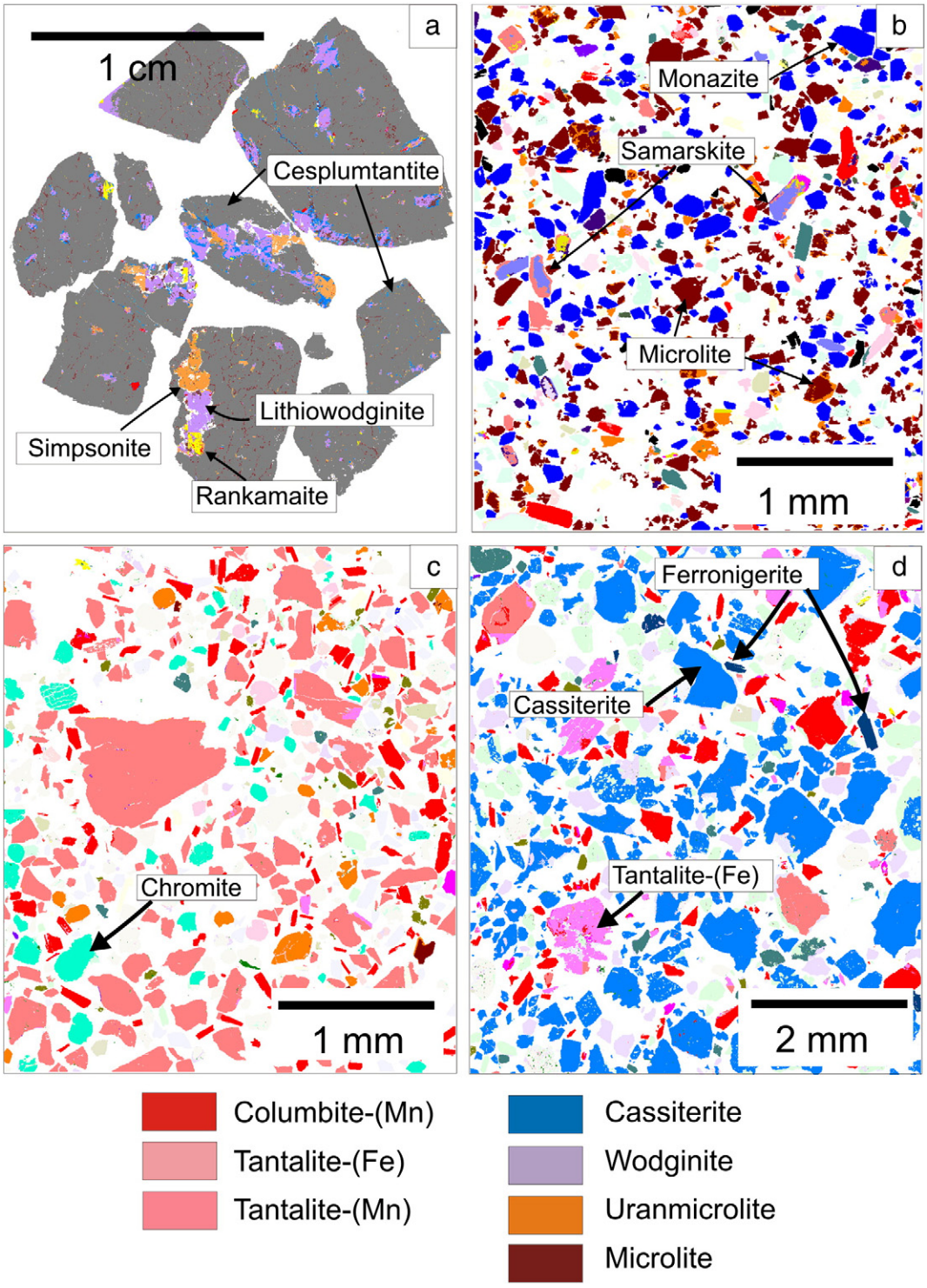

Fig. 3. Representative SEM/MLA maps of ore concentrates from selected African Ta–Nb–Sn pegmatites. (a) Mumba, North Kivu, DRC; sample 581; (b) Marropino, Mozambique; sample 132; (c) Kenticha, Ethiopia; sample 254; (d) Nemba, Rwanda; sample 136.

4.2. Paleoproterozoic (2500–1600 Ma)

4.2.1. Birimian (Ghana, Côte d'Ivoire)

Birimian, or Eburnean-age (2100–2000 Ma) pegmatites are known from greenstone belts and sedimentary basins in West Africa including Burkina Faso, Ghana, south-western Mali, south-western Niger and the Côte d'Ivoire (2.1 in Fig. 1). These pegmatites occasionally contain small concentrations of Nb, Ta, Be and Li, e.g. at Issia, Côte d'Ivoire (Allou et al., 2005; Varlamoff, 1972) and at Kokobin near Akim-Oda, Ghana (Bering, 1976).

Both tantalum potential and production of these countries are small. As of September 2002, inferred and indicated alluvial and eluvial resources at Akim-Oda were 93 tons of tantalum minerals. Resources of alluvial material at Issia are 1.5 million tons of gravels grading 0.006% Ta_2O_5; historical production was approximately 12 tons per year of 63–64% Ta_2O_5 concentrates but fell to an estimated level of 0.4 tons recently (Roskill, 2012).

Several CGM analysed from Kokobin gave Paleoproterozoic ages between 2070 and 2085 Ma (Melcher et al., 2008a; sample 007, Table 2) corresponding with prominent pegmatite veining in Birimian

sedimentary rocks during the final stages of the Eburnean tectonothermal event (Abouchami et al., 1990; Anonymous, 2009; Boher et al., 1992; Hirdes et al., 1992; Oberthür et al., 1998; Taylor et al., 1992). These ages are slightly younger than late Eburnean two-mica or muscovite granites (2088 Ma) and also postdate sedimentation of the Tarkwaian Group that was constrained to 2132–2116 Ma (Davis et al., 1994).

Tantalum minerals at Kokobin were collected from eluvial placers and weathered pegmatite. They consist of large grains of complexly zoned and partly homogeneous columbite-(Mn) to tantalite-(Mn) minerals that are sometimes extensively replaced by microlite-group minerals (Figs. 6c, 7c). Zoned grains frequently reveal rims of columbite-(Fe). From Issia, Allou et al. (2005) reported the occurrence of beryl, tourmaline, garnet, apatite, epidote and Li-rich mica in pegmatites hosted by mica schist. Tantalite-(Fe,Mn) and tapiolite are present in their pegmatite types C and D.

4.2.2. North-eastern DRC (Ubendian; Orientale and northern North Kivu)

The metasedimentary and magmatic rocks of the Paleoproterozoic Ruwenzori (or Buganda-Toro; Cahen and Snelling, 1966; Cahen et al., 1984; Lepersonne, 1974) fold belt that extends into the Kibali-Ituri region of North Kivu (2.2 in Figs. 1 and 2) are crosscut by east–west-trending pegmatitic veins that carry columbite–tantalite, cassiterite and wolframite mineralisation (Etaetu and Mambasa, Orientale Province; Prigogine, 1956; Angermeier et al., 1974; Musée Royal de l'Afrique Centrale, 2005. Placer deposits have been mined until the 1950s. Current mining activities in the region are, however, mainly concentrated on gold deposits associated with greenstone belts. Only few small artisanal mine sites produce cassiterite, coltan and wolframite (Spittaels, 2010).

Several columbite and tapiolite grains from a sample from the Mambasa area yielded a borderline Archean–Paleoproterozoic core age of 2487 Ma, whereas rims, veinlets and also discrete grains yielded ages close to 2000 Ma (Melcher et al., 2008b, 2009). These findings are interpreted to indicate Paleoproterozoic overgrowth on significantly older CGM and probably represent the first documented example of polyphase growth of CGM in pegmatites. Single grains from two placer samples collected further to the south (Liha, Lubero, samples 100, 114) yielded Paleoproterozoic ages only (e.g., with an intercept at 1953 ± 7.4 Ma; Fig. 4b). Twenty-seven single grains from four locations (mostly placer material) investigated in the Archean–Paleoproterozoic transition zone at the southern margin of the Congo Craton include complexly zoned columbite-(Fe) to tantalite-(Fe), tapiolite, and subordinate U-bearing (2–5 wt.% UO_2) microlite (Fig. 6b). Various pyrochlore-supergroup minerals such as microlite (Pb and/or U-rich), and U-bearing pyrochlore occur as inclusions in and replace CGM and tapiolite. Niobian rutile grains intergrown with ilmenite were also observed. Zircon and uraninite occur as inclusions in CGM. The complexly zoned CGM range from Fe-rich to moderately Mn-rich columbite to tantalite (#Mn = 10–54; #Ta = 10–77; Fig. 7d).

4.3. Neoproterozoic (1000–542 Ma)

4.3.1. Kibara Belt (east-central Africa)

The NNE–SSW trending Kibara Belt (sensu lato; 3.1 in Figs. 1 and 2) stretches over a distance of 1300 km from south-western Uganda via Rwanda and Burundi into the Katanga region of the DRC towards the Angola–Zambia–DRC border (e.g., Dewaele et al., 2008; Fernandez-Alonso et al., 2012; Pohl, 1987, 1994; Tack et al., 2010). Recently, the term Kibara Belt has been subdivided by Tack et al. (2010) into the Karagwe–Ankole Belt (KAB) and into the Kibara Belt sensu stricto. Both are separated by an area of Paleoproterozoic (Rusizian) terranes that are in structural continuity with the Ubendian Shear Belt in Tanzania. The Kibara and Karagwe–Ankole Belts mainly consist of Paleo- to Mesoproterozoic clastic sediments that were intruded by several generations of granite.

The Kibara "tin granites" (G4 granites) and associated pegmatites constitute one of the world's largest Ta–Nb–Sn–W provinces. Ta–Nb mineralisation is hosted by zoned or unzoned pegmatites of variable size, whereas Sn mineralisation is more abundant in greisenised zones and hydrothermal quartz veins (Dewaele et al., 2010, 2011). Wolframite is restricted to hydrothermal quartz veins only (De Clerq et al., 2008). In this area, the LCT pegmatites are mineralised with Ta–Nb, Li, Be and phosphates and intrude metasediments, mafic intrusive rocks and older granites. The most fractionated (i.e., Li–Ta-rich) pegmatites are more distant to G4 granite outcrops than the less fractionated Nb–Be-rich pegmatites. This led Varlamoff (1972) to develop a concept of zoned pegmatite mineralisation in Central Africa. Sn–Ta deposits have been mined in the DRC since about 1910 (Angermeier et al., 1974). Manono–Kitotolo in Katanga (DRC) is the largest single pegmatite deposit in the Kibara Belt, constituting an ore resource (Sn, Ta, Li) of 100 million tons (Bassot and Morio, 1989). Extensive mining activities took place in the Kivu and Maniema Provinces, e.g., in the Lugulu (Lulingu) district along the southern margin of the Kasese batholith in South Kivu (e.g., Angermeier et al., 1974; de Kun, 1960). Only 5% of the Ta and Sn resources are hosted in primary deposits (pegmatites and cassiterite-bearing quartz veins), whereas 10% occur in eluvial and 85% in alluvial deposits. Concentrates usually contain 92% cassiterite and 6–7% coltan (with 30 wt.% Ta_2O_5). With the onset of the civil war in the mid-1990s production of Ta and Sn in the Kivu Provinces became largely controlled by armed groups. Garrett and Mitchell (2009) estimate cassiterite exports from the DRC at 18,000–25,000 tons (in 2007–2008) and coltan exports at 360 tons (2007) and 517 tons (2008).

In Rwanda, many mining licences that had previously been owned by the state-controlled Régie d'Exploitation et de Developpement des Mines (REDEMI) have been granted to national and international companies. Most of them are operated in an artisanal way (Fig. 5a). From 1958 to 2005, about 60,000 tons of cassiterite and 5000 tons of coltan were produced (BRGM, 1987; USGS Mineral Commodity Summaries 1990–2005). Recent annual exports (2010) included 749 tons of coltan concentrate and ca. 4000 tons of cassiterite concentrate (BGS World Mineral Production, 2012); these numbers may include material imported from the DRC. Much lower production numbers are reported for Burundi (113 tons Ta_2O_5 from 1997 to 2006; 20 tons in 2010; BGS World Mineral Production, 2012) and Uganda (28 tons Ta_2O_5 from 2000 to 2006; USGS Mineral Commodity Summaries).

Alkaline complexes and carbonatites (e.g., Lueshe, Bingo, Upper Ruvubu) in the Central African rift system host significant resources of Nb (Woolley, 2001). These rocks postdate the Kibara Belt, but radiometric data are equivocal (U–Pb zircon data ca. 750 Ma, Tack, pers. comm. 2010; Rb/Sr whole-rock data of ca. 800–830 Ma; Kampunzu et al, 1998). Lueshe comprises the largest Nb resource in Central Africa (180 Mt at 1% pyrochlore).

4.3.1.1. Radiometric data. U–Pb ages were obtained from CGM in the Kibara Belt (sensu lato) of the DRC, Uganda, Rwanda and Burundi (Table 2, Fig. 4c–g). First columbite data reported for samples from this area were from pegmatites in northern Burundi, revealing ages of 963 + 9/−5 and 968 + 33/−29 Ma (Romer and Lehmann, 1995). New columbite–tantalite U–Pb ages range from ca. 920 to 1030 Ma, with the maximum around 960–990 Ma. This indicates a close association with post-compressional G4 or "tin granites", some of which have been dated at 986 ± 10 Ma (Kasika tin granite, DRC; Tack et al., 2010). There is no clear age variation of pegmatite-hosted mineralisation over the Kibara Belt. A few CGM and cassiterite concentrate samples collected within about 50 km of Lake Kivu in the centre of the East African rift, however, yielded younger U–Pb ages ranging from 500 to 700 Ma (e.g., sample 745 from Kiyanja in the Rutsiro area, Rwanda, Fig. 4f; Table 2). This is interpreted as Pan-African rejuvenation of older mineralised structures. Further research is ongoing to unravel the history of Ta–Sn mineralisation in the belt (Dewaele et al., 2011).

Table 2
Radiometric ages (U–Pb) of Nb–Ta mineralisation in Africa.

Location	Country	Province/Belt	District	Sample no.	Minerals dated	Type of material dated	Dating method[a]	Geologically significant age(s) (Ma)	±2 s (Ma)	MSWD	Degree of concordance (%)[b]	TIMS: n (splits/grains)	LA-ICP-MS: n (spots/grains)	Reference
Bikita	Zimbabwe	Zimbabwe Craton	Victoria Schist Belt	056	Columbite-(Mn)	Single crystal	TIMS 1	2617	1	1.3	89–96 (93)	5/3		
Benson	Zimbabwe	Zimbabwe Craton	Mutoko	098	Wodginite	Few crystals	TIMS 2	2586.7	3.6	0.14	96–98 (97)	3/1		
Kokobin	Ghana	Birimian		007	Columbite-(Fe,Mn)	Few crystals	TIMS 1	2079.6	3.1	59	99–101 (100)	5/2		Melcher et al. (2008a)
				007	Columbite-(Fe,Mn)		TIMS 2	2084.7	0.8	0.08	100	3/1		
				007	Columbite-(Fe,Mn)		LA-ICP-MS	2073.8	8.3	1.08	76–103 (98)		27/2	
G 18, Riv. Liha	DRC	Congo Craton	Orientale	100	Columbite-(Fe)	Concentrate	TIMS 1	1981	8		92–94 (93)	5/5		
				100	Columbite-(Fe)		LA-ICP-MS	1953	7.0	1.09	22–130 (92)		53/4	
G 6, Enehe, Mambasa area	DRC	Congo Craton	Orientale	101	Tantalite-(Fe), columbite-(Fe), tapiolite	Concentrate	TIMS 2	1950.1[c]	0.8	0.76	99–100 (99)	4/1		Melcher et al. (2008b, 2009)
				101	Tantalite-(Fe), columbite-(Fe), tapiolite		LA-ICPMS	2487.8	7.9	0.2	95–102 (99)		53/8	
				101	Tantalite-(Fe), columbite-(Fe), tapiolite		LA-ICPMS	2051	12.0	0.78	36–101 (85)			
Chutes Haute Lenda Lubero	DRC	Congo Craton	North Kivu	114	Tantalite-(Fe), columbite-(Fe), tapiolite	Concentrate	TIMS 1	1980	3	25	99–101 (100)	4/1		
				114	Tantalite-(Fe), columbite-(Fe), tapiolite		TIMS 1	1930	5	65	97–100 (98)	6/1		
				114	Tantalite-(Fe), columbite-(Fe), tapiolite		TIMS 1	1876	20	14	97–99 (98)	4/1		
Mobra	Burundi	Kibara Belt	Ndora	155	Columbite-(Fe)	Single crystal	TIMS 1	934.5	3.9	1.15	96–98 (97)	4/4		
Kivuvu	Burundi	Kibara Belt	Kabarore field		CGM	Single crystal	TIMS	963.7	+9.1/−5.3	1.31	99–100 (99)	4/1		Romer and Lehmann (1995)
Ruhembe	Burundi	Kibara Belt			CGM	Single crystal	TIMS	968	+33/−29	4.85	94–98 (97)	4/1		Romer and Lehmann (1995)
Camp Bisengo	DRC	Kibara Belt	South Kivu	040	Tantalite-(Fe), columbite-(Fe), tapiolite	Concentrate	TIMS 2	973.8	2.2	2.5	98–100 (99)	4/1		
				040	Tantalite-(Fe), columbite-(Fe), tapiolite		LA-ICP-MS	975.2	5.9	1.3	56–117 (94)		52/34	
Kakelo, Camp Vuma	DRC	Kibara Belt	South Kivu	043	Tantalite-(Fe,Mn), columbite-(Fe,Mn), tapiolite	Concentrate	LA-ICP-MS	962.8	+8.7/−8.5	0.5	87–108 (101)		30/30	
Mapimo Mulungu, Nzovu	DRC	Kibara Belt	South Kivu	044	Tantalite-(Fe,Mn), columbite-(Fe,Mn), tapiolite	Concentrate	LA-ICP-MS	960	9.0	0.97	81–113 (100)		35/35	
Mazakala, Shabunda	DRC	Kibara Belt	South Kivu	045	Tantalite-(Fe,Mn), columbite-(Fe,Mn), tapiolite	Concentrate	TIMS 2	971.1[c]	1.5	0.35	97–100 (99)	3/1		Melcher et al. (2008b, 2009)
				045	Tantalite-(Fe,Mn), columbite-(Fe,Mn), tapiolite		LA-ICP-MS	964.3	5.4	0.94	52–117 (97)		54/46	
Kamisuku, Pangi	DRC	Kibara Belt	Maniema	105	Tantalite-(Fe), columbite-(Fe), tapiolite	Concentrate	TIMS 2	992.2[d]	7.8	0.42	84–99 (92)	4/1		
				105	Tantalite-(Fe), columbite-(Fe), tapiolite		TIMS 2	992.8	2.1	0.86	98–99 (99)	2/1		
Kibeke, Pangi	DRC	Kibara Belt	Maniema	106	Tantalite-(Fe), columbite-(Fe), tapiolite	Concentrate	TIMS 1	960	5	–	92–99 (96)	8/8		
Bassin Obea Lubutu	DRC	Kibara Belt	Maniema	110	Tantalite-(Fe), columbite-(Fe), tapiolite	Concentrate	LA-ICP-MS	971.8	7.0	1.2	50–105 (98)		53/36	Melcher et al. (2008a)
Mutiko, Masisi	DRC	Kibara Belt	North Kivu	112	Columbite-(Fe,Mn)	Few crystals	TIMS 1	950.2	4.4	26	95–100 (97)	6/3		
Mwimbi Region, Mwenga	DRC	Kibara Belt	South Kivu	115	Columbite-(Fe,Mn)	Few crystals	TIMS 2	972.3	3	0.3	98–100 (99)	4/1		
Manono	DRC	Kibara Belt	Katanga	119	Columbite-(Mn), tantalite-(Mn)	Concentrate	TIMS 2	940.2	5.1	11.7	99–107 (101)	5/5		
Manono	DRC	Kibara Belt	Katanga	122	Columbite-(Mn), tantalite-(Mn)	Concentrate	TIMS 2	947.3[c]	2.8	0.05	99–123 (105)	4/1		
				122	Columbite-(Mn), tantalite-(Mn)		TIMS 2	947.3 [d]	2.3	1.5	99–123 (105)	4/1		

Muana, Region Mwenga	DRC	Kibara Belt	South Kivu	156	Tantalite-(Fe,Mn)	Single crystal	TIMS 1	937.1	2.4	2.1	95–98 (97)	8/1		
Muhanga	Rwanda	Kibara Belt		041	Columbite-(Fe,Mn), tantalite-(Fe,Mn)	Concentrate	LA-ICP-MS	971.9	4.9	1.2	88–122 (100)		26/7	
Gatumba plant	Rwanda	Kibara Belt	Gatumba	048	Columbite-(Fe,Mn), tantalite-(Fe,Mn)	Concentrate	TIMS 1	1029	19	3.7	95–97 (96)	8/4		Dewaele et al. (2011)
Ruhanga	Rwanda	Kibara Belt	Gatumba	084	Columbite-(Mn), tantalite-(Mn)	Concentrate	LA-ICP-MS	937.6	9.3	1.4	73–102 (92)		41/20	Melcher et al. (2008b, 2009)
Buranga	Rwanda	Kibara Belt	Gatumba	087	Columbite-(Mn), tantalite-(Mn)	Concentrate	TIMS 1	936	14	2.5	98–100 (99)	4/2		Dewaele et al. (2011)
Shori 3 (Gateko)	Rwanda	Kibara Belt	Gatumba	089	Columbite-(Fe,Mn), tantalite-(Fe,Mn), tapiolite	Concentrate	LA-ICP-MS	974.8	8.2	0.96	29–127 (90)		41/20	Dewaele et al. (2011)
Nyabisindu-Gasovu	Rwanda	Kibara Belt	Gatumba	093	Columbite-(Fe), tantalite-(Fe), tapiolite	Concentrate	TIMS 2	951	15	0.38	98–100 (98)	3/1		Dewaele et al. (2011)
Rongi	Rwanda	Kibara Belt	Gatumba	151	Columbite-(Fe)	Single crystal	TIMS 1	931.1	1.2	2.0	100–100 (100)	4/1		
Nyarigamba	Rwanda	Kibara Belt	Gatumba	204	Columbite-(Fe,Mn)	Concentrate	TIMS 1	928	4.5	0.4	97–99 (98)	5/3		Dewaele et al. (2011)
Nkegete	Rwanda	Kibara Belt	Gatumba	216	Columbite-(Fe), tantalite-(Fe)	Few crystals	TIMS 1	939.3	4	3.2	100–102 (101)	4/4		Dewaele et al. (2011)
Nkegete	Rwanda	Kibara Belt	Gatumba	219	Columbite-(Fe,Mn)	Concentrate	TIMS 1	958	0.4	0.8	99–103 (101)	5/4		Dewaele et al. (2011)
Bijyojyo	Rwanda	Kibara Belt	Gatumba	233	Columbite-(Fe,Mn), tantalite-(Fe), cassiterite, zircon	Concentrate	TIMS 1	1177	120	0.32	94–95 (95)	4/2		
				233	Columbite-(Fe,Mn), tantalite-(Fe), cassiterite, zircon		LA-ICP-MS	966.2	+8.7/−8.6	0.9	70–109 (97)		37/31	Dewaele et al. (2011)
Ndiza	Rwanda	Kibara Belt	Gatumba	125	Columbite-(Fe), tantalite-(Fe,Mn)	Single crystal	TIMS 1	936.5	6.6	0.49	99–100 (100)	3/2		
Ntunga	Rwanda	Kibara Belt	Musha–Ntunga	153	Columbite-(Mn)	Single crystal	TIMS 1	935	13	0.92	99–100 (100)	4/1		
Ntunga	Rwanda	Kibara Belt	Musha–Ntunga	235	Tantalite-(Mn), columbite-(Mn), wodginite	Concentrate	TIMS 1	949.2	2.7	0.3	98–100 (99)	5/5		Melcher et al. (2008a)
Nemba	Rwanda	Kibara Belt	Nemba	136	Columbite-(Fe,Mn), tantalite-(Fe,Mn), wodginite	Concentrate	LA-ICP-MS	960.7	7.6	0.51	82–117 (99)		53/31	
Nemba	Rwanda	Kibara Belt	Nemba	169	Columbite-(Mn), tantalite-(Mn)	Concentrate	TIMS 2	951	13	1.8	98–99 (98)	2/1		
Kibingo	Rwanda	Kibara Belt	Rutsiro	150	Columbite-(Mn)	Single crystal	TIMS 1	929.4	6	0.042	97–98 (98)	3/1		
Kiyanja 1	Rwanda	Kibara Belt	Rutsiro	745	Columbite-(Fe)	Concentrate	LA-ICP-MS	577	25	1.03	55–114 (91)		25/25	
Myatano 1	Rwanda	Kibara Belt	Rutsiro	743	Columbite-(Fe)	Concentrate	LA-ICP-MS	940	21	1.6	80–110 (93)		26/26	
Kanungu	Uganda	Kibara Belt		381	Columbite-(Fe,Mn), tantalite-(Fe,Mn)	Concentrate	TIMS 1	983.4 [f]	0.6	0.55	100	2/1		
Mbulema	Uganda	Kibara Belt		383	Columbite-(Fe)	Single crystal	TIMS 1	958.5	3.2	3.2	99–100 (100)	5/3		
Kamativi	Zimbabwe	Kamativi Belt		786	Columbite-(Fe,Mn)	Concentrate	TIMS 2	1031 [c]	8	0.15	100–102 (101)	3/3		
				786	Columbite-(Fe,Mn)		TIMS 2	1037 [d]	5	1	100–102 (101)	3/3		
Homestead	Namibia	Orange River Belt	Tantalite Valley	272	Tantalite-(Mn), columbite-(Mn)	Few crystals	LA-ICP-MS	982.7	5.3	1.4	84–109 (96)		38	Melcher et al. (2008a)
Homestead	Namibia	Orange River Belt	Tantalite Valley	274	Tantalite-(Mn), columbite-(Mn)	Few crystals	LA-ICP-MS	981.4	3.3	0.77	74–111 (94)		43/9	
Homestead	Namibia	Orange River Belt	Tantalite Valley	275	Tantalite-(Mn), columbite-(Mn)	Few crystals	LA-ICP-MS	984.9	2.8	0.87	88–117 (101)		47/6	
Kenticha (quartz unit)	Ethiopia	Arabian–Nubian Shield	Adola Belt		Tantalite-(Mn)	Single crystal	TIMS	529.2	5.4	4.1	95–101 (99)	7/1		Küster et al. (2009)
					Tantalite-(Mn)		TIMS	530.2 [e]	1.3	1.3	99–101 (100)	5/1		Küster et al. (2009)
Kenticha (spodumene unit)	Ethiopia	Arabian–Nubian Shield	Adola Belt		Tantalite-(Mn)	Single crystal	TIMS	530.0	2.3	1.3	98–101 (99)	5/1		Küster et al. (2009)
Bupo	Ethiopia	Arabian–Nubian Shield	Adola Belt		Tantalite-(Mn)	Single crystal	TIMS	529.2	4.1	4.3	101–104 (102)	4/1		Küster et al. (2009)
					Tantalite-(Mn)		TIMS	530.0 [e]	6.4	3.8	101–104 (102)			

(continued on next page)

Table 2 (*continued*)

Location	Country	Province/Belt	District	Sample no.	Minerals dated	Type of material dated	Dating method[a]	Geologically significant age(s) (Ma)	±2 s (Ma)	MSWD	Degree of concordance (%)[b]	TIMS: n (splits/grains)	LA-ICP-MS: n (spots/grains)	Reference
Somabula \gravels	Zimbabwe		Midlands	027	Tapiolite, columbite-(Fe), tantalite-(Fe)	Concentrate	TIMS 2	511	20		97–101 (99)	5/5		Oberthür et al. (2002)
	Madagascar			139	Columbite-(Fe)	Large crystal	TIMS 1	505.4	1.0	2.7	96–100 (98)	5/1		
				139	Columbite-(Fe)		TIMS 2	506.6	2.4	0.23	93–99 (96)	7/1		
				139	Columbite-(Fe)		LA-ICP-MS	506.2	5.0	0.93	97–110 (103)		30/1	
Marropino	Mozambique	Alto Ligonha	Lurio Belt	009	Tantalite-(Mn)	Single crystal	TIMS 2	473.8	3.4	0.46	98–99 (99)	3/1		
				009	Tantalite-(Mn)		TIMS 2	472.9[d]	2.5	0.69	98–99 (99)	3/1		
				126	Tantalite-(Mn)	Few crystals	TIMS 2	465.1	1.9	0.28	73–99 (93)	3/2		
				132	Monazite	Concentrate	TIMS 2	481[f]	1.7	2.6	105–108 (106)	4/1		
				132	Tantalite-(Mn), columbite-(Mn)	Concentrate	LA-ICP-MS	446.6	4.4	1.4	37–123 (88)		34	Melcher et al. (2008b, 2009)
Morrua	Mozambique	Alto Ligonha	Lurio Belt	159	Tantalite-(Mn)	Concentrate	TIMS 2	479.7	2.3	0.18	99–99 (99)	4/1		
				159	Tantalite-(Mn)		TIMS 2	480.0[d]	2	0.17	99–99 (99)	4/1		
Moneia	Mozambique	Alto Ligonha	Lurio Belt	175	Tantalite-(Mn)	Concentrate	LA-ICP-MS	451.9	7.4	1.3	25–140 (92)		55/20	
Moneia	Mozambique	Alto Ligonha	Lurio Belt	178	Tantalite-(Mn)	Concentrate	TIMS 2	440.5[e]	0.5		99–100 (99)	3/1		
Rubikon	Namibia	Damara Belt	Karibib	004	Columbite-(Mn)	Single crystal	TIMS 2	505.5	2.6	1.7	99–101 (100)	2/1		
				004	Columbite-(Mn)		TIMS 2	506.0[d]	2.3	1.4		2/1		
				004	Columbite-(Mn)		LA-ICP-MS	499.7	12.0	0.73	85–103 (93)[g]		16/1	
Bauchi-Province	Nigeria	Jos Plateau	Guli–Richi	148	Columbite-(Fe), cassiterite	Concentrate	LA-ICP-MS	197.8	1.6	1.4			54/54	

[a] TIMS: literature data; TIMS 1: BGR; TIMS 2: University Toronto; LA-ICP-MS: University Frankfurt.
[b] Degree of concordance = ($^{206}Pb/^{238}U$ age × 100 / $^{207}Pb/^{206}Pb$ age), range and average (in brackets).
[c] Average $^{207}Pb/^{206}Pb$ age.
[d] Pb–Pb isochron age.
[e] Average $^{206}Pb/^{238}U$ age.
[f] Average $^{207}Pb/^{235}U$ age.
[g] No reliable $^{207}Pb/^{206}Pb$ ages due to low ^{207}Pb yields.

4.3.1.2. Mineralogy. This study forms the first regional summary on heavy minerals in this Ta–Nb–Sn province since the pioneering work of Prigogine (1956) and de Kun (1960). It also includes data previously published in Lehmann et al. (2008) and Dewaele et al. (2011) and is based on a total of 82 MLA analyses of Ta–Nb–Sn ore concentrate samples and on electron microprobe analyses of 53 polished sections.

Kibaran pegmatites cover a wide array of mineralogical compositions, with a characteristic predominance of CGM among the heavy minerals, and their wide compositional range. The nearly 10,000 analyses presented in Fig. 7e plot in all areas of the "columbite quadrilateral" except for pure tantalite-(Mn) and the miscibility gap to tapiolite. The density-contoured diagram indicates a general Fe–Mn fractionation trend. However, Nb–Ta fractionation is observed at many individual locations. Cassiterite is abundant, but is not present in all concentrates, either due to the lack of cassiterite in some mineralised systems or to effective manual-automated beneficiation of concentrates. On the other hand, the presence of large amounts of cassiterite not intergrown with TNO indicates that different styles of mineralisation may have been sampled in some concentrates. Greisen and quartz vein-type mineralisations usually lack CGM but also contribute to eluvial and alluvial placer deposits. Thus, the proportion of cassiterite intergrown with CGM and TNO is a reliable indicator of the co-occurrence of Sn and Ta–Nb minerals. MLA data for 25 concentrate samples (Dewaele et al., 2011) show that this proportion ranges from 2.5 to 28% (median, Md: 6.2%) in eight pegmatite deposits in the Gatumba area of Rwanda, whereas the proportion of CGM intergrown with cassiterite ranges from 0.1 to 7.8%. Furthermore, ilmenite and rutile are omnipresent and wolframite may occur in significant quantities. Zircon, monazite, xenotime, apatite and garnet are typically present in small amounts only, whereas sulphides are mostly absent probably due to weathering (Table 1). Apart from CGM (comprising on average 91% of the TNO) (Fig. 6e–h), the following TNO were identified: tapiolite (average 3.2%, locally up to 78%) (Fig. 6h), wodginite–ixiolite (1.7%, up to 35%) (Fig. 6f), pyrochlore-supergroup minerals (mainly microlite; average 2.5%, up to 86%) (Fig. 6d, h) and Ta–Nb rutile (1.1%, up to 40%). Foordite–thoreaulite was found in one sample only (Kubitaka, DRC, composing 7.5% of this sample) (Fig. 6d), but has been reported from a few other locations as well, including Manono and Rutsiro (Černý et al., 1988; Uher et al., 2008). REE–U–Ta-rich oxides are rare and larger concentrations of fergusonite and euxenite were only encountered in one sample from Lutenga, South Kivu. Although bismutotantalite was discovered in a pegmatite in south-western Uganda (Gamba Hill, Busiro County, Ankole; Wayland and Spencer, 1929), neither bismutotantalite nor stibiotantalite were found in the samples analysed in the present work. Other rare phases include simpsonite, rankamaite (von Knorring and Fadipe, 1981; von Knorring et al., 1969), cesplumtantite and lithiowodginite that were all identified only in samples from the Mumba area, North Kivu (DRC). Rynersonite was previously described from Wampewo/Mengo, Uganda (von Knorring and Fadipe, 1981).

Table 1 illustrates an enormous mineralogical diversity of pegmatite-hosted Ta mineralisation within the Kibara Belt. The Manono (DRC), Nemba and Musha–Ntunga districts (both in Rwanda) are characterised by Mn-rich CGM ranging from columbite to tantalite. In the Kivu Provinces, Pangi (Maniema, DRC), Gatumba and Rutsiro in Rwanda, as well as in some pegmatites from Burundi (Ndora) and Uganda (Kanungu), CGM vary from Fe- to Mn-rich columbite, with occasional development of Fe- and Mn-rich tantalite. Tapiolite is more abundant in districts with Fe-dominated CGM than in those pegmatites dominated by Mn-dominated CGM. Abundant wodginite, on the other hand, is associated with the Mn-rich pegmatites. Large concentrations of primary U-rich microlite were observed in phosphate-rich pegmatites of the Gatumba district only, namely at Buranga and Nyarigamba (Rwanda).

4.3.2. Kamativi Schist Belt (western Zimbabwe)

Paragneisses of the Kamativi Schist Belt (3.2 in Fig. 1) that forms part of the Paleoproterozoic Magondi Belt (Petters, 1991), were intruded by poorly zoned Sn–Ta–W- and amblygonite–spodumene–beryl-bearing pegmatites (Rijks and van der Veen, 1972; von Knorring, 1970; Watson, 1962). These pegmatites are of early Neoproterozoic age (990 ± 15 Ma).

Cassiterite and Ta–Nb mineralisation is significant in mica selvage zones. The Kalinda and Kamativi mines were in intermittent production from 1937 until 1994, annually producing 1200 tons of cassiterite and 60 tons of tantalum concentrates by the end of their production period (Fetherston, 2004). Coarse grains collected at the Kapata mine consist of cassiterite. Concentrates labelled "Kamativi" from the collection of the University of Harare consist of columbite-(Fe,Mn), tantalite-(Fe,Mn) and cassiterite (Fig. 7f) in varying proportions. Some tapiolite, wodginite, garnet, monazite, zircon and tourmaline occur as additional heavy minerals (Table 1). U–Pb dating using TIMS yielded a Pb–Pb age of 1031 ± 8 Ma for three columbite grains (Table 2). Age estimates using the method of Gäbler et al. (2011) on CGM range from 925 to 1026 Ma for different concentrate samples.

4.3.3. Orange-River Pegmatite Belt (Namibia, South Africa)

One of the largest pegmatite provinces in Africa with over 12,000 known pegmatites is the Orange-River Pegmatite Belt (3.3 in Fig. 1), extending from the northwestern Cape Province of South Africa into southern Namibia. Some of the pegmatites are rare-element bearing, e.g. the Noumas pegmatite in the Steinkopf–Vioolsdrif area, which has been intermittently mined for feldspar (Gevers et al., 1937; Minnaar, 2006; Schutte, 1972).

The Mesoproterozoic Tantalite Valley igneous complex in southern Namibia and South Africa is part of the high-grade metamorphic Namaqualand Province and is attributed to the late- to post-kinematic Namaquan orogeny (580 °C, 4–5.5 kb) at 1100–1000 Ma (Becker et al., 2006). It is composed of mafic magmatic rocks (olivine gabbro) and gneisses. LCT-family ("Skimmelberg-type") pegmatites intruded the layered mafic to ultramafic sequence along prominent shear zones as symmetrically zoned bodies, up to 1 km long and more than 10 m thick (Fig. 5b). They consist of quartz, K-feldspar, albite, muscovite, spodumene, lepidolite, amblygonite, beryl, Bi and Ta minerals and various phosphates (Diehl, 1992; von Knorring and Condliffe, 1987). Some of the pegmatites in the Tantalite Valley Complex have been mined until the 1970s and in the early 2000s. Their total reserves have been estimated at 0.74 million tons at 430 ppm Ta_2O_5 (Fetherston, 2004).

4.3.3.1. Radiometric data. CGM from the Homestead pegmatite in the Tantalite Valley, Namibia, yield consistent U–Pb ages of ca. 985 Ma (samples 272, 274, 275; Table 2, Fig. 4h), in partial agreement with previous K–Ar (muscovite; 920 Ma), Rb–Sr (muscovite, biotite, lepidolite; 956–1090 Ma) and ^{207}Pb–^{206}Pb measurements (monazite, gadolinite, uraninite, euxenite, allanite; 880–1040 Ma) for different pegmatites in the Namaqualand Complex carried out by Burger et al. (1965) and Nicolaysen and Burger (1965).

4.3.3.2. Mineralogy. In the Homestead pegmatite, tantalite-(Mn) (Fig. 6i) predominates in the albite and lepidolite zones over columbite-(Mn,Fe) that was identified in garnet-rich samples of the intermediate zone only (Fig. 7f; Graupner et al., 2010; van Lichtervelde et al., 2011). Alteration to Pb–U-bearing microlite is commonly observed. Amblygonite, spodumene, lepidolite, beryl, Bi minerals (including native bismuth) and various phosphates have been reported from the Tantalite Valley pegmatites (Diehl, 1992; von Knorring and Condliffe, 1987). In the past, cassiterite-bearing pegmatites containing accessory tourmaline, garnet, fluorite and beryl have also been mined from the Namaqualand Metamorphic Complex (e.g., Aukam; Diehl, 1992). The Noumas and related pegmatites in the South African part (northern Cape Province) of the Orange River Belt carry beryl, columbite, tantalite, microlite and spodumene (Boelema and Hira, 1998; von Knorring and Fadipe, 1981). Some of the pegmatites in the Kenhardt and Gordonia districts (South Africa) host abundant rare earth minerals, such as monazite, gadolinite, allanite, euxenite, fergusonite and zircon (Burger et al., 1965).

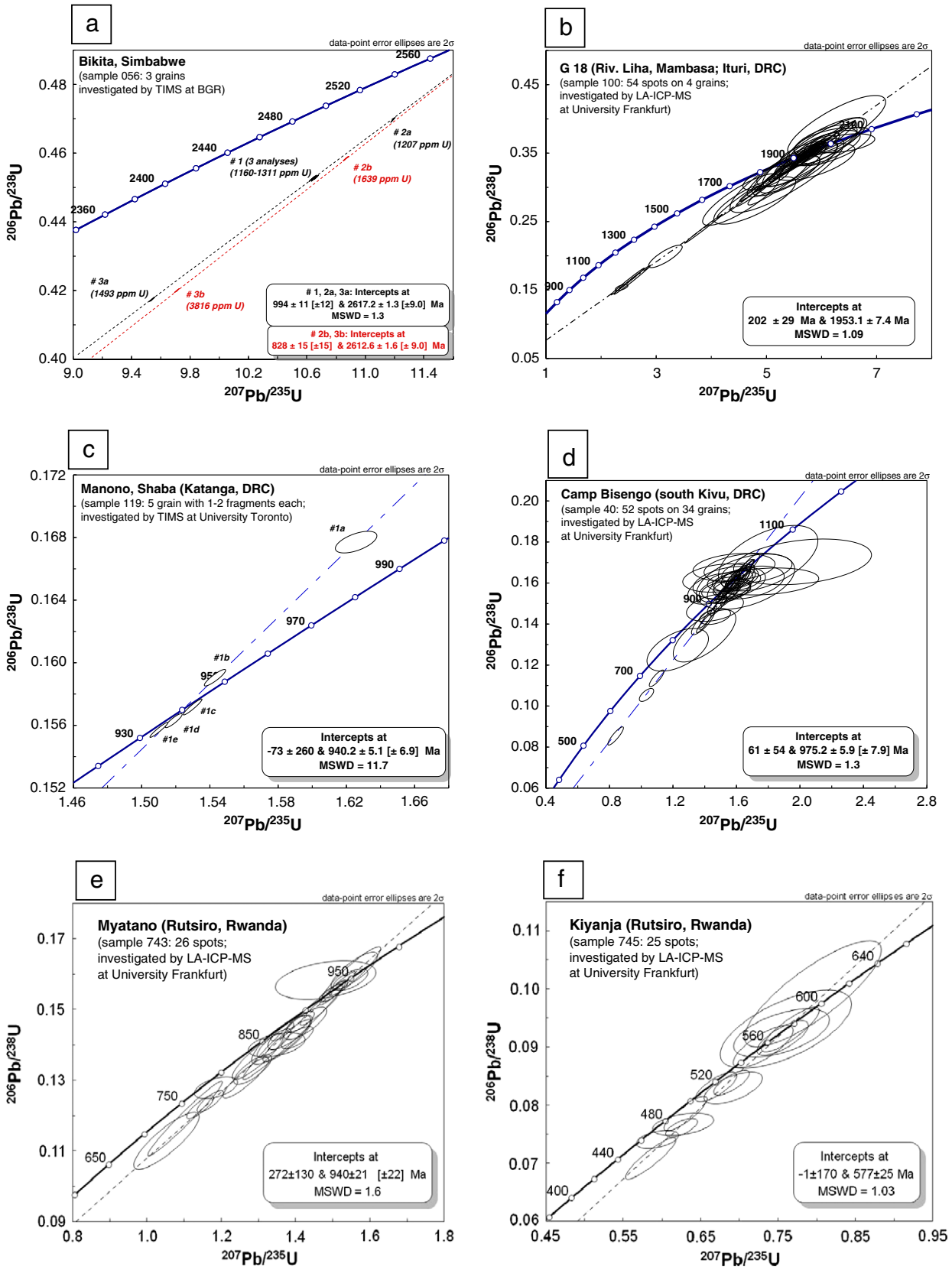

Fig. 4. U–Pb concordia diagrams of CGM from (a) Bikita (Zimbabwe), sample 056; (b) Liha (DRC), sample 100; (c) Manono (DRC), sample 119; (d) Camp Bisengo, South Kivu (DRC), sample 040; (e) Myatano (Rwanda), sample 743; (f) Kiyanja (Rwanda), sample 745; (g) Kanungu (Uganda), sample 381; (h) Homestead (Namibia), sample 275; (i) Marropino (Mozambique), sample 009; (j) Moneia (Mozambique), sample 175; (k) Rubikon (Namibia), sample 004; (l) Bauchi (Nigeria), sample 148.

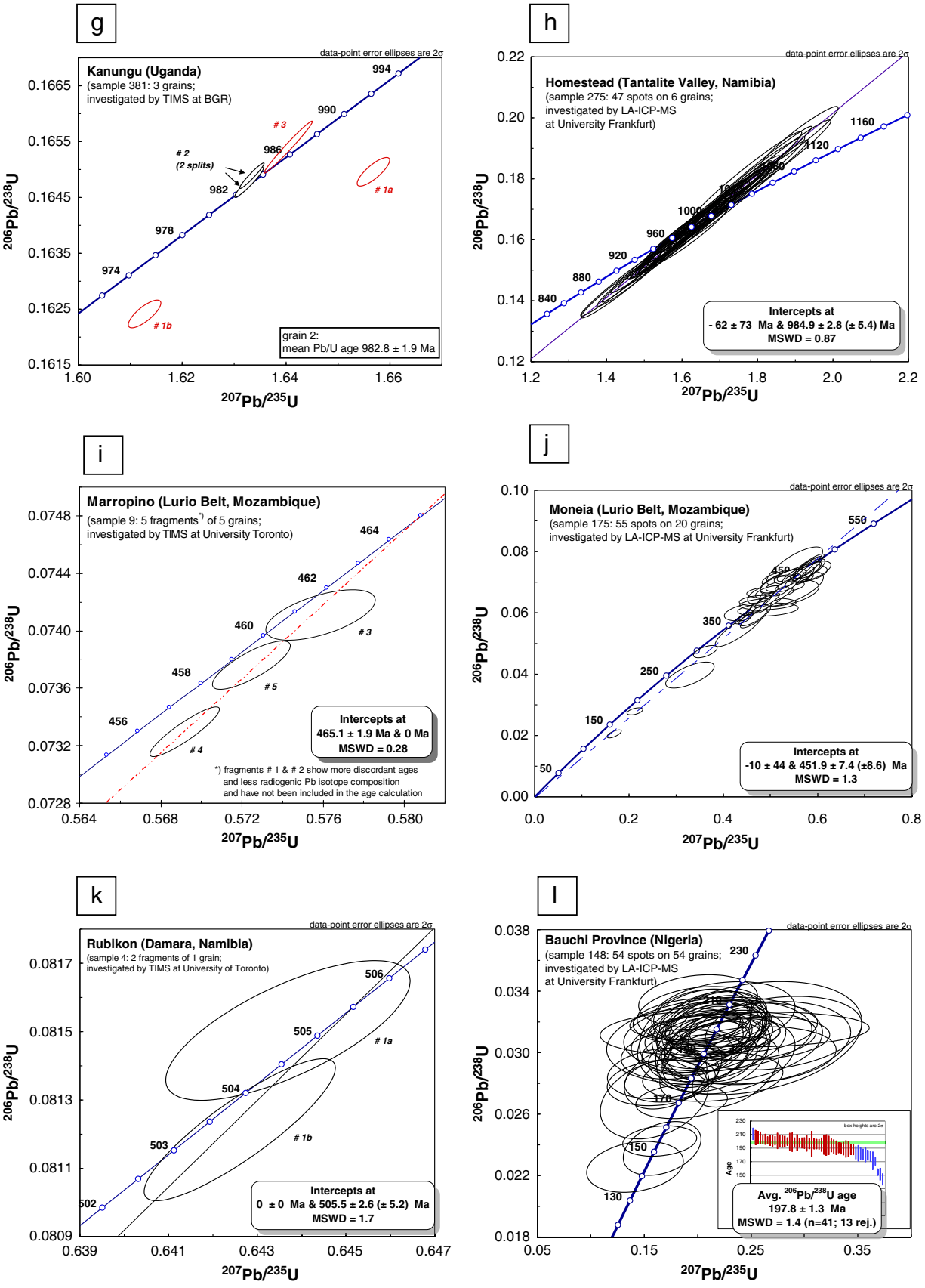

Fig. 4 (*continued*).

Fig. 5. Tantalum pegmatite deposits. (a) Bijyojo, Gatumba district, Rwanda. View into open pit generated by ground-sluicing; kaolinitised pegmatite under a laterite cover. (b) The metagabbro-hosted Homestead pegmatite, level 2, Tantalite Valley district, Namibia, with wall zone (WZ), albite zone (AZ) and relict quartz core zone (QZ); (c) Kenticha, Ethiopia; view into the open pit from distance; (d) Marropino, Mozambique; contact between muscovite and albite zones.

Tantalite and columbite from Homestead, single crystals of columbite-(Mn) and tantalite-(Mn) from the Steinkopf district, and a columbite-(Mn) crystal from an unknown locality (labelled "Namaqualand") were analysed in the present study.

4.4. Late Neoproterozoic to early Paleozoic (Pan-African)

Pan-African mobile belts are found across much of Africa; the East African Orogenic Belt is a major structure extending from the Eastern Desert of Egypt through Ethiopia into Mozambique and Madagascar (Mozambique Belt; Fritz et al., 2013). There are numerous areas within the Pan-African mobile belts surrounding the Archean to Proterozoic cratonic nuclei that host abundant pegmatites, which all are late with respect to the Pan-African orogenies (Stern, 1994). Pegmatite provinces of similar age are also found in the Damara Belt of central Namibia and in the Older Granites of Nigeria. Rare-metal granites are restricted to the Arabian–Nubian Shield (ANS) that constitutes the northern part of the East African Orogenic Belt.

4.4.1. Rare metal granites of the Eastern Desert (Egypt)

In the ANS (4.1 in Fig. 1), Ta mineralisation occurs in peraluminous rare-metal granites, in rare-element pegmatites (e.g., Kenticha, Ethiopia; Abu Dabbab and Nuweibi, Egypt; Majayahan, Somalia; Umm al Suquian, Saudi Arabia) and in peralkaline rare-metal granites (e.g., Ghurayyah, Saudi Arabia). Mineralisation is associated with a post-accretionary magmatic phase ranging in age from 610 Ma in the north to 530 Ma in the south (Küster, 2009). The deposits of Abu Dabbab (total resource 44.5 million tons of ore at 250 g/t Ta_2O_5 and 0.09% Sn) and Nuweibi (98 million tons of ore at 143 g/t Ta_2O_5 and 95 g/t Nb_2O_5; Gippsland Limited, 2013) in the Eastern Desert are hosted by small cupolas of highly evolved rare-metal granites that have been subjected to albitisation and greisenisation (El-Sharkawy, 2001; Sharara, 2000). At Abu Dabbab, fine-grained disseminated Ta and Sn ore minerals occur within the cupola, in marginal pegmatitic phases and external quartz veins and stockworks. At Nuweibi, the contact between granite and its host rock is marked by a stockscheider and a quartz cap. Ta mineralisation (with little Sn) in the eastern, more albite-rich part of the massif constitutes a large resource, whereas the western part is of lower grade.

4.4.1.1. Radiometric data. U–Pb age estimates for tantalite from Nuweibi suggest a Pan-African age close to 550 Ma. On the other hand, U–Pb age estimates for cassiterite from the Abu Dabbab, Nuweibi and Igla granites are significantly older, i.e. 616–685 Ma (BGR, unpubl. data). The rare-metal granites of Egypt are poorly dated because zircons are small, irregular and partly metamict; single-crystal evaporation analyses of 10 zircon grains from Nuweibi yielded Pan-African ages ranging from 610 ± 34 Ma to 425 ± 24 (Helba et al., 1997). Post-collisional alkaline A-type granites in the Eastern Desert hosting Sn–Mo mineralisation in quartz veins have been dated as late Neoproterozoic (620–630 Ma) using U–Pb SHRIMP zircon dating (Ali et al., 2012), with evidence that zircons were affected by late corrosive fluids.

4.4.1.2. Mineralogy. The rare-element granites of Abu Dabbab, Nuweibi and other localities in the Eastern Desert contain zoned columbite-(Fe), columbite-(Mn) and tantalite-(Mn), in addition to tapiolite, ixiolite–wodginite, stibiotantalite, microlite and cassiterite that is commonly intergrown with CGM and wodginite (Abdalla et al., 1998; Helba et al., 1997; Jahn, 1996); all are usually of small grain size (<100 μm) (Figs. 6j, 7g). In addition, microlite, (REE-rich) zircon, monazite, xenotime-(Yb), thorianite, REE fluoro-carbonates and fluorite were identified as accessory phases in mineralised granites from Abu Dabbab and Nuweibi.

4.4.2. Pegmatites of Ethiopia and Somalia

In Ethiopia, Ta mineralisation is mainly restricted to the Adola Belt in the southern part of the country (Küster et al., 2009; Tadesse and Zerihun, 1996). The Kenticha, Bupo and Shuni Hill pegmatites are part of a significant pegmatite cluster. The zoned and layered pegmatites of the LCT family (complex spodumene subtype according to the classification of Černý, 1991a) contain tantalite-(Mn) and spodumene, in addition to amblygonite and beryl. The Kenticha pegmatite, which is a significant Ta producer, has indicated reserves of 9000 tons of "tantalum products" (presumably concentrates; Roskill, 2012), and a grade of 150 g/t Ta_2O_5 in fresh rock (Fetherston, 2004). Production rose from 127 tons in 2007 to 445 tons of Ta and Nb concentrates in 2011 (Roskill, 2012); the concentrates commonly grade 55–60% Ta_2O_5.

After the discovery of Ta mineralisation by the British Geological Survey in the 1950s, several deposits have been explored and partly exploited in Somalia, among them a cassiterite- and spodumene-bearing LCT pegmatite at Majayahan with resources of 1.6 Mt grading 0.018% Ta_2O_5 (Küster et al., 2009). The current annual Ta production from pegmatites in Somalia is estimated close to 10 tpa (Roskill, 2012).

4.4.2.1. Radiometric data. Late Pan-African ages have been determined for tantalite from the Kenticha and Bupo pegmatites (ca. 530 Ma; Küster et al., 2009). Columbite from the Dalan and Majayahan pegmatites in Somalia gave similar U–Pb age estimates (530 Ma). Rb–Sr muscovite ages of 465 Ma in these pegmatites most probably indicate a resetting event (Küster, 1995; Lenoir et al., 1994b).

4.4.2.2. Mineralogy. The Kenticha LCT-pegmatite contains a continuous suite of CGM from columbite-(Fe) to columbite-(Mn) and tantalite-(Mn) (Figs. 6k, 7h), with rare ixiolite, tapiolite, and Ta-bearing rutile (Table 1); cassiterite is rare. Concentrates from the plant contain on average 79% TNO composed of CGM (~95%), pyrochlore-supergroup minerals (microlite, partly U-rich; ~5%), rare tapiolite and wodginite (<0.1% each). Several crystals of columbite-(Fe) from Majayahan were also investigated.

4.4.3. Alto Ligonha Province (northern Mozambique)

The Mozambique Belt comprises Mesoproterozoic and Neoproterozoic material reworked during the Pan-African orogeny (Fritz et al., 2013). The Alto Ligonha Province (4.3 in Fig. 1) is an important rare-metal pegmatite province, which has produced gemstones, industrial minerals and rare metals (REE, Be, Nb–Ta, Li, U–Th) between the 1950s and 1974, and from 1994 onward. A total of 12 pegmatite fields with 46 pegmatite groups and more than 100 single pegmatite occurrences are known (Cronwright, 2005); these correlate with, and are probably derived from, late- to post-orogenic, undeformed, equigranular, subaluminous to peraluminous A-type granites of Pan-African age.

The pegmatites of Alto Ligonha are concentrated mainly in the Nampula Subprovince, located at the southern end of the Mozambique Belt (Cronwright, 2005; Hutchinson and Claus, 1956). In addition to several pegmatite types barren with respect to CGM, three groups of economically important rare-element pegmatites are associated with Pan-African granites (Barros and Vicente, 1963; Lächelt, 2004):

(1) Sodic pegmatites (also referred to as "sodalithic" due to the occurrence of plagioclase and lithium minerals in these rocks), which are usually well zoned and contain beryl, CGM, microlite, tourmaline, lepidolite, spodumene, amblygonite and a variety of accessory minerals. These pegmatites constitute the most important group and occur mainly in amphibole schists, amphibolites and mica schists. They correspond to the complex spodumene and lepidolite–albite–spodumene types of the LCT family of Černý (1991a);
(2) Potassic pegmatites (beryl-columbite subtype, LCT family) with beryl and CGM, minor polycrase–euxenite, monazite, ilmenite and bismuthite; occurrence of these pegmatites is not restricted to specific host rock lithologies.
(3) Potassic pegmatites with metamict U, Th and REE minerals. These rocks are equivalent to the rare-earth type and show attributes of both the LCT and NYF families.

The deeply weathered Marropino "sodalithic" pegmatite (7.4 Mt ore total resources at 223 g/t Ta_2O_5; Roskill, 2012) in the Melela pegmatite field intruded into mafic gneisses and schists of the Mesoproterozoic Morrua Formation (Fig. 5d). The main ore body extends over 1 km in ENE–WSE direction and is up to 80 m thick. In 2006, 81 tons of Ta_2O_5 have been produced at Marropino (Schwela, 2007); an output of 45 tons of Ta_2O_5 was reported for 2011 (Roskill, 2012). Ore concentrates from Marropino are characterised by high concentrations of radiogenic and rare-earth elements present in monazite, zircon, bismutotantalite, samarskite and euxenite. In the Melela pegmatite field at Morrua, 50 km north of Marropino, 1300 tons of tantalite concentrates were mined from 1957 to 1979, in addition to microlite (119 tons), beryl and bismuthite (Cronwright, 2005). Exploration drilling indicated the presence of six pegmatites with thicknesses exceeding three metres that can be followed for over 1 km along strike. Resources are estimated at 7.8 Mt at 463 g/t Ta_2O_5 (Roskill, 2012). Ninety km north of Marropino, large reserves of Ta ore are associated with thick (up to 50 m) zoned pegmatites at Mutala (Munhamola, Moneia) in the Alto Molocue pegmatite field (Mutala resources: 10.3 Mt at 236 g/t Ta_2O_5). The Naquissupa and Muiane pegmatites are located in the Alto Ligonha pegmatite field northeast of Mutala. Historical production (1937–1978) from Muiane is 185 tons of columbite–tantalite, with additional beryl, lepidolite and bismuthite (Cronwright, 2005); the deposit contains a resource of 1.4 Mt grading 250 g/t to 40 m (Roskill, 2012). The Mocuba–Mugeba and Munhiba zone in the southwestern part of the pegmatite province hosts, among many others, the Somipe pegmatite, which is a member of the potassic pegmatite group (see before) and corresponds to the beryl-columbite or REE groups of the rare element pegmatite classification (Cronwright, 2005). The largest production of columbite–tantalite in Alto Ligonha is recorded from the potassic rare-earth-type Boa Esperanca pegmatites (18,300 tons in 1937–1961) in the Errego–Ribaue zone, in the northernmost part of the province (Cronwright, 2005).

4.4.3.1. Radiometric data. U–Pb age determinations for tantalite and monazite from Alto Ligonha record pegmatite formation from 480 to 440 Ma (samples 009, 126, 132, 159, 175, 178; Table 2, Fig. 4i, j). These U–Pb data are in line with previously obtained data for Pan-African granites in Alto Ligonha, which include Rb–Sr and U–Pb ages close to 490 Ma and a SHRIMP zircon age of 453 ± 17 Ma (Cronwright, 2005).

4.4.3.2. Mineralogy. The pegmatites within the Alto Ligonha Province are mineralogically variable, and display features characteristic of both the NYF and the LCT families (Cronwright, 2005; Lächelt, 2004; Sahama, 1980). The mineralogy of the economically important Marropino pegmatite is heterogeneous, being partly dominated by primary microlite (44% of the TNO, average of 7 concentrate samples), partly by CGM (53%) and characterised by the presence of bismutotantalite (2.1%) and euxenite–samarskite (1.1%). Tapiolite, wodginite–ixiolite and cassiterite have not been identified (Table 1, Fig. 6l, n). Monazite, xenotime and garnet are additional abundant heavy minerals. CGM are represented by Mn-rich columbite and tantalite; however, Fe-rich columbite is also present (Fig. 7i). The Moneia pegmatites mainly contain tantalite-(Mn), with less abundant tantalite-(Fe), microlite (4%), as well as ilmenite and garnet. The Morrua pegmatites are similar in composition, being dominated by tantalite-(Mn) (94%) and microlite (6%). Bismuth minerals, gahnite, rutile and monazite have been described previously (Cronwright, 2005). In contrast, CGM from a concentrate from Muiane follow a fractionation trend from columbite-(Mn) to tantalite-(Mn), and Sc-rich ixiolite was identified. A concentrate from Somipe consists

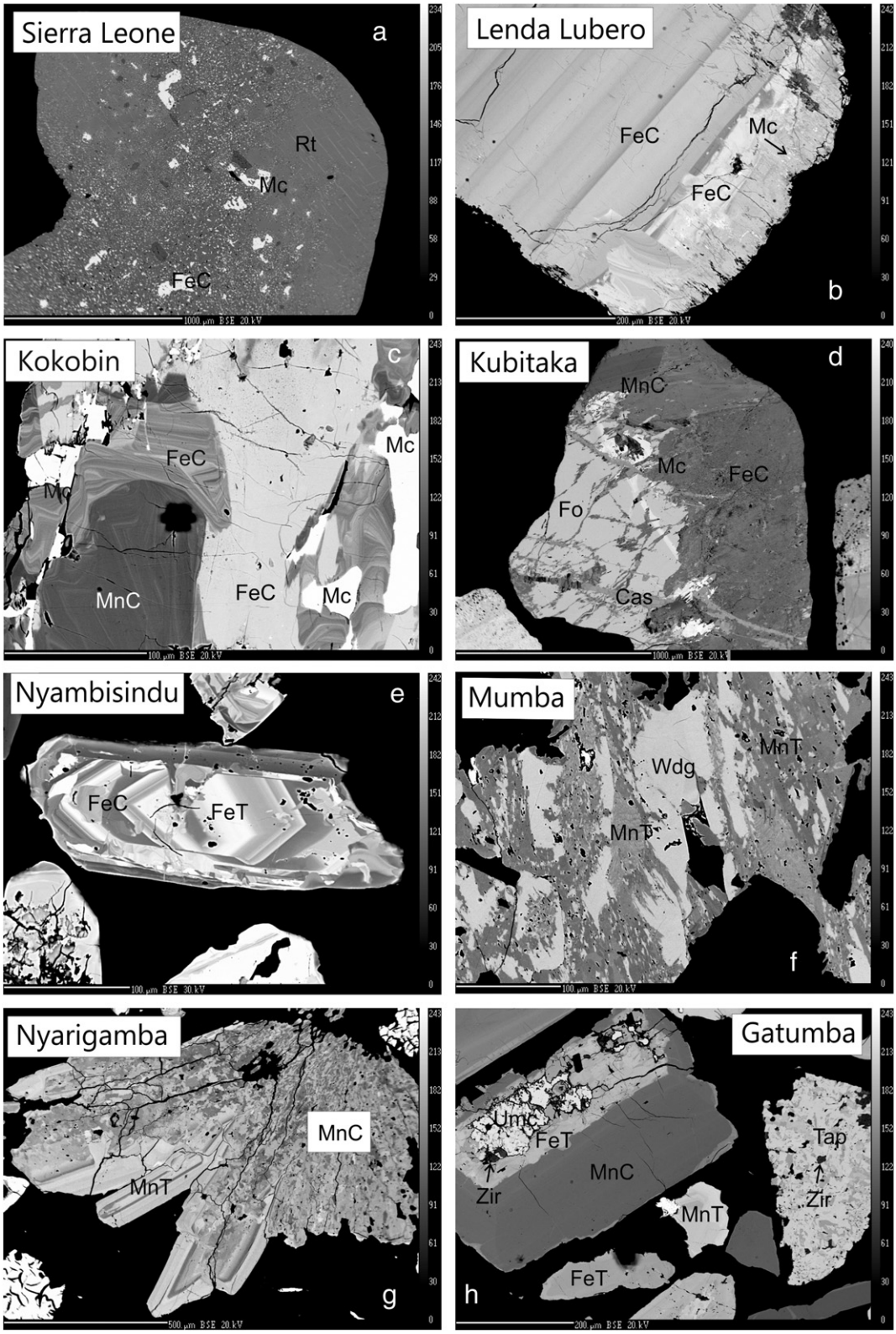

Fig. 6. Back-scatter electron images of Ta–Nb oxide assemblages from various African Ta provinces. (a) Maburagwa, Sierra Leone, sample 538 (image number 9510/1a); (b) Lenda Lubero, DRC, sample 114 (7829/6c); (c) Kokobin, Ghana, sample 007 (3704/4h); (d) Kubitaka, DRC, sample 721 (8824/3a); (e) Nyabisindu, Rwanda, sample 093 (7758/3b); (f) Mumba, DRC, sample 113 (7828/3c); (g) Nyarigamba, Rwanda, sample 088 (7753/7b); (h) Gatumba, Rwanda, sample 049 (7735/2c); (i) Homestead, Namibia, sample 285 (8119/2b); (j) Abu Dabbab, Egypt, sample 779 (9286/6a); (k) Kenticha, Ethiopia, sample 254 (8084/11a); (l) Marropino, Mozambique, sample 132 (7878b/1f); (m) Sesam, Namibia, sample 097 (7812/2a); (n) Marropino, Mozambique, sample 131 (7877/16a); (o) Lema, Nigeria, sample 403 (8457/14a); (p) Jos, Nigeria, sample 059 (7741/3b). Abbreviations: FeC, columbite-(Fe); FeT, tantalite-(Fe); MnC, columbite-(Mn); MnT, tantalite-(Mn); Mc, microlite; UMc, U-rich microlite; PbMc, Pb-rich microlite; Rt, rutile; Fo, foordite; Cas, cassiterite; Wdg, wodginite; Tap, tapiolite; Zir, zircon; BiT, bismutotantalite; Sam, samarskite; SbT, stibiotantalite.

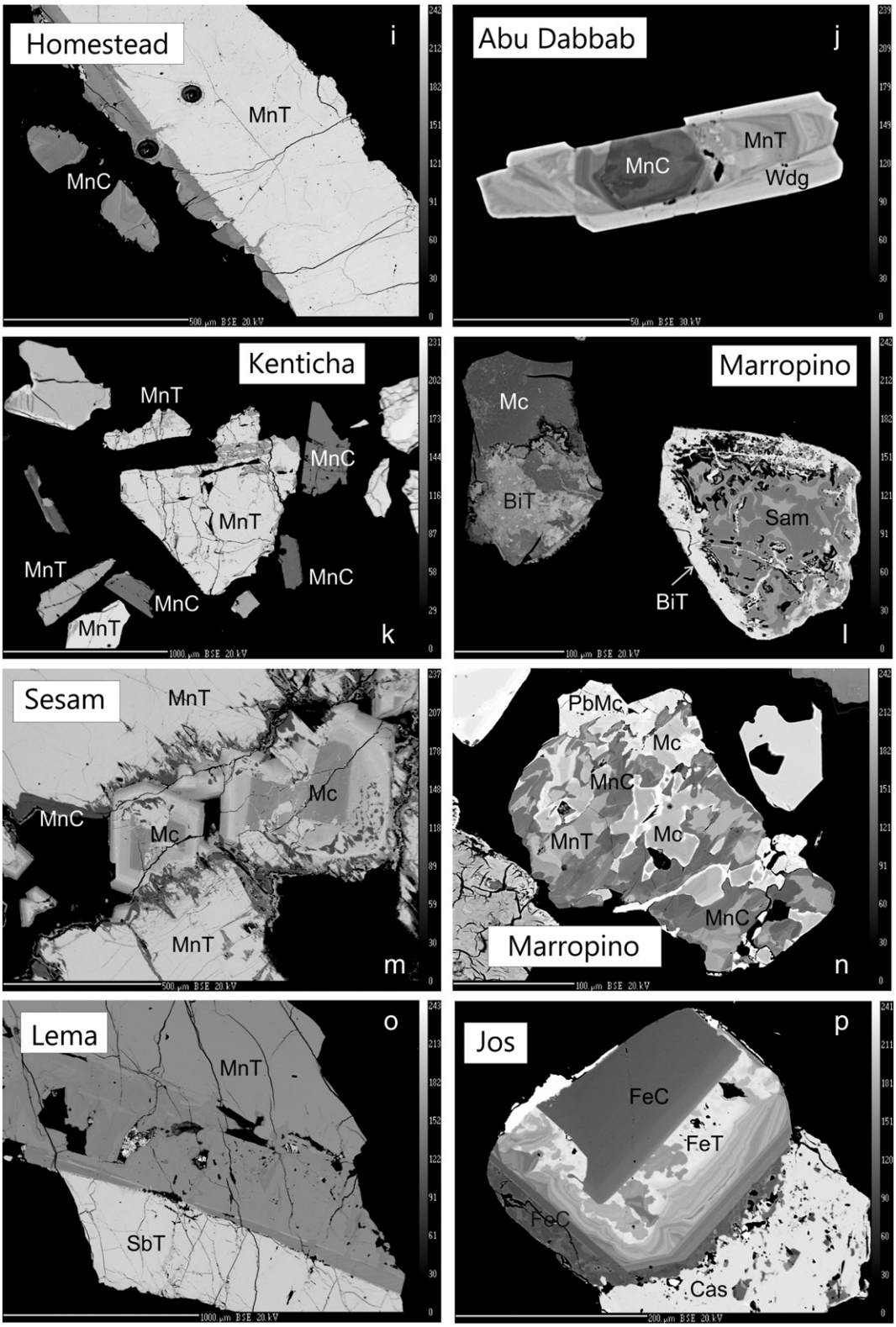

Fig. 6 (*continued*).

of monazite, xenotime, microlite, euxenite and 16% columbite-(Fe) (Fig. 7i). The "sodalithic" pegmatites are often characterised by the absence of cassiterite, which has been described only from less fractionated potassic amazonite- and tourmaline-bearing pegmatites (Cronwright, 2005; Dias and Wilson, 2000).

4.4.4. Damara Belt (Namibia)

Rare-metal pegmatites in the central zone of the Damara Belt (4.4 in Fig. 1) contain Li, Be, Sn and Nb–Ta mineralisation (Diehl, 1992; Keller, 1991; Reuning, 1923). Tin-bearing pegmatites are concentrated in four parallel belts among which the NE-trending, 100 km long and 8 km

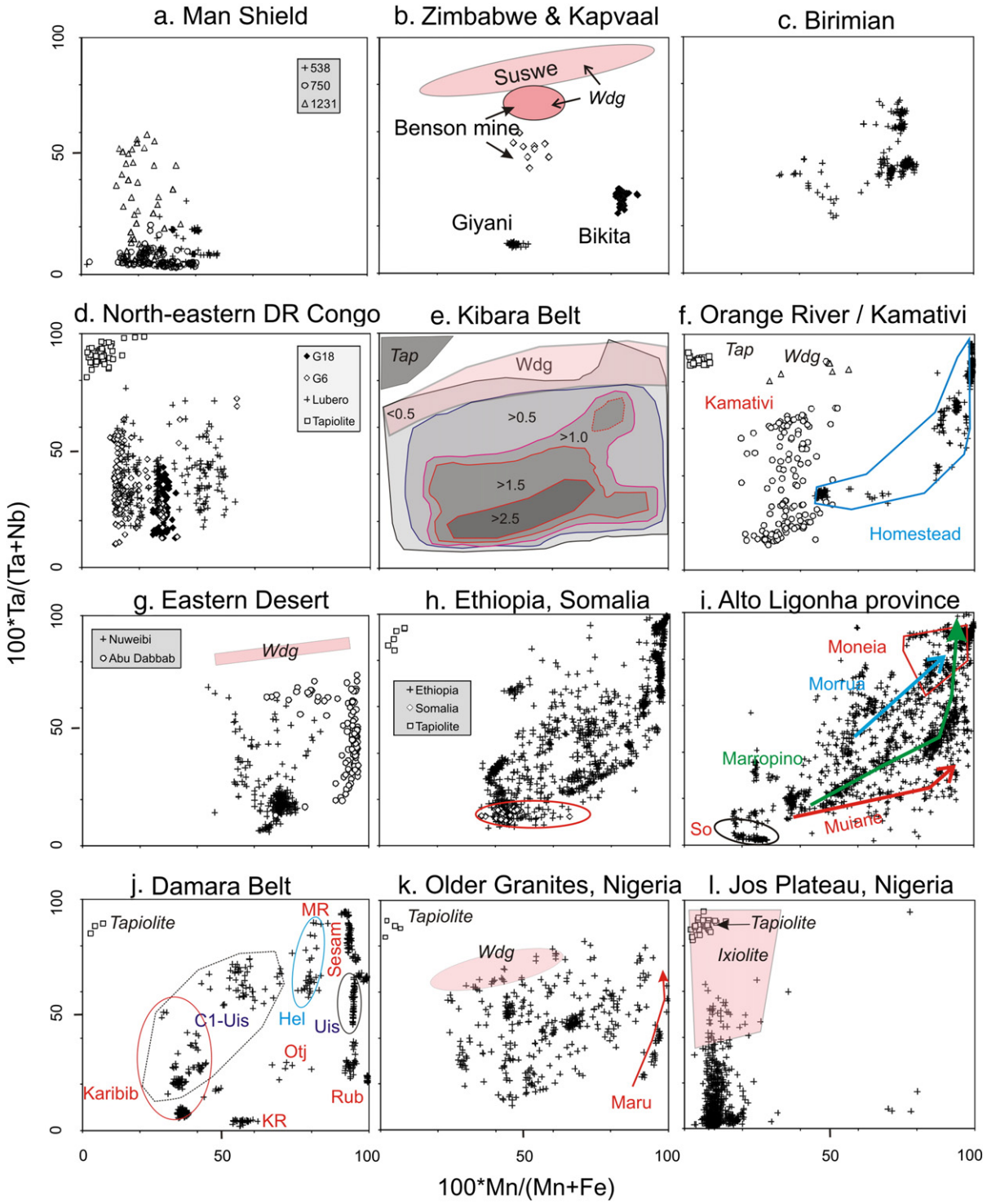

Fig. 7. Diagrams showing variations in #Mn and #Ta [i.e. 100 * Mn / (Mn + Fe) versus 100 * Ta / (Ta + Nb)] for CGM (symbols), tapiolite (open quadrangles; field in the Kibara Belt diagram) and wodginite–ixiolite (triangles in panel f, otherwise fields only) in African Ta ore provinces. Abbreviations used: ANS, Arabian–Nubian Shield; Cgm, columbite–tantalite-group minerals; Hel, Helicon; KR, Klein Rössing; MR, Mon Repos; Otj, Otjimbingwe; Rub, Rubikon; So, Somipe; Wdg, wodginite. Arrows indicate fractionation trends in subgroups of analyses. For the Kibara Belt, data were density-contoured using an R-script; numbers indicate densities of points for N = 10,275.

wide Cape Cross–Uis Belt is the most important one. Many of the pegmatites, attaining a maximum thickness of 50 m, are unzoned and carry cassiterite, columbite–tantalite, ixiolite, tapiolite and wodginite. Historically, the tin pegmatites of Uis were the most important Ta producers in Namibia and one of the world's largest hard rock tin mining operations (35,000 t cassiterite concentrate produced from 1924 to 1990; Diehl, 1992). Resources in the Uis area are estimated at 7.2 million tons (500 g/t Ta_2O_5) in the Three Aloes mine, 2 million tons (240 g/t Ta_2O_5) in the so-called B1 and C1 pegmatite prospects, and a low-grade (60 g/t Ta_2O_5) resource of 4 million tons in the slimes dam of the Uis tin mine which was closed in 1989 (Fetherston, 2004; Roskill, 2012). The complexly zoned pegmatites around Usakos and Karibib (Southern Tin Belt; Karibib Pegmatite Belt) were mined for a long time for amblygonite–montebrasite, lepidolite, petalite, pollucite, beryl, Nb–Ta minerals, bismuth, feldspar, mica, quartz and gemstones. The extensive Li pegmatite bodies at Helikon and Rubikon carry minor

Nb–Ta minerals. However, adjacent satellite veins at Rubikon are extraordinarily rich in Ta. Tantalum minerals have been described from many pegmatites in the Karibib area (e.g., Keller, 1991; von Knorring and Fadipe, 1981). Ta was also mined from the Donkerhoek (Orion) and Tsaobismund pegmatites in the Okahandja Pegmatite Belt in the southern Damara Province.

4.4.4.1. Radiometric data. One columbite-(Mn) crystal from Rubikon yielded a U–Pb (TIMS) age of ca. 505 Ma (sample 004; Table 2, Fig. 4k). U–Pb age estimates from various localities cluster around 400–500 Ma. Tkachev (2011) noted ages of 508–509 Ma for the southern segment and 492 Ma for the northern segment of the Damara Pegmatite Belt (Jung et al., 2000).

4.4.4.2. Mineralogy. The mineralogy of numerous zoned and unzoned pegmatites in the central Damara Belt has been extensively studied (e.g., Baldwin et al., 2005; Diehl, 1992; Fransolet et al., 1986; Frindt et al., 2004; Keller and von Knorring, 1989; von Knorring, 1985; von Knorring and Fadipe, 1981). TNO range from columbite-(Fe) to tantalite-(Mn) and also include tapiolite, wodginite and microlite (Fig. 7j). Specimens investigated in this study are columbite-(Fe) from Omaruru, columbite-(Mn) from Rubikon, Klein Rössing and Karibib, tantalite-(Mn) from Helikon, tantalite-(Mn) with some microlite from Donkerhoek (Fig. 6m), tantalite-(Mn) and wodginite from Uis and tantalite-(Mn) from the Strathmore pegmatites.

4.4.5. Older Granites (Nigeria)

The Precambrian basement of Nigeria is intruded by granites of Pan-African age (Older Granites) and associated Sn–Nb–Ta-bearing pegmatites (ca. 562–545 Ma; Akintola and Adekeye, 2008; Küster, 1990; Matheis, 1987; Matheis and Caen-Vachette, 1983) (4.5 in Fig. 1). Okunlola (1998, 2005) and MMSD (2012) outlined seven pegmatite fields in south-western Nigeria (Oke-Ogun, Ibadan–Osogbo, Kabba–Isanlu, Ijero–Aramoku and Lema–Share–Ndeji) and central and northern Nigeria (Nasarawa–Keffi and Kushaka–Birni Gwari) hosting at least 3000 sizeable pegmatite veins (length 10–1500 m, width up to 50 m). Such pegmatites intrude (i) pelitic to semi-pelitic schists with minor associated amphibolites and dolerites (e.g. Oke–Ogun, Lema–Share) or (ii) gneisses, granites and meta-volcanics (Ibadan–Osogbo, Ijero–Aramoku; Okunlola, 2005). Production numbers are subordinate to the Sn–Nb–Ta placer deposits on the Jos Plateau (see below). However, increasing artisanal activity is noted (Obomhense, 2008). In the Ijero area, 247 tons of cassiterite, 13 tons of columbite and 5 tons of tantalite were produced from 1944 to 1970. In the Egbe area (Kabba–Isanlu field), 117 tons of cassiterite and 39 tons of columbite–tantalite were mined between 1950 and 1970 (Schaetzl, 1971).

4.4.5.1. Radiometric data. U–Pb age estimates for CGM from granite-related pegmatites in SW and NW Nigeria range from 450 to 560 Ma. Rb–Sr analyses of muscovite from pegmatites indicate emplacement between 535 and 555 Ma (Matheis, 1987; Tkachev, 2011).

4.4.5.2. Mineralogy. Pegmatite-hosted Ta–Nb–Sn mineralisation associated with the Older Granites is diverse. Fe- and Mn-dominated CGM as well as stibiotantalite, form the majority of TNO present in the pegmatites (Okunlola, 2005). Okunlola and Oyedokun (2009) assigned Ta–Nb pegmatites around Igbeti (Oke–Ogun field) to the LCT family; the opaques are mainly CGM, rutile and magnetite. Tantalite-(Mn) is more common at Lema (Lema–Share–Ndeji field) and cassiterite-rich tantalite-(Fe) and stibiotantalite are concentrated in the Ijero and Ibadan–Osogbo fields, whereas Fe-rich CGM are associated with the Nasarawa–Keffi and Isanlu–Kabba fields (Okunlola, 2005).

Samples from five regions studied in the present project (Olode, Ibadan–Osogbo field; Lema, Lema–Share–Ndeji field; Komu and Sepeteri, Oke–Ogun field; Maru Belt), reveal a large compositional spread for CGM with all end members present (Fig. 7k), as well as tapiolite, wodginite, microlite (partly rich in U), abundant ilmenite, nigrine (ilmenite–rutile

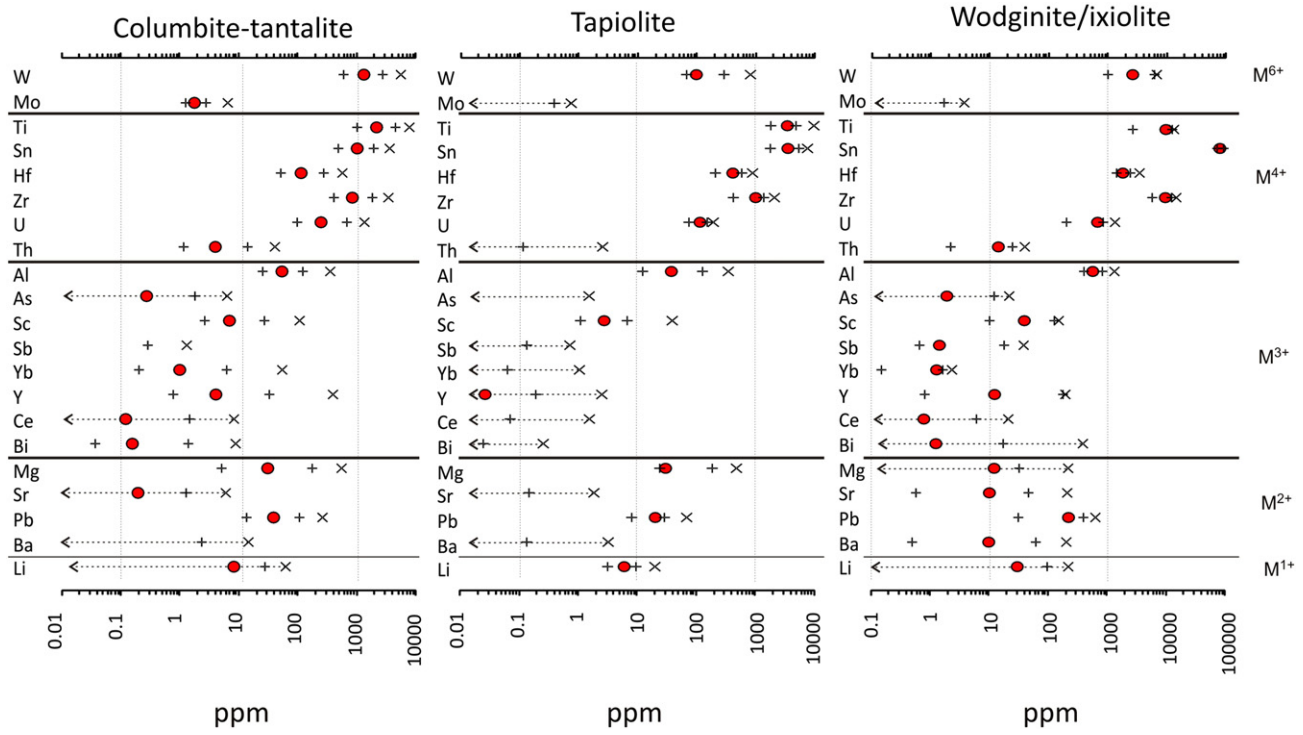

Fig. 8. Minor and trace element distributions in CGM, tapiolite and wodginite–ixiolite from African deposits. The median (red dots), 25th and 75th percentiles (crosses) and 90th percentile (x) are shown. The dataset comprises 5138 LA-ICP-MS datasets for CGM, 174 for tapiolite and 122 for wodginite–ixiolite (excluding analyses of lithiowodginite and W-ixiolite). Elements are arranged according to their assumed valence and ionic radius in an octahedral coordination. Arrows are shown to indicate that certain values (P25 and sometimes the median) are below the detection limits of LA-ICP-MS.

intergrowths) and, in a few cases, cassiterite. Stibiotantalite (Fig. 6o) was identified as a major component in samples from Lema. In a concentrate sample from this location with 65% total TNO, stibiotantalite forms 9% of the TNO; in addition, microlite (53%) and CGM (37%) dominated by columbite-(Mn) (49%), are present. An ilmenite-rich concentrate from Sepeteri contains 8% TNO; Ta–Nb–Sn minerals are dominated by cassiterite (51%) and CGM (48%), with some wodginite and Ta-bearing rutile (Table 1).

4.4.6. Madagascar

On the island of Madagascar, which forms the southern extension of the Mozambique Belt (4.5 in Fig. 1), syntectonic (750–600 Ma) and

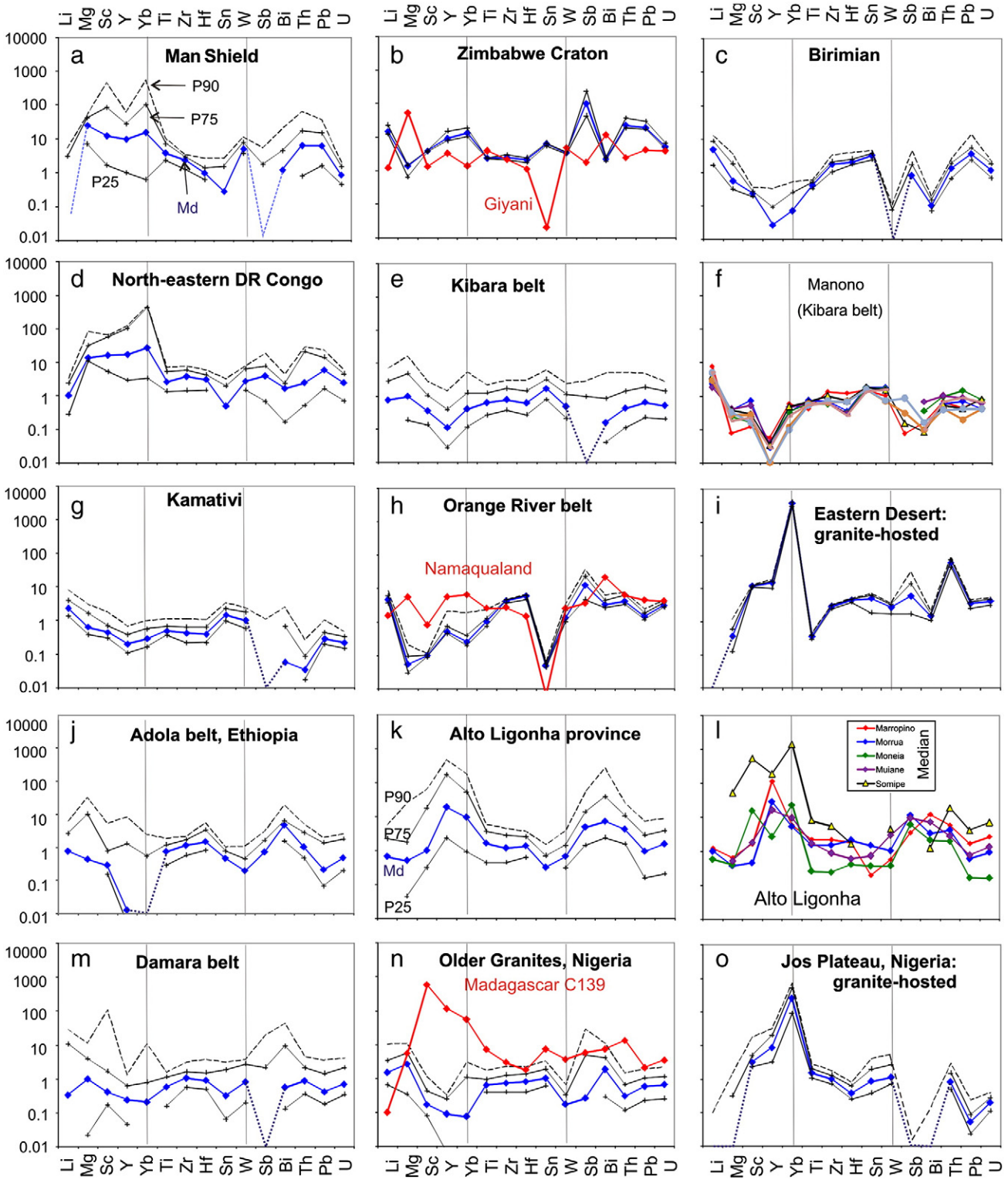

Fig. 9. Trace element diagrams normalised to an average CGM composition (see text for explanation). For each province, the median (Md, blue line with diamond symbols), P25 (lower line with cross symbols), P75 (upper line with cross symbols) and P90 (upper stippled line) are presented. Patterns in red refer to single crystals only. Examples are given illustrating the homogeneity of median values from concentrates derived from a single pegmatite deposit (Manono, Kibara Belt), and the variation of median values within a province (Alto Ligonha Province).

Table 3
Median composition of CGM in 29 Ta ore provinces (these values are taken as the basis for normalisation in Figs. 8, 10 and 11).

Province	Country	N (LA)	Li	Mg	Sc	Y	Yb	Ti	Zr	Hf	Sn	W	Sb	Bi	Th	Pb	U	#Mn	#Ta
Man Shield	Sierra Leone	111	bdl	741	211	206	25	15,737	2478	165	244	10,070	bdl	0.69	40	362	238	27.8	8.7
NE Congo Craton	DRC	83	9	403	238	359	43.30	8950	3820	508	352	5911	0.76	0.94	15	338	1036	26.7	31.5
Birimian	Ghana	127	40.3	17.3	3.4	0.66	0.14	1319	1776	340	2537	182	0.15	0.06	8	206	492	75.3	46.0
Kibara Belt	Rwanda, Burundi, DRC	4964	7.24	30	5.47	2.54	0.7	2158	819	103	1276	1015	bdl	0.09	2.5	40	237	52.8	31.8
Kamativi Belt	Zimbabwe	63	21	19	6.5	4.15	0.46	1541	426	66	1205	2680	bdl	0.03	0.21	17	93.7	36.7	27.1
Orange River Belt	Namibia	82	19	7	7	36	0.43	6425	4734	655	47	3438	2.17	2.86	136	746	4779	98.9	83.9
Eastern Desert	Egypt	69	bdl	13	173	265	5595	1305	2679	719	4998	3374	1.62	0.89	312	174	1537	69.3	20.0
Adola Belt	Ethiopia	534	7	13	4	0.26	bdl	1742	1141	244	385	543	0.14	2.66	6	12	202	75.3	48.8
Alto Ligonha Province	Mozambique	979	4.6	14	17	547	13.2	5156	1131	246	276	1403	0.59	3.37	23.1	54	692	80.9	47.3
Damara Belt	Namibia	401	bdl	24	6	5	0.29	2866	985	159	341	4385	bdl	0.35	4.91	22	286	92.6	27.5
Older granites	Nigeria	208	10	116	4	2	0.25	1974	835	153	701	355	0.08	0.92	1.82	33	285	59.5	46.2
Younger Granites	Nigeria	175	bdl	bdl	46	175	407	4556	994	62	535	1903	bdl	bdl	4.97	3	83	10.5	4.6
Pampean Province	Argentina	99	bdl	49	3	10	0.59	1274	778	169	319	321	0.09	0.57	0.55	38	339	80.6	37.8
Sao Joao del Rei	Brazil	171	12	4	3	605	74	2782	1012	177	1691	1122	0.73	0.65	44	237	429	85.6	52.6
Amapa	Brazil	42	2	716	1286	1205	211	6545	1051	94	169	4697	bdl	0.06	6	59	130	14.1	12.5
Aracuai	Brazil	45	6	293	64	25	5.79	5640	889	57	793	4150	0.19	0.12	3.23	42	462	44.1	18.5
Borborema	Brazil	154	bdl	167	19	12	0.11	6778	1644	221	60	1982	0.65	1.91	4.67	60	630	74.3	59.2
Black Hills, SD	USA	60	20	160	42	1.37	1.54	2746	752	120	2685	1403	0.23	0.06	0.78	58	176	40.8	38.7
Tanco	Canada	129	70	14	3976	0.11	0.15	13,997	2069	304	4943	1944	18.60	0.74	33	370	2202	80.2	51.3
Wodgina, WA	Australia	17	25	bdl	1	20.83	4.39	752	323	74	1288	404	0.14	0.14	6	118	171	92.7	71.2
Greenbushes, WA	Australia	69	6	442	379	2.10	1.48	4073	285	45	1245	3957	20.49	2.70	1.21	27	71	45.3	48.4
Fregenda–Almendra	Portugal, Spain	109	187	3	15	10	1.59	1421	2690	293	2357	2621	0.08	0.17	7	24	570	98.6	26.5
Hagendorf	Germany	31	17	7	22	22	2.16	8507	8988	927	1568	7096	bdl	0.05	11	131	2463	22.1	12.5
Austroalpine	Austria	38	6	378	3	4	0.39	1649	1143	125	1982	1348	0.24	0.44	6	19	452	66.0	23.6
Finnish Lapland	Finland	30	1	161	115	533	60	14,475	3326	1230	567	1670	0.51	3.75	60	305	731	42.7	61.2
Kolmozero	Russia	96	11	107	4	6	0.30	2575	962	278	858	1831	0.36	0.58	5	118	235	56.1	43.8
Orlovka	Russia	48	12	11	892	272	566	5168	773	233	883	6592	0.07	1.43	55	15	739	89.3	26.5
Phuket	Thailand	50	bdl	322	497	177	33	4663	804	71	536	10,459	bdl	0.15	4	6	136	22.7	7.5
Bastar	India	63	10	41	13	64	3.07	6445	1771	141	1852	4718	2.08	0.20	15	181	384	38.5	47.6
P25			1	13	4	4	0.39	1742	819	103	352	1348	bdl	0.12	4	24	202	38.5	23.6
Median			7	30	17	21	1.59	4073	1051	169	858	1982	0.15	0.57	6	58	384	59.5	37.8
P75			17	167	173	206	33.45	6445	2069	293	1691	4385	0.65	0.94	23	181	692	80.6	48.4

N = number of grains analysed by LA-ICP-MS. bdl = median below detection limit.

Table 4
Representative analyses of columbite-group minerals from African Ta–Nb deposits. Major element oxides in wt.% (by electron-microprobe), trace elements in ppm (by LA-ICP-MS), if not otherwise noted.

Sample	114	105	083	028	275	775	782	140	258	007	131	158	004	286	059	403	095	002
Country	CD	CD	RW	BI	NA	EG	EG	ET	ET	GH	MZ	MZ	NA	NA	NG	Nigeria	ZA	ZW
Location	Lenda Lubero	Kamisuku Pangi, Kivu	Gasasa	Ruhembe	Tantalite Valley Mine	Abu Dabbab	Nuweibi	Kenticha, qtz core	Shuni Hill	Kokobin	Marropino Mine	Morrua	Rubikon	Uis	Bauchi province	Lema, Kwara state	Namaqua-land	Bikita
Mineral	FeC	MnC	FeC	MnC	MnT	MnT	MnC	MnT	FeC	MnC	MnC	MnT	MnC	MnC	FeC	FeT	MnC	FeC
Texture	Oscillatory zoned grain	Rim of zoned grain		Oscillatory zoned grain	Zoned grain	Zoned grain	Zoned grain	Homogeneous grain	Homogeneous grain	Weakly zoned grain	Homogeneous grain with microlite rim	Homogeneous grain	Complex zoned grain	Weakly zoned grain	Weakly zoned grain, homogeneous core	Weakly zoned grain	Homogeneous grain	Homogeneous grain
#Mn	44	62	23	55	99	93	73	95	42	77	58	63	100	94	6	50	62	84
#Ta	43	50	32	27	83	50	21	82	38	46	24	59	24	46	2	57	23	34
MnO	7.83	10.18	4.40	10.07	14.14	15.98	15.35	13.78	7.88	12.88	10.75	10.39	18.22	15.95	1.37	8.21	11.97	14.67
FeO	10.28	6.20	15.13	8.27	0.16	1.29	5.68	0.73	10.81	3.93	7.94	6.07	bdl	0.97	21.16	8.36	7.31	2.76
Nb_2O_5	35.84	29.15	45.33	48.80	8.86	30.94	54.37	9.82	39.47	33.67	51.44	24.21	52.96	34.45	73.31	26.27	53.05	42.05
Ta_2O_5	44.14	47.90	35.19	30.30	73.46	50.79	23.86	74.05	40.09	47.28	26.89	57.59	27.85	48.53	2.60	56.73	25.65	35.59
TiO_2	1.02	2.32	0.45	0.12	0.56	0.66	0.38	0.23	0.54	0.26	2.34	1.22	0.01	0.08	1.01	0.33	1.38	1.24
SnO_2	0.04	1.81	0.14	0.14	0.00	0.19	0.20	0.09	0.04	0.34	0.05	0.25	0.02	0.15	0.01	0.10	bdl	0.85
WO_3	0.24	0.27	0.20	0.16	0.33	0.15	0.17	0.05	0.05	0.03	0.28	0.31	0.11	0.04	0.26	0.01	0.64	0.81
total wt.%	99.38	97.82	100.84	97.87	97.51	100[a]	100[a]	98.76	98.88	98.39	99.69	100.04	99.17	100.17	99.71	100[a]	100[a]	97.97
Li	0.7	40	1.7	5	85	bdl	bdl	2.8	0.4	56	23	17	400	92	0.6	18	16	118
Mg	62	9	7	6	0.8	37	49	6	285	13	679	15	0.5	0.3	5	166	200	17
Al	44	298	47	41	116	1166	117	59	29	88	49	83	40	36	2.1	63	60	106
Sc	18	8	2.7	2.6	1.6	500	128	2.6	2.0	4	1213	6	bdl	0.3	79	41	12	51
Sr	bdl	2.4	bdl	0.4	1.1	15.5	4.0	bdl	0.1	11.2	0.1	3.6	0.9	0.1	0.4	0.1	2.7	0.7
Y	24.6	7.6	3.3	3.4	11.4	70	101	0.3	11.5	0.5	10,461	687	30.6	bdl	798	1.2	112.6	317.0
Zr	3051	11,360	2353	652	4725	552	947	1691	1426	1829	3016	2295	1118	664	1022	168	2679	2399
Sb	0.22	0.21	0.10	0.31	0.75	1.68	1.49	0.23	bdl	0.27	1.18	16.50	1.66	bdl	bdl	1.80	0.31	6.27
Hf	686	2651	374	118	1126	251	275	673	365	341	422	373	338	130	59	76	221	367
Pb	161	752	10	12	71	49	24	5	13	671	50	76	24	7	0.7	1.5	267	1963
Bi	0.19	0.15	bdl	0.19	1.44	21.87	5.23	2.55	0.06	0.10	8.04	0.79	43.80	0.06	bdl	4.95	11.61	1.39
Th	27	49	bdl	4	26	33	61	13	27	10	61	72	9	1.9	10	0.9	35	274
U	857	2815	133	187	1374	381	476	230	539	753	1482	898	819	289	153	13	1717	3075
La	bdl	0.50	bdl	0.31	0.26	1.16	0.53	bdl	bdl	1.08	0.71	2.87	bdl	bdl	0.30	0.01	0.02	0.03
Ce	0.20	1.23	bdl	0.61	0.67	5.27	2.49	bdl	0.16	8.05	13.90	5.27	bdl	bdl	5.43	0.12	0.10	0.50
Pr	0.07	0.13	bdl	0.08	0.13	1.66	1.10	bdl	0.08	0.33	7.72	0.92	bdl	bdl	2.45	bdl	0.03	0.15
Nd	1.07	0.34	bdl	0.25	0.73	6.39	7.55	bdl	0.95	1.11	95	4.41	bdl	bdl	21	0.02	0.28	1.12
Sm	5.20	0.32	0.14	0.75	7.89	13.55	19.02	bdl	13.20	0.39	246	19.90	0.76	bdl	30	bdl	1.12	5.04
Eu	bdl	0.13	bdl	0.17	0.04	bdl	bdl	bdl	bdl	0.13	0.03	0.04	bdl	bdl	0.32	bdl	bdl	0.06
Gd	9.98	0.58	bdl	1.18	27.40	14	22	bdl	24.50	0.19	623	68.10	11.40	bdl	62	bdl	4.60	12.70
Tb	2.60	0.18	0.07	0.33	6.91	20	23	bdl	5.34	0.06	156	27.30	9.67	bdl	35	0.01	3.20	7.78
Dy	8.68	1.18	0.74	1.71	9.08	272	314	bdl	8.36	0.29	938	123.00	23.90	bdl	424	0.14	23.38	50.90
Ho	0.50	0.17	0.19	0.34	0.13	66	87	bdl	0.24	0.05	125	10.20	0.38	bdl	138	0.07	3.30	5.72
Er	0.49	0.50	0.64	0.98	0.19	395	522	bdl	0.26	0.12	288	16.80	0.29	bdl	638	0.45	8.23	15.10
Tm	0.06	0.11	0.08	0.23	0.03	182	205	bdl	0.04	0.02	47	2.26	0.03	bdl	156	0.15	1.39	3.38
Yb	0.26	0.65	0.65	1.23	0.24	2799	2787	0.08	0.54	0.23	372	17.30	0.07	bdl	1542	1.99	9.43	29.50
Lu	bdl	0.07	0.05	0.17	0.06	434	460	bdl	0.09	0.03	49	1.61	0.03	bdl	252	0.48	1.03	3.66

[a] Major elements by LA-ICP-MS.

post-tectonic pegmatites are distinguished (Petters, 1991). The younger pegmatites (ca. 500 Ma, Delbos, 1965; ca. 565 Ma, De Vito et al., 2006; monazite ages of 554 ± 34 and 492 ± 15 Ma, Berger et al., 2006) are typically interpreted as members of the NYF family or the REE-rich type of the rare-element pegmatite class (Ercit, 2005a) and contain rare U–REE–Ta–Nb oxides (De Vito et al., 2006; von Knorring and Condliffe, 1987) in addition to beryl and various gemstones. Cassiterite seems to be absent, and Ta minerals are Sc-rich. During the past 15 years, no Ta–Nb production has been reported, although large quantities of beryl and gemstones (tourmaline, sapphire, ruby) have been produced from pegmatites and associated rocks (Yager, 2013). A large, unzoned single grain of columbite-(Fe) with rare inclusions of cassiterite, euxenite and rutile from an unknown location in Madagascar yielded an age of ca. 506 Ma (sample 139; Table 2). This crystal was used as an in-house reference standard for major and trace elements (Gäbler et al., 2011).

4.5. Mesozoic

4.5.1. Jos Plateau (central Nigeria)

On the Jos Plateau (5.1 in Fig. 1), about 50 anorogenic peralkaline and alkaline granitic ring complexes are known. They form the Jurassic Younger Granites (213–141 Ma) that intruded a Precambrian gneiss–migmatite complex during incipient rifting which resulted in the opening of the Benue trough (Mücke and Neumann, 2006; Woolley, 2001; Wright et al., 1985). Biotite granites constitute the youngest of these granites, containing cassiterite and columbite-(Fe) as an accessory phase in greisen and metasomatic albitised zones, associated with wolframite and sulphides (Kinnaird, 1985). In placers, cassiterite is associated with columbite, rutile, ilmenite, zircon, monazite, xenotime, and thorite with rare magnetite and chromite. Alluvial tin placer deposits were mined from 1913 until the 1980s. Reserves are given as 140,000 tons of cassiterite and 70,000 tons of columbite (Wright et al., 1985). In "younger" placer deposits, the columbite–cassiterite ratio ranges from 1:20 to 1:3, whereas columbite is absent in "older" placers (Wright et al., 1985). In the 1970s, Nigerian columbite production ranged between 1000 and 2000 tons per year. From 2002 to 2006, 838 tons of columbite concentrates averaging 5–10% Ta_2O_5 were exported (USGS Mineral Commodity Summaries, Mobbs, 2009). However, these numbers seem to underestimate the current situation in artisanal mining (Obomhense, 2008).

4.5.1.1. Radiometric data. One concentrate (columbite, cassiterite, zircon) derived from placer material yielded a columbite U–Pb (LA-ICP-MS) age of 198 Ma, i.e. Jurassic (sample 148; Table 2, Fig. 4l). Although most grains analysed are concordant, the spread of U–Pb ages from 150 to 210 Ma indicates contributions from multiple sources.

4.5.1.2. Mineralogy. Heavy mineral concentrates obtained from the Jos Plateau are characterised by columbite-(Fe) as the dominant TNO, with some compositions plotting in the tantalite-(Fe) and columbite-(Mn) compositional fields (Figs. 6p, 7 l). Tapiolite, ixiolite, microlite, fergusonite, euxenite and cassiterite are usually present (Kinnaird, 1985; Mücke and Neumann, 2006). The common occurrence of wolframian ixiolite is noteworthy. In a total of six concentrates investigated quantitatively, TNO make up between 5 and 86%, followed in abundance by cassiterite, ilmenite and zircon (Table 1). Rutile, wolframite and thorite are common major to minor phases in the concentrates.

5. Mineral chemistry of columbite–tantalite, tapiolite, wodginite and ixiolite in African Ta provinces

The chemical composition of the examined CGM, tapiolite and wodginite–ixiolite is highly variable, as illustrated by Figs. 7 and 8. However, major as well as trace elements show regional characteristics that, in many cases, allow the distinction of ore provinces based on the composition of a representative number of TNO grains. The #Mn–#Ta diagrams (Fig. 7) illustrate the major element variation of CGM, tapiolite and ixiolite–wodginite, essentially reflecting differentiation of and fractional crystallisation from melts. The degree and type of variation of trace element concentration in CGM is complex and depends on multiple factors, including crystal-chemical parameters (e.g., ionic radius, charge), melt chemistry (e.g., presence of fluxing elements), internal differentiation of the melt, reaction with host rocks, and probably melt-source characteristics (e.g., Černý and Němec, 1995). All these factors are superimposed on each other and may result in characteristic trace element signatures specific to TNO from different ore provinces.

In order to illustrate regional variations in CGM chemistry, trace element patterns normalised to a global CGM average were constructed (Fig. 9). A "global CGM median" was calculated from the median values obtained for each element in a suite of CGM from 29 ore provinces (Table 3). In addition to the median values calculated for the 12 African provinces in the present work, median values for 17 other province are used; these are from South America (Pampean Province, Argentina; Borborema, Amapa, Sao Joao del Rei and Aracuai, all Brazil), North America (Tanco, Canada; Black Hills, South Dakota), Asia (Bastar, India; Phuket, Thailand), Australia (Greenbushes, Wodgina), Europe (Hagendorf Province, Germany; northern Finland; eastern Alps, Austria; Fregeneda–Almendra pegmatite field, Portugal and Spain) and Russia (Orlovka rare-metal granite, Transbaikalia; Kolmozero rare-element pegmatite, Kola). Elements were arranged with the light elements on the left (Li, Mg, Sc), followed by selected HFSE (Y, Yb, Ti, Zr, Hf, Sn, W), Sb, Bi, and the radioactive and radiogenic elements (Th, Pb, U). The normalising values obtained by this approach are, in ppm: Li 7.2; Mg 29.8; Sc 17; Y 20.8; Yb 1.6; Ti 4073; Zr 1051; Hf 169; Sn 858; W 1982; Sb 0.15; Bi 0.57; Th 6.1; Pb 58; and U 384. As trace element concentrations within the dataset do not show a normal distribution, robust statistical parameters were chosen to illustrate variations within each province: the median (Md), P25 (25th percentile) and P75 (75th percentile) to illustrate the variation around the median, and P90 to approximate the maximum values and eliminate outliers. The diagrams illustrate that the variation of trace element concentrations varies systematically around the median and that the P25 and P75 curves are often parallel to the median curves. Trace element concentrations in tapiolite and wodginite–ixiolite were also normalised to the median CGM value, and are compared to the median and P75 values of the co-existing CGM populations (Fig. 10).

The REE + Y concentrations were normalised to average chondrites (Anders and Grevesse, 1989), and the median, P25, P75 and P90 values are presented for CGM in Fig. 11, and for the other minerals in Fig. 12. REE patterns are classified using the nomenclature and parameters suggested by Graupner et al. (2010) that are based on the relative abundances of the chondrite-normalised concentrations of the LREE (La to Sm), MREE (Gd to Ho + Y) and HREE (Er to Lu) and the presence or absence of anomalies quantified as $Eu/Eu^* = (Eu_N / (0.5 * (Sm_N + Gd_N)))$ and $Ce/Ce^* = (Ce_N / (0.5 * (La_N + Nd_N)))$, as follows:

Type 1: $HREE_N > MREE_N$, with subtype [1a] showing high $HREE_N/MREE_N$ ratios, [1b] showing intermediate $HREE_N/MREE_N$ ratios (>1), [1c] characterised by $LREE_N$ enrichment, and [1d] by negative Y anomalies. Type 1 patterns usually have small to moderate negative Eu anomalies.

Type 2: $HREE_N \leq MREE_N$, with subtype [2a] showing $HREE_N/MREE_N$ ratios close to 1, [2b] showing intermediate $HREE_N/MREE_N$ ratios (<1), and [2c] characterised by low $HREE_N/MREE_N$ ratios ($\ll 1$). Type 2 patterns have prominent negative Eu anomalies and variable $LREE_N$ concentrations, but usually $LREE_N < MREE_N$.

Type 3: patterns lacking Eu anomalies, with subtype [3a] corresponding to highly fractionated (steeply positive) patterns with $HREE_N > MREE_N > LREE_N$, [3b] to moderately fractionated patterns with $MREE_N > LREE_N$, and [3c] to unfractionated (flat) patterns.

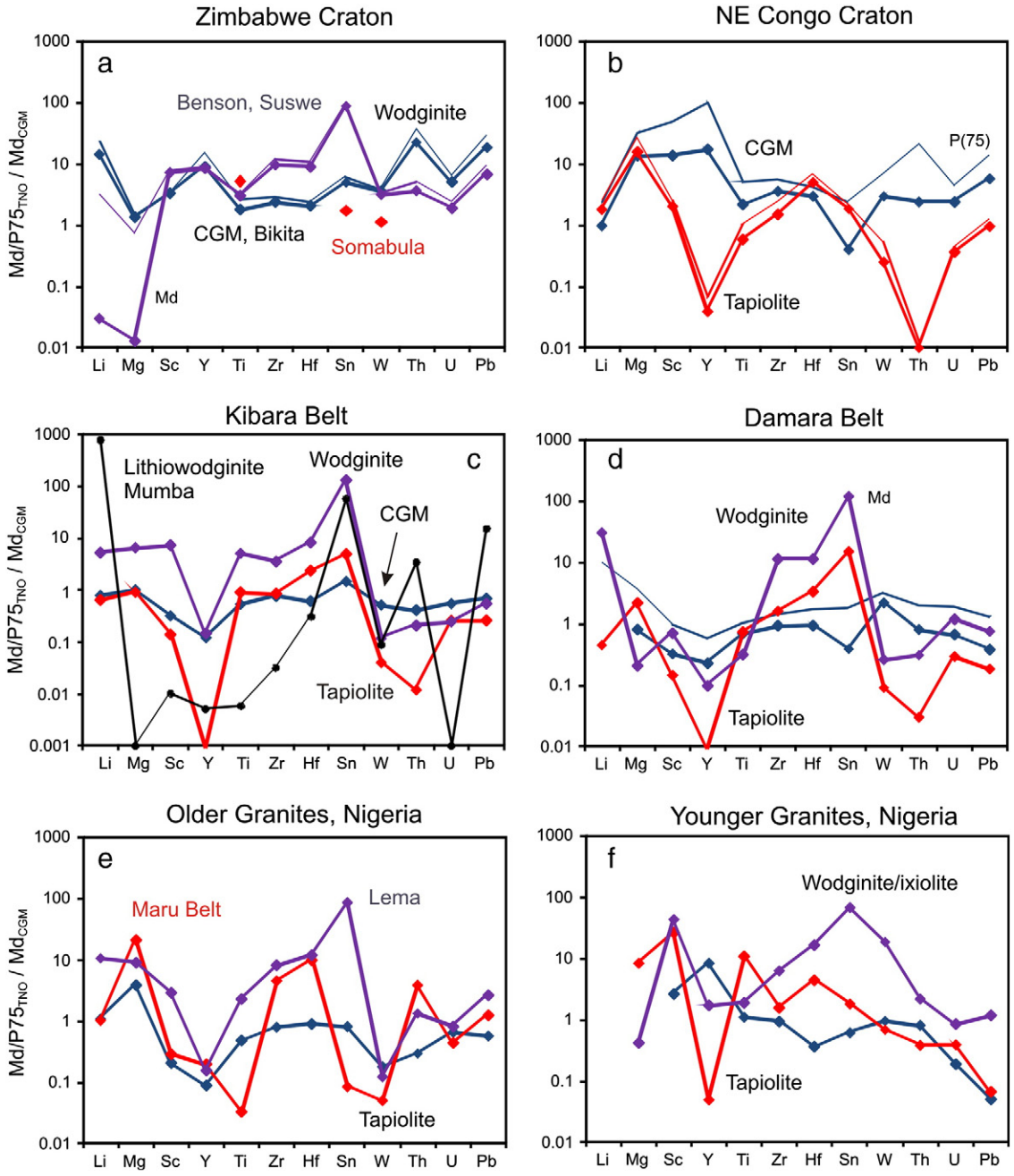

Fig. 10. Summary trace element diagrams for CGM (blue line), tapiolite (red line) and wodginite–ixiolite (violet line). Median (lines with symbols) and P75 values (lines without symbols) normalised to average CGM composition. a) Zimbabwe Craton (CGM from Bikita, wodginite from Benson mine and Sutswe; tapiolite from the Somabula gravels, microprobe data only); b) NE Congo Craton; c) Kibara Belt; d) Damara Belt; e) Older Granites (Nigeria); f) Younger Granites, Jos Plateau (Nigeria).

The $HREE_N$–$MREE_N$ ratios vary from >5 (sometimes >10; subtype [3a]) to ≤1 (subtype [3c]).

Type 4: $LREE_N = HREE_N > MREE_N$, concave (trough-like) shapes. In many cases, the MREE and Eu are below the detection limit of the method, and the presence of Eu anomalies cannot be established.

Type 5: $LREE_N > MREE_N = HREE_N$; this is the only type showing decreasing values from the $LREE_N$ to the $HREE_N$. A weak Eu anomaly (positive in subtype [5a] and negative in subtype [5b]), and a positive Ce anomaly may be present. Patterns from the Adola Belt (Ethiopia) form an individual subtype [5c] with slightly increasing values for the heaviest REE_N.

In the following section, the main characteristics of TNO compositions for each province are discussed and some outstanding median values are quoted. For illustration, the reader is referred to Figs. 9–12. Representative analyses of CGM are shown in Table 4. Summary data (Md, P25 and P75 values) for CGM are presented in Table 5, and for tapiolite, wodginite and ixiolite in Table 6.

5.1. Archean

5.1.1. Man Shield (Sierra Leone)

Homogeneous grains of columbite–tantalite-(Fe) and columbite-(Fe) inclusions in Nb–Ta rutile are characterised by variable #Mn (5–50), low #Ta values (<60; Fig. 7a) and low concentrations of Sn (Md, 244 ppm; Tables 3, 5). Concentrations of other elements are high compared to those in other provinces: Ti (Md, 1.6 wt.%), W (1.07 wt.%), Th (40 ppm), Pb (362 ppm), Mg (741 ppm), Sc (211 ppm), and REE

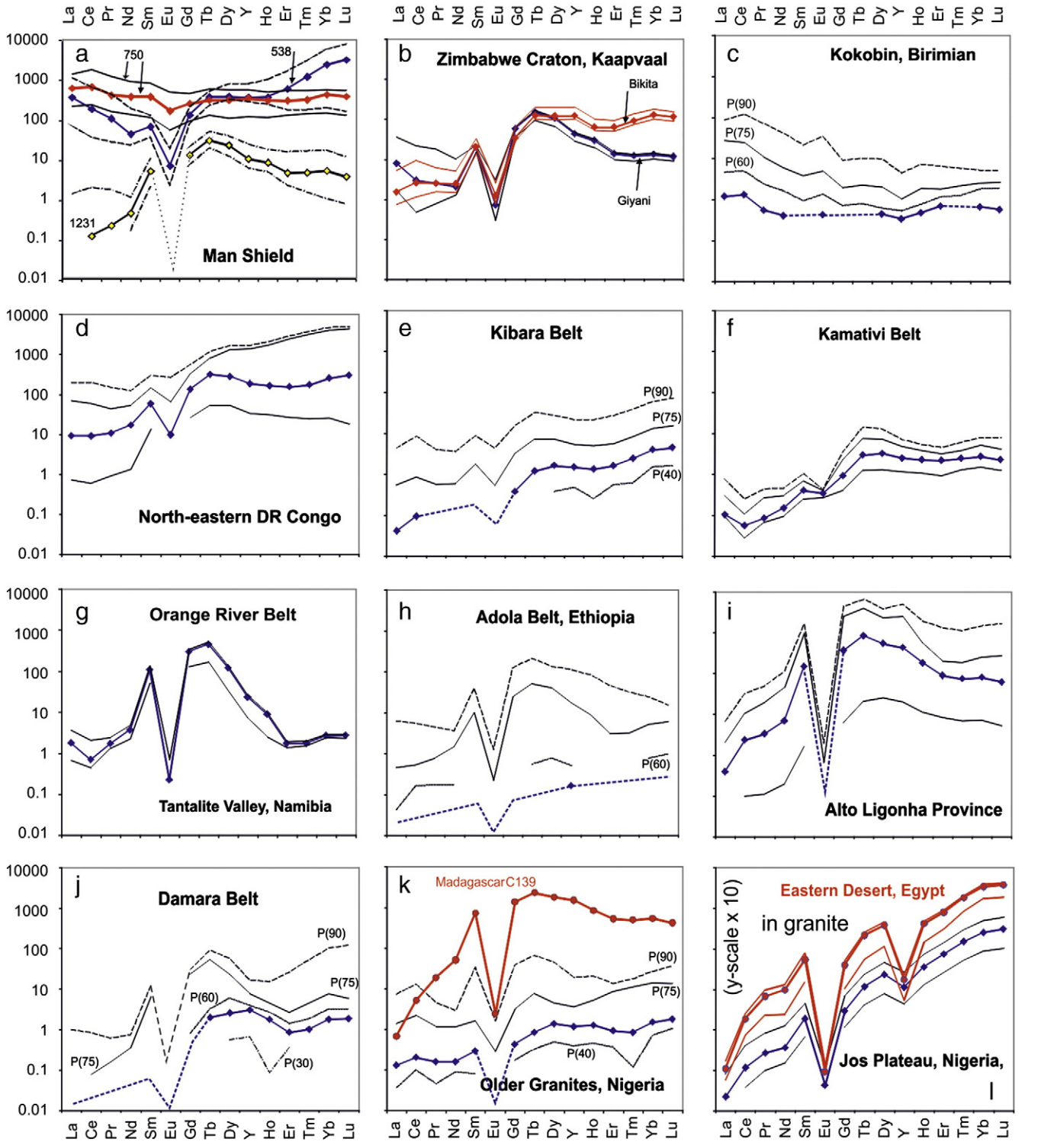

Fig. 11. Chondrite-normalised REE + Y diagrams for CGM from African Ta provinces. If not otherwise stated, the median (blue line with diamond symbols) and P25 and P75 (black lines) are given; the upper broken line is P90. Broken blue lines are estimated data. Red patterns are additional sample populations: a) Three different columbite-(rutile) concentrates from Sierra Leone, with median, P25 and P75 for each sample; b) Bikita, Zimbabwe; k) average of the internal reference material from Madagascar (Gäbler et al., 2011); l) Abu Dabbab and Nuweibi, Egypt, ANS (Arabian–Nubian Shield). Note that in Fig. (l), the y-scale must be multiplied by 10.

(Y, 205 ppm; Yb, 25 ppm) (Fig. 9a). Although only three concentrate samples were available for study, the variability of trace element concentrations is large. This also applies to the REE that are presented as median and P25/P75 of the three individual samples to account for the extreme heterogeneity (Fig. 11a). REE patterns are of subtype [1c] with $HREE_N > MREE_N$ (sample 538), subtype [2c] with $HREE_N < MREE_N$ (sample 1231) and of type 5 with $LREE_N > MREE_N > HREE_N$ (sample 750; Fig. 11a). The $LREE_N$ are variably enriched or depleted and patterns often show a prominent negative Eu anomaly (Md $Eu/Eu^* = 0.83$ to 0.02).

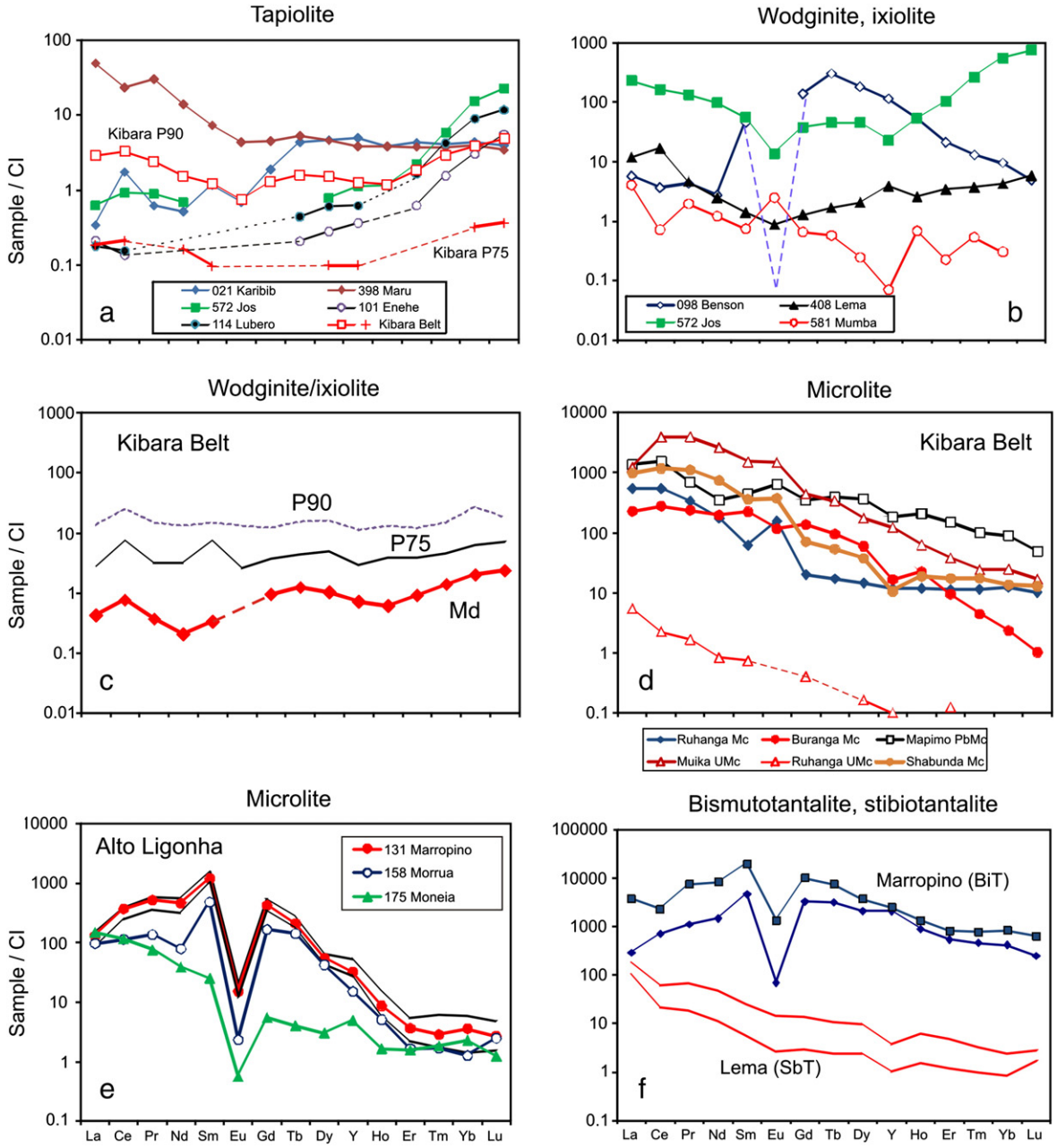

Fig. 12. Chondrite-normalised REE + Y diagrams for tapiolite, wodginite–ixiolite, microlite, bismutotantalite and stibiotantalite from Ta provinces in Africa. a) Tapiolite: median of grains from Karibib (Damara Belt, N = 1), Maru Belt (Older Granites, Nigeria, N = 4), Jos (Younger Granites, Nigeria, N = 4), Enehe (NE Congo Craton, N = 10), Lubero (NE Congo Craton, N = 7); P90 and P75 of 87 grains from the Kibara Belt; b) Wodginite–ixiolite: median of several measurements from Benson mine (Zimbabwe Craton, N = 50), Lema (Older Granites, Nigeria, N = 1), Jos (Younger Granites, Nigeria, N = 4), Mumba (lithiowodginite; Kibara Belt, DRC, N = 13); c) Wodginite–ixiolite from the Kibara Belt, median, P90 and P75 (N = 46); d) Microlite (Mc), U-rich microlite (UMc) and Pb-rich microlite (PbMc) from different pegmatite deposits in the Kibara Belt: Ruhanga (sample 084, N = 14 for Mc, N = 15 for UMc), Buranga (sample 086, N = 16), Mapimo Mulungu (sample 044, N = 1), Bionga mine, Shabunda (sample 108, N = 6), Muika, Katanga (sample 116; N = 1); e) Microlite from Marropino (N = 12), Morrua (N = 11) and Moneia (N = 13; Alto Ligonha, Mozambique); f) Bismutotantalite from Marropino (sample 132, Mozambique), stibiotantalite from Lema (sample 403, Older Granites, Nigeria).

5.1.2. Congo Craton

See Section 5.2.2.

5.1.3. Zimbabwe Craton (Zimbabwe)

Columbite-(Mn) from Bikita has low Mg (19 ppm) and high Sn, W, U (2852 ppm), Th (247 ppm), Pb (1743 ppm), Li (225 ppm), As (9 ppm), Sb (25 ppm), Sc, and REE + Y contents (Figs. 9b, 10a, 11b, Table 5). Columbite–tantalite from the Benson mine is more Fe- and Ta-rich than columbite from Bikita (Fig. 7b), and is also higher in Ti and Sn. At the Benson mine and Sutswe, abundant wodginite is characterised by variable #Mn (20–98) and high #Ta (>65) (Fig. 7b), elevated concentrations of Sc, Y, Zr, Hf, Sn, and low Ti (Fig. 10a). The wodginite grains from Benson mine reveal subtype [2a] REE patterns with variable $LREE_N$, prominent negative Eu anomalies, and moderate to low $HREE_N/MREE_N$ ratios (Fig. 12b).

5.1.4. Kaapvaal Craton (South Africa)

The trace element pattern of columbite (#Mn = 46, #Ta = 12; Fig. 7b) from the Giyani area is similar to the Bikita sample in its low Sc and high U and W concentrations. However, the Giyani sample has high Mg (1532 ppm) and very low Sn (15 ppm) concentrations (Fig. 9b). The REE patterns of columbite-(Mn) from Bikita and Giyani are weakly fractionated and of subtype [2a/2b] with negative Eu anomaly (Md $Eu/Eu^* = 0.04$) (Fig. 11b).

5.2. Paleoproterozoic

5.2.1. Birimian (Ghana)

Columbite-(Mn) and tantalite-(Mn) from Kokobin have higher-than-average concentrations of Li (40 ppm), Sn, Zr, Hf, U, and low Mg, Sc, Y, W (182 ppm) and Bi (Fig. 9c, Table 5). REE patterns of CGM from Kokobin are generally parallel with $LREE_N > HREE_N$ (Md $La_N/Yb_N = 7$; subtype [5b]) and frequently show positive Eu (Md $Eu/Eu^* = 1.33$) and also Ce anomalies (Fig. 11c).

5.2.2. North-eastern DRC

The CGM are Fe-rich to moderately Mn-rich columbite to tantalite (#Mn = 10–54; #Ta = 10–77; Fig. 7d) characterised by high concentrations of Mg (403 ppm), Sc (238 ppm), REE (Y, 359 ppm; Yb, 43 ppm), Zr (3820 ppm), Hf (508 ppm), W (5300 ppm), U (1036 ppm), as well as low Li and Sn (400 ppm) (Table 5). The general shape of the normalised pattern is similar to CGM from the Man Shield (Fig. 9d). REE patterns are variable and represent subtypes [1a] (Liha) and [1b] (Enehe); negative Eu anomalies are present, and the $HREE_N/MREE_N$ ranges from <1 to >1 (Fig. 11d). Tapiolite is common as large homogeneous grains partly replaced by CGM. Similar to the CGM, tapiolite is high in Sc, Mg, Hf, and low in Y, Ti and Th (Fig. 10b). REE patterns of tapiolite are similar to those of the coexisting CGM and characterised by high $HREE_N/MREE_N$ ratios (samples 101 and 114, Fig. 12a).

5.3. Neoproterozoic

5.3.1. Kibara Belt (east-central Africa)

Major element compositions of CGM in the Kibara Belt vary over a wide range (#Mn = 2–100; #Ta = 0–98; Fig. 7e). Compared to many other provinces, average Kibaran CGM have elevated concentrations of Ti, Sn, W and Zr. Magnesium, Li and REE contents show much variation but tend to be low, whereas Sc, Sb and Bi concentrations are generally low (Fig. 9e; Table 5). Normalised spidergrams for TNO from individual pegmatites reflect unique characteristics of the ore-forming systems. For example, 11 concentrates from the important Manono–Kitotolo pegmatite (Katanga, DRC) all display comparable trace element patterns (Fig. 9f). The CGMs from Manono are characterised by higher-than-average concentrations of Li, Sn, W, and a marked depletion of Mg, Sc, REE + Y and Bi (Figs. 9f, 13a; Table 5). CGM in the phosphate-bearing Buranga pegmatite in the Gatumba district of Rwanda, on the other hand, are enriched in Mg (>100 ppm) and Bi (Md, 3 ppm) relative to CGM from other pegmatites in the Kibara Belt, but have low Li, W, Th and U contents, most probably due to presence of abundant primary U-rich microlite. Samples from the Nyarigamba pegmatite, a few km northwest of Buranga, are also Bi-enriched, but Mg-poor. These examples demonstrate that the concentrations of some trace elements in individual pegmatites in the Kibara Belt may differ significantly. However, the overall pattern as mentioned above can be observed in most individual pegmatites.

Most of the chondrite-normalised REE patterns are flat or weakly fractionated consistent with type 3 or subtype [4a] (Fig. 11e). Because the Eu concentrations are low, the presence of Eu anomalies could not be established in many cases. However, those analyses that have higher than average REE concentrations show small negative Eu anomalies only (Md $Eu/Eu^* = 0.59$). More prominent negative Eu anomalies were observed in a few samples (e.g., from pegmatites in Maniema and Katanga). Some localities (e.g., Mbuye, Rwanda) are characterised by positive Ce anomalies.

Tapiolite is a common mineral in many pegmatites of the Kibara Belt and may constitute up to 20% of the TNO (Table 1). It is usually high in Sn, but low in Sc, Y, W and Th (Fig. 10c). REE concentrations are very low; P90 and P75 values of tapiolite from the Kibara pegmatites reveal flat chondrite-normalised patterns (Fig. 12a).

Small amounts of ixiolite–wodginite are present in many samples. They mostly form complex zoned grains intergrown with CGM, tapiolite, cassiterite, microlite and also foordite–thoreaulite. They are most abundant in the South Kivu, averaging 3% of the TNO in samples from this area (Table 1). The chemical composition of Kibaran ixiolite–wodginite is variable, ranging from 0 to 100 for #Mn and from 20 to 100 for #Ta (Fig. 7e). Some grains are extremely rich in TiO_2 (up to 22 wt.%), SnO_2 (up to 35 wt.%), ZrO_2 (up to 10 wt.%), HfO_2 (up to 1.2 wt.%), and moderately rich in WO_3 (up to 4 wt.%), Sc, Li, Mg, and Bi (Fig. 10c). Most REE patterns are of type 3 (low fractionation, no Eu anomalies), but type 5 and subtype [1b] patterns are also present (Fig. 12c). Lithiowodginite (up to 0.9 wt.% Li) from Mumba (North Kivu, DRC) displays an unusual REE pattern with $LREE_N = MREE_N > HREE_N$ (sample 581, Fig. 12b). This phase has very low Mg, Sc, Ti, Zr and U concentrations (Fig. 10c).

5.3.2. Kamativi Schist Belt (Zimbabwe)

The chemical composition of CGM from Kamativi is similar to the average Kibaran CGM (Fig. 7f), although they appear to be Li enriched, but Bi- and Th-depleted (Fig. 9g, Table 5). CGM have low REE concentrations (Md Yb = 0.4 ppm) and their patterns are of subtypes [2a] or [3a]; Eu anomalies are virtually undetectable because of the low concentrations of Sm, Eu and Gd. However, negative Ce anomalies appear to be present (Fig. 11f). Tapiolite is an accessory phase (ca. 1–2%), often occurring as euhedral homogeneous grains, but also intergrown with cassiterite and tantalite-(Fe). Tapiolite is low in trace elements except for SnO_2 (Md = 0.73 wt.%). Wodginite (#Mn = 30–60) is a very rare phase in the concentrates investigated, and is commonly intergrown with tantalite-(Mn, Fe). It is rich in Zr, Hf and W, but low in Ti.

5.3.3. Orange River Pegmatite Belt (South Africa–Namibia)

Tantalite-(Mn) from the Homestead pegmatite in the Tantalite Valley has low concentrations of Sn (50 ppm), Sc, Mg and HREE, but high concentrations of Zr (4734 ppm), Hf (655 ppm), U (4779 ppm), as well as Li, Sb, and Y (Fig. 9h, Table 5). Single crystals analysed from the Steinkopf district (South Africa) and a sample labelled "Namaqualand", also have low Sn concentrations. This observation is regarded as a distinctive feature of the pegmatite mineralisation throughout the Orange River Belt. REE patterns of tantalite-(Mn) from the albite zone in the Homestead pegmatite are enriched in Sm_N and $MREE_N$ and reveal prominent negative Eu anomalies (Md $Eu/Eu^* = 0.01$), highly fractionated $HREE_N/MREE_N$ ($\ll 1$) as well as highly variable $LREE_N$ (Fig. 11g). Chondrite-normalised patterns are of subtype [2c]. Nb-rich rims coating tantalite-(Mn) have higher REE concentrations and $HREE_N/MREE_N$ up to ~10. Columbite-(Mn) from the garnet–tourmaline zone is $LREE_N$-enriched and has $HREE_N/MREE_N < 1$ (Graupner et al., 2010).

5.4. Late Neoproterozoic to Early Paleozoic (Pan-African)

5.4.1. Rare metal granites of the Eastern Desert (Egypt)

Ta mineralisation in rare-element granites of Nuweibi and Abu Dabbab consists mainly of columbite-(Mn) and some tantalite-(Mn) (Fig. 7g) that both have low concentrations of Li and Ti, but high concentrations of Sc, REE and Th (Fig. 9i, Table 5). Yttrium is depleted relative to the other REE, but still averages to 265 ppm. REE patterns of columbite-(Mn) from Abu Dabbab and Nuweibi (Egypt) are highly fractionated and display negative Eu and Y anomalies (subtype [1d]) (ANS; Fig. 11l). Tapiolite found in concentrates from Abu Dabbab is high in Sn, but low in Ti and W. Mn- and Ta-rich wodginite (Fig. 7g) associated with, and often coating, CGM (Fig. 6j) was observed at both Abu Dabbab (common) and Nuweibi (rare). At Abu Dabbab, wodginite is rich in Ti, Zr, Hf and Sc.

5.4.2. Pegmatites of Ethiopia and Somalia

Ta deposits in the Ethiopian Adola Belt (Kenticha, Bupo, Shuni Hill) contain CGM ranging from columbite-(Mn,Fe) to tantalite-(Mn) (Fig. 7h) and characterised by low concentrations of most trace

Table 5
Summary data for CGM from African Ta provinces. Major element oxides and #Mn, #Ta by EPMA and LA-ICP-MS ("all"); trace elements by LA-ICP-MS.

Province		Man Shield			Bikita			Congo Craton			Birimian			Kibara Belt			Kamativi Belt		
		Sierra Leone			Zimbabwe			DRC			Kokobin						Zimbabwe		
Age		Archean			Archean			Paleoproterozoic			Paleoproterozoic			Neoproterozoic			Neoproterozoic		
Measurements	(all/LA)	261/111			98/59			503/83			363/127			10,275/4964			197/63		
Parameter		median	P25	P75	median	P25	P75	median	P25	P75	median	P25	P75	median	P25	P75	median	P25	P75
#Mn		27.81	21.90	34.49	84.27	84.11	84.45	26.75	15.44	29.22	75.33	71.58	76.98	52.85	33.59	71.75	36.68	32.33	40.93
#Ta		8.68	4.99	16.73	33.53	33.03	33.84	31.50	24.20	40.82	46.00	43.59	60.43	31.82	18.35	50.20	27.08	17.88	51.37
Li	ppm	bdl	bdl	22	225	169	288	9	3	22	40	14	73	7	bdl	26	21	12	36
Be	ppm	bdl	bdl	bdl	0.66	0.36	1.34	bdl	bdl	1.42	bdl	bdl	0.32	bdl	bdl	bdl	bdl	bdl	bdl
Mg	ppm	741	216	1258	19	18	21	403	333	940	17	10	55	30	6	152	19	12	48
Al	ppm	176	54	796	131	115	157	114	62	144	72	51	122	50	25	114	59	31	228
Sc	ppm	211	28	1448	56	55	57	238	76	852	3.41	2.80	4.04	5.47	2.20	17.00	6.50	4.45	10.48
TiO_2	wt.%	2.63	1.59	4.98	1.25	1.22	1.27	1.35	0.73	2.77	0.22	0.17	0.28	0.36	0.15	0.67	0.26	0.19	0.36
As	ppm	2.70	0.30	6.13	9.35	6.04	24.70	3.06	bdl	43.25	bdl	bdl	8.09	0.20	bdl	2.25	0.80	bdl	1.98
Sr	ppm	2.27	0.20	10.77	1.30	0.84	3.63	3.41	0.74	23.70	2.21	0.34	17.07	0.27	bdl	1.25	0.20	bdl	1.02
Y	ppm	205	21	588	320	315	336	359	61	2125	0.67	bdl	2.57	2.54	0.58	9.91	4.15	2.22	8.10
Zr	ppm	2650	2289	3135	2432	2362	2494	3820	1444	6000	1776	1002	2142	819	392	1746	427	225	644
Mo	ppm	16	3	34	6.77	6.56	7.05	6.16	3.04	7.26	3.54	1.43	4.29	1.57	1.02	2.29	1.30	1.20	1.50
SnO_2	wt.%	0.031	0.004	0.170	0.643	0.607	0.664	0.048	0.012	0.197	0.322	0.228	0.369	0.162	0.078	0.306	0.146	0.097	0.223
Sb	ppm	bdl	bdl	0.26	25.35	12.96	59.90	0.76	0.13	1.50	0.15	bdl	0.32	bdl	bdl	0.18	bdl	bdl	bdl
Ba	ppm	6.75	bdl	80.01	5.74	1.10	9.32	5.86	0.72	27	1.84	bdl	12.60	bdl	bdl	2.06	bdl	bdl	0.90
La	ppm	15.71	bdl	127	0.49	0.24	1.51	2.34	0.28	17	0.33	0.04	6.36	0.01	bdl	0.16	bdl	bdl	bdl
Ce	ppm	41.20	bdl	260	2.83	0.80	6.19	5.82	0.41	37	0.91	0.08	14.40	0.06	bdl	0.57	bdl	bdl	0.13
Pr	ppm	3.01	bdl	26	0.35	0.18	0.59	1.14	0.09	4.23	0.06	bdl	0.96	bdl	bdl	0.06	bdl	bdl	0.01
Nd	ppm	10.19	bdl	89	1.42	1.13	2.77	8.25	0.73	25	0.28	bdl	2.69	bdl	bdl	0.31	bdl	bdl	bdl
Sm	ppm	4.60	bdl	20	4.84	4.08	5.16	8.68	2.59	22	bdl	bdl	0.76	bdl	bdl	0.31	0.02	bdl	0.12
Eu	ppm	0.17	bdl	1.55	0.07	0.06	0.14	0.73	0.00	4	0.03	bdl	0.28	bdl	bdl	0.03	bdl	bdl	bdl
Gd	ppm	10.48	2.74	33	12.65	11.70	13.50	27.40	5.14	63	0.08	bdl	0.59	0.09	bdl	0.79	0.11	bdl	0.39
Tb	ppm	4.99	1.17	14	7.71	7.13	8.24	12.16	2.10	30	bdl	bdl	0.12	0.05	bdl	0.34	0.11	0.03	0.27
Dy	ppm	32.91	6.24	91	49.60	48.55	54.60	79.00	13.60	328	0.12	bdl	0.73	0.44	0.07	2.24	0.84	0.35	1.95
Ho	ppm	6.79	0.50	20	5.72	5.50	5.96	9.58	1.92	98	0.03	bdl	0.12	0.08	bdl	0.32	0.14	0.06	0.26
Er	ppm	19.95	1.05	83	15.00	14.65	15.70	28.40	4.64	385	0.12	bdl	0.29	0.28	0.07	1.05	0.35	0.16	0.55
Tm	ppm	3.39	0.15	23	3.38	3.22	3.49	4.40	0.67	78	bdl	bdl	0.05	0.06	bdl	0.24	0.07	0.03	0.11
Yb	ppm	24.99	0.99	165	29.85	28.50	31.10	43.30	5.27	670	0.13	bdl	0.39	0.69	0.19	2.43	0.46	0.26	0.91
Lu	ppm	3.39	0.10	19	3.74	3.62	3.92	8.51	0.70	107	0.02	bdl	0.06	0.12	0.03	0.41	0.06	0.03	0.13
Hf	ppm	165	108	235	374	353	388	508	250	714	340	281	435	103	46	238	66	38	109
WO_3	wt.%	1.270	0.920	1.932	0.838	0.781	0.882	0.672	0.370	1.559	0.023	0.019	0.028	0.128	0.056	0.302	0.252	0.146	0.446
Pb	ppm	362	96	873	1743	1634	1963	338	95	815	206	126	325	40	15	115	17	11	26
Bi	ppm	0.69	bdl	2.63	1.38	1.23	1.51	0.94	0.09	1.35	0.06	0.03	0.09	0.09	0.02	0.40	0.03	bdl	0.39
Th	ppm	40	5	108	247	229	284	15	3	128	7.98	4.01	11.65	2.52	0.70	8.74	0.21	0.11	0.52
U	ppm	328	175	597	2852	2678	3013	1036	300	1929	492	277	791	237	94	634	94	66	142

#Mn = 100 * Mn / (Mn + Fe); #Ta = 100 * Ta / (Ta + Nb).

Orange River Belt			PEastern Desert			Adola Belt			Alto Ligonha province			Damara Belt			Older Granites			Younger Granites		
Tantalite Valley			Egypt			Ethiopia			Mozambique			Namibia			Nigeria			Nigeria		
Neoproterozoic			Pan-African			Pan-African			Pan-African			Pan-African			Pan-African			Mesozoic		
614/82			317/69			1423/534			1660/979			623/401			381/208			877/175		
median	P25	P75	median	P25	P75	median	P25	P75	median	P25	P75	median	P25	P75	median	P25	P75	median	P25	P75
98.96	97.45	99.14	69.30	68.12	74.65	75.29	47.41	95.60	80.93	54.57	93.05	92.56	47.42	98.25	59.53	44.86	72.93	10.48	9.38	11.85
83.90	77.15	87.34	20.06	16.91	37.65	48.81	27.54	73.94	47.34	24.74	76.82	27.48	21.08	65.50	46.27	34.47	54.39	4.58	2.62	12.04
19	9	44	bdl	bdl	bdl	7	bdl	24	5	bdl	19	bdl	bdl	92	10	4	27	bdl	bdl	bdl
0.84	0.24	1.66	bdl	bdl	bdl	bdl	bdl	bdl	bdl	bdl	bdl	bdl	bdl	bdl	bdl	bdl	bdl	bdl	bdl	bdl
7	2	9	13	8	37	13	bdl	302	14	4	138	24	1	109	116	51	202	bdl	bdl	9
196	155	240	91	72	1048	44	33	74	54	27	101	43	30	66	50	28	100	bdl	bdl	14
7.45	1.46	8.92	173	158	185	4.17	2.20	11	17	4.70	282	5.58	2.30	17	3.53	1.62	10	46	34	73
0.55	0.41	0.75	0.19	0.16	0.21	0.39	0.15	0.64	0.86	0.23	2.03	0.29	0.08	0.59	0.34	0.23	0.59	0.79	0.56	1.08
0.51	0.29	0.92	1.03	bdl	3.28	bdl	bdl	0.72	0.70	bdl	3.30	bdl	bdl	5.00	bdl	bdl	0.28	bdl	bdl	14.96
15.41	2.71	42.26	3.99	2.72	11.99	0.42	bdl	0.87	0.03	bdl	1.22	bdl	bdl	1.23	0.61	0.17	1.01	bdl	bdl	0.12
36	11	39	265	86	335	0.26	0.11	27	547	14	4066	4.76	0.82	12	1.83	0.18	5.60	175	67	418
4734	4234	5679	2679	947	3077	1141	590	1722	1131	426	2968	985	569	1544	835	467	1622	994	725	1332
2.92	2.61	6.88	54	22	60	1.79	1.29	4.56	2.59	1.64	4.99	1.62	1.10	16.60	1.47	1.27	2.04	50	21	78
0.006	0.005	0.007	0.488	0.178	0.626	0.046	0.021	0.078	0.035	0.005	0.093	0.030	0.008	0.180	0.100	0.060	0.200	0.084	0.038	0.197
2.17	1.02	4.76	1.62	0.32	3.78	0.14	bdl	0.32	0.59	0.19	1.69	bdl	bdl	0.64	0.08	bdl	0.94	bdl	bdl	bdl
9.11	1.63	16.96	2.29	0.35	8.15	bdl	bdl	0.79	bdl	bdl	2.44	bdl	bdl	1.23	0.24	bdl	1.96	bdl	bdl	bdl
0.41	0.16	0.85	0.25	0.14	0.40	bdl	bdl	0.11	0.08	bdl	0.33	bdl	bdl	bdl	0.03	bdl	0.33	0.05	bdl	0.19
0.42	0.27	1.25	11	4	15	bdl	bdl	0.32	1.12	0.05	4.74	bdl	bdl	0.05	0.12	bdl	1.33	0.70	0.22	2.38
0.15	0.12	0.21	6	2	9	bdl	bdl	0.07	0.23	0.00	1.67	bdl	bdl	0.01	0.01	bdl	0.10	0.24	0.09	0.76
1.66	1.01	2.15	44	11	59	bdl	bdl	0.67	2.07	0.04	21	bdl	bdl	0.16	0.07	bdl	0.53	1.62	0.70	5.77
15.99	7.34	19.75	78	22	113	bdl	bdl	1.44	14	0.18	132	bdl	bdl	0.94	0.04	bdl	0.25	2.75	0.96	6.52
0.01	bdl	0.04	0.05	bdl	0.07	bdl	bdl	0.01	bdl	bdl	0.04	bdl	bdl	bdl	bdl	bdl	0.02	0.02	bdl	0.07
58.21	24.90	67.51	78	20	99	bdl	bdl	4.70	49	0.79	378	bdl	bdl	4.55	0.09	bdl	0.62	5.69	2.22	12.99
16.46	6.07	18.87	78	20	93	bdl	bdl	1.86	22	0.50	118	0.07	bdl	1.96	0.03	bdl	0.28	4.19	1.47	8.49
29.31	8.10	32.72	924	272	1097	bdl	bdl	10.02	107	3.01	538	0.62	0.09	5.66	0.34	0.03	1.10	56	19	113
0.49	0.14	0.55	233	80	267	bdl	bdl	0.50	10	0.35	36	0.10	bdl	0.25	0.07	bdl	0.30	20	7	40
0.27	0.22	0.31	1263	499	1430	bdl	bdl	0.50	14	0.87	39	0.13	0.05	0.43	0.15	0.03	1.37	117	41	222
0.04	0.04	0.05	441	204	503	bdl	bdl	0.08	1.80	0.13	6	0.02	bdl	0.11	0.02	bdl	0.27	36	12	70
0.43	0.39	0.48	5595	2799	6297	bdl	bdl	0.86	13.18	0.95	51	0.29	bdl	1.25	0.25	0.02	2.29	407	143	821
0.07	0.06	0.07	922	460	1039	bdl	bdl	0.15	1.51	0.09	5	0.05	bdl	0.14	0.04	0.01	0.33	74	26	149
655	596	967	719	483	806	244	136	566	246	123	480	159	85	288	153	85	283	62	42	105
0.342	0.256	0.576	0.639	0.384	0.824	0.048	0.038	0.113	0.177	0.073	0.401	0.181	0.046	0.679	0.044	0.014	0.090	0.276	0.181	0.679
746	91	1036	174	62	224	12	4	80	54	15	119	22	9	75	33	15	60	2.98	1.33	4.98
2.86	2.00	3.64	0.89	0.74	1.81	2.66	0.89	3.55	3.37	0.74	23.71	0.35	0.08	7.61	0.92	0.18	2.11	bdl	bdl	bdl
136	26	187	312	107	425	6.13	2.86	16.80	23.10	9.49	49.36	4.91	2.36	12.12	1.82	0.78	4.49	4.97	2.97	9.17
4779	1341	7011	1537	647	2032	202	85	765	692	156	1348	286	118	802	285	113	532	83	47	118

Table 6
Summary data for wodginite/ixiolite and tapiolite from African Ta provinces. Major element oxides and #Mn, #Ta by EPMA and LA-ICP-MS ("all"); trace elements by LA-ICP-MS ("LA").

Province		Zimbabwe			Kibara Belt			Damara Belt, Namibia			Older Granites		
Parameter		Median	Q1	Q3	Median	Q1	Q3	Median	Q1	Q3	Median	Q1	Q3
Measurements	(all/LA)	103/50			302/60			7/6			17/2		
Mineral		Wdg	Wdg	Wdg	Wdg	Wdg	Wdg	Wdg	Wdg	Wdg	Wdg	Wdg	Wdg
#Mn		47.30	45.61	49.44	65.70	45.21	80.18	56.91	55.46	62.38	39.28	25.88	45.21
#Ta		71.97	69.30	76.37	84.02	78.19	88.49	78.54	77.55	78.90	76.91	72.11	80.51
Li	ppm	bdl	bdl	29	70	0.71	160	279	267	300	97	90	103
Be	ppm	bdl	bdl	bdl	bdl	bdl	0.32	bdl	bdl	bdl	bdl	bdl	0.24
Mg	ppm	bdl	bdl	22	20	1.25	136	6	bdl	12	272	214	330
Al	ppm	611	506	1010	412	325	685	1278	1165	1424	2019	1374	2663
Sc	ppm	124	107	131	9	5	21	12	12	12	50	44	57
TiO_2	wt.%	2.02	1.75	2.15	0.65	0.13	1.66	0.21	0.19	0.25	1.69	1.45	5.07
As	ppm	13.75	7.90	21.32	0.57	bdl	1.89	0.59	bdl	2.93	0.18	0.01	0.34
Rb	ppm	bdl	bdl	bdl	0.03	bdl	0.39	4.48	bdl	13.86	0.96	0.40	1.53
Sr	ppm	38	11	147	2.11	0.05	20.40	4.81	2.46	7.40	3.98	1.95	6.02
Y	ppm	178	164	190	0.79	0.33	3.77	2.06	1.99	2.32	3.23	1.80	4.67
Zr	ppm	10,254	9590	12,588	6362	2893	9150	12,120	12,079	12,657	8605	5578	11,631
Mo	ppm	bdl	bdl	bdl	1.5	bdl	2.6	0.78	bdl	0.82	0.58	0.54	0.62
SnO_2	wt.%	10.43	9.72	11.28	13.18	10.35	15.46	13.44	12.64	13.75	9.84	9.24	12.11
Sb	ppm	21.43	14.18	37.89	0.71	0.17	0.99	0.78	0.70	1.03	7.64	4.15	11.14
Ba	ppm	23.74	6.11	117.78	5.67	0.16	66.19	4.89	4.45	9.86	8.90	4.35	13.44
La	ppm	1.19	0.27	5.80	0.04	bdl	0.45	bdl	bdl	bdl	1.39	0.69	2.08
Ce	ppm	2.11	0.72	8.50	0.07	bdl	2.03	bdl	bdl	bdl	5.05	2.52	7.58
Pr	ppm	0.34	0.09	1.16	bdl	bdl	0.22	bdl	bdl	bdl	0.21	0.10	0.31
Nd	ppm	1.24	0.71	3.10	bdl	bdl	1.11	bdl	bdl	0.03	0.54	0.26	0.83
Sm	ppm	6.67	5.87	7.96	bdl	bdl	0.37	0.12	0.10	0.13	0.10	0.04	0.15
Eu	ppm	bdl	bdl	0.05	bdl	bdl	0.08	bdl	bdl	bdl	0.02	0.01	0.04
Gd	ppm	27.35	24.07	29.30	0.16	bdl	0.42	0.44	0.40	0.54	0.15	0.10	0.20
Tb	ppm	10.95	9.64	11.93	0.03	bdl	0.14	0.21	0.19	0.22	0.04	0.02	0.05
Dy	ppm	43.72	39.53	47.93	0.13	bdl	0.81	0.67	0.64	0.81	0.27	0.15	0.38
Ho	ppm	2.98	2.68	3.24	0.02	bdl	0.08	0.03	bdl	0.04	0.08	0.05	0.11
Er	ppm	3.35	3.03	3.69	0.11	bdl	0.22	0.05	0.05	0.06	0.33	0.22	0.43
Tm	ppm	0.31	0.28	0.34	bdl	bdl	0.06	bdl	bdl	bdl	0.06	0.05	0.08
Yb	ppm	1.55	1.39	1.70	0.23	bdl	0.61	bdl	bdl	bdl	0.62	0.58	0.66
Lu	ppm	0.12	0.11	0.14	0.03	bdl	0.10	bdl	bdl	bdl	0.13	0.13	0.14
Hf	ppm	1553	1469	1883	2407	1409	3033	1952	1898	1996	2036	1508	2565
WO_3	wt.%	0.73	0.63	0.81	0.10	0.02	0.20	0.07	0.06	0.15	0.03	bdl	0.08
Tl	ppm	0.57	0.27	1.33	0.05	bdl	0.20	0.26	0.22	0.47	0.14	0.07	0.22
Pb	ppm	398	290	539	31	18	101	45	40	53	154	78	231
Bi	ppm	91.14	1.81	381.42	0.22	0.04	2.13	0.04	bdl	0.04	0.59	0.41	0.76
Th	ppm	22	17	32	3.57	1.01	12	1.89	1.65	2.16	8.19	4.18	12
U	ppm	827	773	1028	243	155	495	515	468	625	352	182	522

#Mn = 100 * Mn / (Mn + Fe); #Ta = 100 * Ta / (Ta + Nb).

elements, especially of the REE. Hafnium and Bi are the most enriched of all trace elements (Fig. 9j, Table 5). REE patterns are variable, ranging from type 4 to more REE-enriched patterns with negative Eu anomalies in columbite-(Mn) (type 2 of Graupner et al., 2010; see also Friese, 2010; Küster et al., 2009) (Fig. 11h). Tantalite-(Mn) from Bupo shows $LREE_N$–$HREE_N$ fractionated patterns at elevated REE concentrations (type 5), whereas columbite-(Fe) from Shuni Hill has the highest REE concentrations of CGM from this belt, prominent negative Eu anomalies and strong $MREE_N$–$HREE_N$ fractionation (subtype [2c]; $HREE_N/MREE_N \ll 1$). Only one grain of a Sn- and Ti-bearing ixiolite–wodginite was detected in the numerous concentrate and drill core samples from the Kenticha mine.

5.4.3. Alto Ligonha Province (northern Mozambique)

CGM compositions range from columbite-(Fe) to pure tantalite-(Mn) (Fig. 7i) and are characterised by high concentrations of REE (Y, 547 ppm), Hf, Bi (3.4 ppm), Sb, and to some extent Sc, Li and U. Sn (280 ppm) and Mg are low (Fig. 9k, Table 5). Individual pegmatites mainly differ in the concentrations of Sc and REE + Y (Fig. 9l). The REE patterns of the CGM from Alto Ligonha are characterised by extreme negative Eu anomalies (Md $Eu/Eu^* = 0.001$) and subtype [1b] ($HREE_N = MREE_N$) and type 2 ($HREE_N < MREE_N$) (Fig. 11i). The within-deposit variation (Fig. 13b) is small except at Moneia, but $HREE_N/MREE_N$ ratios differ significantly between different deposits, being low at Marropino (Md $Yb_N/Tb_N = 0.02$), Muiane (0.2) and Morrua (0.1), variable at Moneia and high at Somipe (10).

5.4.4. Damara Belt (Namibia)

The CGM from the Damara Belt, usually Mn-rich columbite and tantalite (Fig. 7j) have low concentrations of most trace elements, especially Sc, REE + Y and Sb. Lithium, Mg, Sc, Sb and Bi are quite variable (Table 5). Sn (240 ppm) is also well below the normalising value (Fig. 9m). The REE patterns are either of subtype [3a] with weak Eu anomalies, of subtype [2c] with $HREE_N$–$MREE_N$ fractionation and moderate negative Eu anomalies (Md $Eu/Eu^* = 0.1$), or of subtype [1b] (Fig. 11j). Tapiolite was observed in samples from the Karibib Pegmatite Belt, showing high Zr, Hf and Sn concentrations and REE patterns of subtype [1c] (Fig. 12a). Wodginite grains are of intermediate composition (#Mn = 53–75) (Fig. 7j), and are low in Ti, W, Mg, Sc and high in Li (Md = 280 ppm), Zr and Hf (Fig. 10d). REE concentrations are low and chondrite-normalised patterns are of subtype [2c].

5.4.5. Older Granites (Nigeria)

CGM are characterised by large variations in major element concentrations (#Mn = 23–100; #Ta = 9–79; Fig. 7k) and generally low trace element concentrations, especially with regard to Sc, REE + Y, W and Sb (Table 5). The Sb and Bi contents exhibit large variations (Fig. 9n).

Jos, Nigeria			Congo Craton			Kibara Belt			Jos, Nigeria		
Median	Q1	Q3	Md	Q1	Q3	Md	Q1	Q3	Md	Q1	Q3
36/4			51/17			505/145			27/4		
Wdg	Wdg	Wdg	Tapiolite	Tapiolite	Tapiolite	Tapiolite	Tapiolite	Tapiolite	Tapiolite	Tapiolite	Tapiolite
13.02	4.66	24.67	3.68	2.51	7.92	4.08	2.86	6.99	1.86	1.38	2.51
69.55	41.40	79.98	87.20	85.06	87.78	88.83	87.17	91.42	81.96	77.20	87.08
bdl	bdl	bdl	17	8	23	6	3	9	bdl	bdl	bdl
bdl	bdl	bdl	bdl	bdl	0.22	bdl	bdl	4.19	bdl	bdl	bdl
13	4	29	470	418	809	27	18	83	251	47	603
1697	604	2748	10	9	13	39	14	124	256	150	395
750	384	1384	35	9	42	2	1	4	451	305	716
1.84	1.14	3.17	0.42	0.27	0.93	0.63	0.27	1.04	1.95	1.45	6.87
bdl	bdl	bdl	bdl	bdl	bdl	bdl	bdl	bdl	bdl	bdl	bdl
bdl	bdl	bdl	bdl	bdl	0.10	bdl	bdl	0.03	bdl	bdl	0.36
9.15	6.89	15.11	0.18	0.06	1.04	bdl	bdl	0.09	bdl	bdl	0.07
36	17	230	0.81	0.25	1.39	0.02	bdl	0.07	1.04	0.20	2.14
6660	3167	9484	1593	797	2581	891	397	1281	1684	1495	2656
180.4	141.5	280.2	0.47	0.36	0.52	bdl	bdl	0.3	2.8	1.8	3.2
7.86	6.30	9.32	0.11	0.04	0.27	0.49	0.25	0.71	0.55	0.24	1.01
0.84	0.44	0.95	0.15	bdl	2.29	bdl	bdl	0.08	bdl	bdl	0.34
9.07	8.02	21.45	0.20	bdl	1.11	bdl	bdl	0.05	bdl	bdl	0.02
53.67	20.72	195.44	0.05	bdl	0.10	bdl	bdl	bdl	0.06	bdl	1.26
98.73	29.86	380.14	0.09	bdl	0.10	bdl	bdl	0.02	0.27	bdl	2.22
11.98	3.07	52.33	bdl	bdl	0.02	bdl	bdl	bdl	0.03	bdl	0.20
44.34	10.10	202.91	bdl	bdl	0.12	bdl	bdl	bdl	0.12	bdl	0.72
8.10	2.11	41.92	bdl	bdl	bdl	bdl	bdl	bdl	bdl	bdl	0.03
0.77	0.20	4.44	bdl	bdl	bdl	bdl	bdl	bdl	bdl	bdl	bdl
7.45	2.29	31.72	bdl	bdl	0.07	bdl	bdl	bdl	bdl	bdl	0.02
1.65	0.95	6.92	0.02	bdl	0.03	bdl	bdl	bdl	bdl	bdl	bdl
11.04	9.37	52.22	0.09	bdl	0.19	bdl	bdl	bdl	0.06	bdl	0.23
2.97	1.85	15.42	bdl	bdl	0.04	bdl	bdl	bdl	0.02	bdl	0.09
16.12	6.47	83.33	0.11	0.03	0.29	bdl	bdl	bdl	0.33	0.21	0.58
6.36	1.89	28.94	0.04	0.01	0.10	bdl	bdl	bdl	0.14	0.10	0.20
89.83	23.50	375.71	0.50	0.27	1.46	bdl	bdl	bdl	1.89	1.01	3.05
18.16	4.57	73.89	0.15	0.05	0.29	bdl	bdl	bdl	0.44	0.26	0.69
2830	885	5487	853	366	1165	396	193	513	761	447	1294
4.22	1.28	7.26	0.09	0.04	0.15	bdl	bdl	0.05	0.33	0.13	0.40
2.63	0.51	4.60	na	na	na	0.03	bdl	1.47	bdl	bdl	0.09
68	52	101	56	41	72	15	8	24	3.85	3.38	6.10
0.84	0.70	0.99	bdl	bdl	bdl	bdl	bdl	bdl	bdl	bdl	bdl
14	12	73	bdl	bdl	bdl	bdl	bdl	0.10	2.38	bdl	5.18
366	133	696	156	139	186	111	69	133	169	121	198

REE are weakly fractionated and mostly form patterns of subtypes [1d] and [5a], with common positive Ce anomalies and moderate negative Eu anomalies (Md Eu/Eu* = 0.45) (Fig. 11k). Tapiolite is present in concentrates from the Maru Belt, and is high in Mn, Zr, Hf, but low in Nb, Ti, Sn and W; the REE patterns are of type 5 ($LREE_N > MREE_N = HREE_N$; Fig. 10a). Some grains analysed from Lema and Sepeteri are ferrowodginite and wodginite with #Mn = 19–60 and #Ta = 64–85 (Fig. 7k). Ferrowodginite has high concentrations of Ti, Zr, Hf, Li, Mg, and low W (Fig. 10e). REE patterns are of type 4 (Fig. 12b).

5.4.6. Madagascar

One large homogeneous columbite-(Fe) crystal (#Mn = 44, #Ta = 12) from an unknown locality shows extreme concentrations of Sc (8300 ppm) and MREE, and low levels of Li and LREE (Fig. 9n; Gäbler et al., 2011). The REE pattern is of subtype [2a] with low concentrations of both, $LREE_N$ and $HREE_N$, extremely high concentrations of $MREE_N$ and a large negative Eu anomaly (Fig. 11k).

5.5. Mesozoic

5.5.1. Jos Plateau (Nigeria)

Columbite-(Fe) (Fig. 7l) from the Jos Plateau reveals high REE (Y, 175 ppm; Yb, 407 ppm), Ti, W and Zr (1000 ppm), and low Li, Mg, Hf, Sb, Bi, Pb and U contents (Fig. 9o, Table 5). The concentrations of Mo (50 ppm; not shown in normalised diagrams) are the highest documented in this study. REE patterns are of subtype [1d], showing prominent negative Eu (Md Eu/Eu* = 0.03), and small negative Y anomalies (Fig. 11l). Tapiolite is high in Ti, Zr, Hf, Nb and HREE (Fig. 12a), and low in Mn, Li, Y, U and Pb (Fig. 10f). Sn-, Ti- and W-bearing ixiolite is a minor constituent (<1%) of the placer deposits derived from Mesozoic granitic ring complexes. The grains are mostly Fe-rich (#Mn < 20), but #Mn locally increases up to 85 (Fig. 7l). The concentrations of TiO_2 (up to 5 wt.%), Zr, Hf, Sc and Y are intermediate to high, whereas those of WO_3 range from <1 to 50 wt.%. Concentrations of Li, Mg, U, As and Sb are low (Fig. 10f). The REE distributions follow a modified subtype [1d] patterns characterised by $LREE_N$ and $HREE_N$-enrichment and weak negative Eu and Y anomalies (Fig. 12b).

6. Mineral chemistry of other Ta–Nb oxides

6.1. Pyrochlore-supergroup minerals

Minerals of the pyrochlore supergroup are second in abundance to CGM in most rare-element pegmatites and rare-metal granites. In the dataset obtained in the present work (>1300 EPMA and 100 LA-ICP-MS analyses), members of the microlite group predominate over pyrochlore-group minerals (91 vs. 9%, respectively); the relative contributions of Ti, Sb and W in the B site are small. Fluorine concentrations

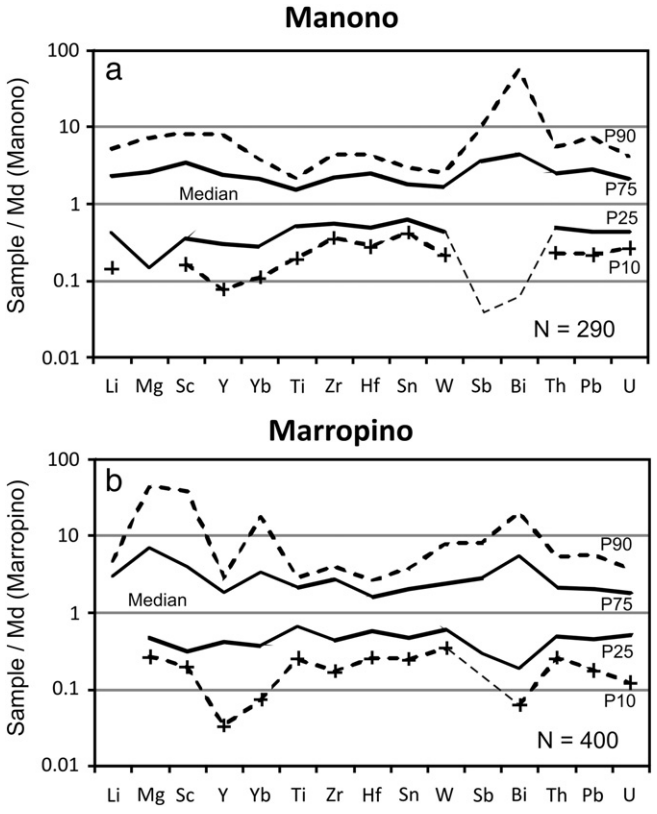

Fig. 13. Normalised trace element diagrams showing P10, P25, P75 and P90 for the Manono (DRC) and Marropino (Mozambique) deposits. Analyses are normalised to the median value calculated from of all point analyses from each location.

were measured in only 20% of grains; therefore, the precise assignment of these compositions to individual pyrochlore-supergroup species is not possible. Ca is the dominant A-site cation (65% of the analyses) followed by Na, U, Pb, Sb and Bi. None of the analyses can be classified as Sn-, K-, Y- or Ce-rich.

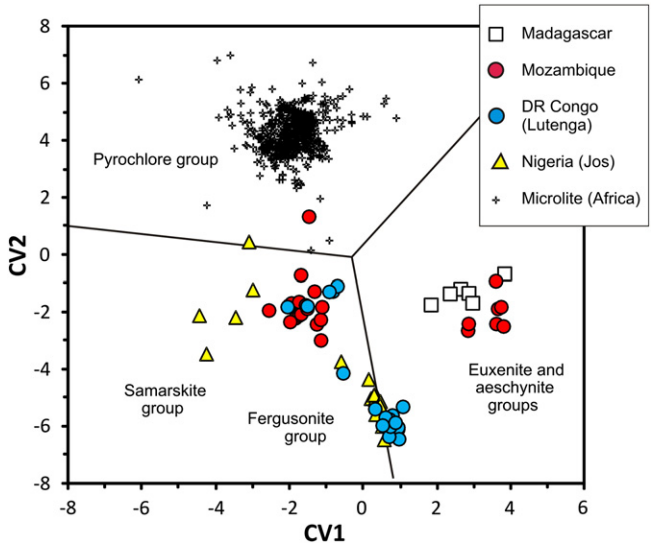

Fig. 14. Empirical discrimination diagram for (Y,REE,U,Th)–(Nb,Ta,Ti) oxide minerals from rare-element pegmatites and granites (after Ercit, 2005b). MD = Madagascar; NG = Jos, Nigeria; MZ = Mozambique; DRC = DR Congo; Data for 774 analyses of microlite from African Ta deposits are shown for comparison. CV1 = 0.245 Na + 0.106 Ca − 0.077 Fe* + 0.425 Pb + 0.220 Y + 0.280 LREE + 0.137 HREE + 0.100 U* +0.304 Ti + 0.097 Nb + 0.109 Ta* − 12.81 (oxide wt.%); CV2 = 0.102 Na − 0.113 Ca − 0.371 Fe* − 0.167 Pb − 0.395 Y − 0.280 LREE − 0.265 HREE − 0.182 U* −0.085 Ti − 0.166 Nb − 0.146 Ta* + 17.29 (oxide wt.%); Fe* = Fe + Mn; U* = U + Th; Ta* = Ta + W.

In most deposits, microlite-group minerals are secondary phases, commonly replacing CGM, tapiolite and wodginite–ixiolite. In some occurrences, however, microlite is a primary phase that predates, postdates, or crystallises contemporaneously with CGM (e.g., Marropino, Mozambique).

Cation proportions were calculated using normalisation to 2 B-site cations, and ratios of A- and B-site cations are used to discriminate different members of the group. In addition, the statistical approach of Ercit (2005b) shows that most of the data plot in the pyrochlore-group field and thus are compositionally distinct from the samarskite- and euxenite–aeschynite-groups (Fig. 14). Many analyses deviate from the ideal 1:1 ratio of A to B cations in the pyrochlore supergroup. In Pb- and U-rich phases, this ratio is often lower than 0.5, caused by vacant sites in the structure.

The chemical composition of microlite-group minerals is quite variable. Although Ca and Na are the dominant A cations (Md = 11.7 wt.% CaO and 3.7 wt.% Na_2O), significant Pb (up to 19 wt.% PbO_2 in microlite) and U (up to 30 wt.% UO_2) may be present. Fluorine concentrations reach up to 3.5 wt.% and correlate well with Na. Median and maximum concentrations (P90) of selected minor elements are: TiO_2 (0.55 wt.%, 1.74 wt.%), MnO (0.21 wt.%, 0.58 wt.%), FeO (0.02 wt.%, 0.36 wt.%), SnO_2 (0.27 wt.%, 1.48 wt.%). Scandium, As, Y, Zr, Sb, Ba, Ce, Hf, W and Th are rarely present at levels detectable by electron-microprobe. In a smaller LA-ICP-MS dataset, traces of Li (<400 ppm), Be (<40 ppm), Mg (<240 ppm), Sc (<50 ppm), As (<600 ppm), Rb (<100 ppm), Sr (<1.2 wt.%), Y (<400 ppm), Zr (<1300 ppm), Hf (<650 ppm), and Bi (<6300 ppm) were detected in microlite.

Concentration levels of minor elements in microlite-group minerals may serve to distinguish among the studied ore provinces. Antimony is a fingerprint for the deposits in Mozambique (Md ca. 500 ppm), whereas Ti is typically high in microlite from Paleoproterozoic deposits bordering the Congo Craton (Md = 1.3 wt.% TiO_2), and Th is enriched in accessory microlite of Jos (Nigeria) (>1 wt.% Th). A microlite-group mineral with an average BaO content of 9.5 wt.%; ("bariomicrolite", now discredited: Atencio et al., 2010) is present in samples from Marropino (Mozambique) and at various locations in the Kibara Province. Despite its frequent occurrence as an alteration product, the Ba-rich microlite is observed in primary associations with cesplumtantite and tantalite-(Mn) at Mumba (North Kivu Province, DRC). Stibiomicrolite, always intergrown with stibiotantalite, is present at Lema (Nigeria) and in the Buranga pegmatite (Rwanda). Bi-rich microlite was detected only at Nyarigamba (Rwanda), where it forms rims on U-rich microlite and tantalite-(Mn). Pb-rich pyrochlore-group minerals are secondary phases that replace CGM and other TNO, as well as primary microlite.

In contrast to the TNO discussed previously, microlite-group minerals are generally enriched in $LREE_N$ relative to the $MREE_N$ and $HREE_N$, yielding type 5 patterns according to the classification of Graupner et al. (2010) (Fig. 12d, e). Microlite from the Kibaran deposits usually has La_N/Yb_N ratios ranging from 10 to 100 and small positive Eu anomalies (Fig. 12d). Microlite from the Alto Ligonha Province, Mozambique, on the other hand, shows REE patterns with strong negative Eu anomalies (Fig. 12e). The REE patterns are somewhat similar to those from coexisting CGM (type 2); however, the microlite is clearly enriched in all $LREE_N$ (see also Graupner et al., 2010).

6.2. Bismutotantalite [Bi(Nb,Ta)O_4] and stibiotantalite [Sb(Nb,Ta)O_4]

Both minerals are rare in the studied pegmatite provinces, but were identified in a few complex TNO assemblages. Bismutotantalite is present in the Marropino pegmatite, Mozambique. Stibiotantalite is abundant at Lema, Nigeria. At Marropino, bismutotantalite is altered and intimately intergrown with microlite, euxenite, CGM and xenotime (Fig. 6l). The composition is non-stoichiometric, with Si, Ca, Al, Mn, Fe and Pb present at the wt.% level; UO_2 may reach 10 wt.%, and ThO_2

2 wt.%, respectively. In addition, Y, Zr and Sn concentrations are up to 1 wt.%. The #Ta value ranges from 12 to 58, and 100 * Bi/(Bi + Sb) is higher than 99, i.e. virtually no Sb is present. REE concentrations are high ($LREE_N$ between 1000 and 10,000 times CI) and give patterns of subtype [2b], similar to those in CGM and microlite from the same deposit (Fig. 12f). At Lema, Nigeria, stibiotantalite (Fig. 6o) shows higher #Bi values (0–20) and less variable #Ta values (60–95) compared to its counterpart from the Greenbushes pegmatite, Western Australia. Zoned grains contain minor Fe, Mn, Sn, Ca, Al and significant Pb (>7000 ppm). The REE concentrations are weakly to moderately LREE-enriched, and normalised patterns are of type 4 (Fig. 12f).

6.3. U–Y–REE-rich Ta–Nb-oxides

(Y,REE,U,Th)–(Nb,Ta,Ti) oxide minerals are nearly ubiquitous constituents of REE-enriched granitic pegmatites, especially of the NYF type, and of rare-metal granites (Ercit, 2005a). In the present compilation that mainly focuses on LCT pegmatites, these minerals were encountered less frequently (Table 1), and were only in a few cases characterised by EPMA. Microprobe analyses were classified using the method of Ercit (2005b) (Fig. 14).

Fergusonite [(Y,REE)$(Nb,Ta)_2O_4$] is locally abundant in concentrates from the rare-metal granites of Jos, Nigeria. In the Kibara Belt, fergusonite, occurring as a primary phase associated with columbite-(Fe) and tapiolite, was detected only in a few concentrates from South Kivu, DRC (e.g., Lutenga). Fergusonite from the Jos Plateau has high concentrations of Th (1–10 wt.% ThO_2) and U (0.3–4.5 wt.% UO_2). No Th was detected by microprobe in the material from Lutenga and UO_2 is <2.5 wt.%, but these samples contain significant WO_3 (<6.6 wt.%).

In addition to fergusonite, the samples from Jos, Lutenga and the Marropino pegmatite in Mozambique contain complex Ca–Fe–Sn–W-bearing Ta–Nb–Y–Th–U-phases, such as *samarskite* [(Y,Ce,U,Fe,Nb)(Nb,Ta,Ti)O_4] or *ishikawaite* [(U,Fe,Y)$(Nb,Ta)O_4$] (Hanson et al., 1999). These phases are easily identifiable by the characteristic Fe contents (typically 8–15 wt.% FeO) compared to fergusonite, euxenite and aeschynite-group minerals. Samarskite is frequently found in anorogenic pegmatite suites, but is also present in NYF family orogenic pegmatites.

Euxenite [(Y,Ca,Ce,U,Th)$(Nb,Ta,Ti)_2O_6$] was identified as inclusions in columbite-(Fe) from Madagascar and in some pegmatites of Mozambique (Marropino, Somipe). In contrast to minerals of the samarskite group, euxenite contains significant TiO_2 (ca. 20 wt.%). These minerals are commonly metamict and altered (e.g., hydrated), and therefore their unambiguous identification on the basis of chemical data is problematic. Furthermore, close structural and compositional relationships exist between the aeschynite and euxenite groups. Euxenite is typically found in metasomatic assemblages associated with alkaline granites, and with rare-metal granites of the NYF family.

6.4. Other Ta–Nb-rich phases

A Ca–Nb–Ta oxide [$Ca(Nb,Ta)_2O_6$], most likely *fersmite* isostructural with euxenite, is a rare phase in the examined samples. It has been positively identified as inclusions in Ta-rich rutile from the Archean Man Shield, Sierra Leone.

Simpsonite [$Al_4(Ta,Nb)_3O_{13}(OH)$] was observed only at Mumba (Kibara Province, DRC), in an unusual assemblage as intergrowths with cesplumtantite, lithiowodginite and microlite. Simpsonite is zoned with respect to its #Ta values (73–96) and contains minor concentrations of SnO_2 (0.5–2.5 wt.%). Černý and Ercit (1989) noted that simpsonite had been found only at nine localities, three of which had economic concentrations of Ta (e.g., Bikita and Benson pegmatites, Zimbabwe; von Knorring and Hornung, 1963), and that it is restricted to highly fractionated complex pegmatites of the low-pressure petalite subtype.

A Ta–Pb–Cs oxide, probably *cesplumtantite* [$(Cs,Na)_2Pb_3Ta_8O_{24}$], with 1.5–3.4 wt.% Cs_2O from two samples from the same area (Mumba, North Kivu, Kibara Belt), shows different #Ta (72–75 and 90–92, respectively) and minor levels of Na, Ca, Ba (<3.5 wt.%), Sn (<6 wt.%), and Sb (<2.5 wt.%). Cesplumtantite is known from Manono, DRC (Uher et al., 2008) and occurs as irregular grains in association with thoreaulite, simpsonite, lithiotantite, calciotantite and rankamaite.

Grains of *foordite* [ideally $Sn^{2+}Nb_2O_6$] with #Ta = 29–48, <0.3 wt.% Sb and <8 wt.% Pb were identified as homogeneous to zoned grains in a concentrate from Kubitaka, Maniema (DRC); foordite is replaced by microlite, columbite-(Mn) and cassiterite (Fig. 6d). Its Ta-dominant counterpart thoreaulite was discovered by Buttgenbach (1933), whereas foordite was recognised by Černý et al. (1988) and subsequently investigated by Uher et al. (2008). So far, these unusual Sn^{2+}-bearing phases are only known from the Kibara Belt of the DRC (Manono, Katanga; Kubitaka, Punia in Maniema), Rutsiro in Rwanda (Gitebi and Sebeya river), Minas Gerais in Brazil (Lavra Urubú), Ungursai pegmatite swarm, Kalba in Kazakhstan, and rare-element pegmatites of Siberia (Nekrasov et al., 1984). All primary occurrences are linked to complex LCT-family pegmatites of the spodumene or petalite subtypes. Due to the presence of Sn^{2+}, foordite–thoreaulite grains are considered to precipitate under low fO_2 (10^{-21} and 10^{-26} Pa at 600 and 400 °C; Nekrasov et al., 1984) and low activities of Fe, Mn, Na, Ca and F, precluding the crystallisation of common pegmatite minerals such as cassiterite, columbite–tantalite or microlite.

Rankamaite [$(Na,K,Pb)_{3-x}Al(Ta,Nb)_{10}(O,OH)_{30}$], with #Ta = 70–75, is an alteration product of cesplumtantite at Mumba (DRC). The fine-grained fibrous minerals have been identified only in simpsonite-bearing pegmatites (Černý and Ercit, 1989). Atencio et al. (2011) describe the crystal chemistry of rankamaite from the Urubu pegmatite in Brazil.

Columbite-(Mg) [$MgNb_2O_6$] was identified only in a concentrate from Muhanga (Rwanda). It contains low MnO (<0.6 wt.%) and FeO (<3.4 wt.%) and no detectable Ta. In Russia and Tajikistan, columbite-(Mg) has been identified in pegmatites hosted by dolomitic marble, in association with Nb-rich rutile, cordierite, dravite, spinel, andalusite and kyanite (Anthony et al., 1997; Mathias et al., 1963).

Several phases could not be unequivocally identified due to their small grain size, complex chemical composition or the paucity of available reference material. One of these phases, occurring as inclusions in Nb-rich rutile from the Man Shield (Sierra Leone), is particularly rich in Sc_2O_3 (10.7–16.0 wt.%), TiO_2 (9.6–18.3 wt.%), FeO (13–16 wt.%), Nb_2O_5 (34–36 wt.%), and Ta_2O_5 (23–26 wt.%), in addition to significant ZrO_2 (3–4 wt.%), MnO (<1 wt.%), SnO_2 (0.5 wt.%), HfO_2 (0.3–0.7 wt.%) and WO_3 (0.5–1.5 wt.%) contents. This phase may be recalculated to the idealised formula $(Sc,Fe)_2(Nb,Ta,Zr,Ti)_3O_{10}$, with #Ta ~ 20. Very similar textures and compositions were described from Nb-rich rutile and its breakdown products from Eptevann, Norway (Černý and Chapman, 2001).

6.5. Rutile

The rutile structure allows for incorporation of cations of different valence via coupled substitution mechanisms. In rare-metal granites and rare-element pegmatites, Ti^{4+} is substituted by Ta^{5+}, Nb^{5+}, Sn^{4+}, Fe^{3+}, Fe^{2+} and Mn^{2+} (commonly, Fe > Mn). Scandium, Zr and W may be present in appreciable concentrations, as well. The maximum concentrations of substituent elements documented in this study (based on more than 350 EPMA data) are: 47 wt.% Ta_2O_5, 44 wt.% Nb_2O_5, 20 wt.% FeO, 3 wt.% MnO, 6.6 wt.% SnO_2, 3.8 wt.% WO_3, 2.3 wt.% Sc_2O_3, 0.4 wt.% ZrO_2, 0.13 wt.% HfO_2 and 0.06 wt.% UO_2. Nb–Ta-enriched rutile is virtually always exsolved into a variety of phases including CGM, ixiolite and others (Černý and Chapman, 2001; Dill et al., 2007).

Rutile is a minor constituent in many of the investigated rare-element pegmatites and granites (Table 1). It is most abundant in placer deposits from the Man Shield, Sierra Leone [Nb-rich variety with inclusions of columbite-(Fe); Fig. 6a]. In most other concentrates, rutile

makes up less than 3% of the TNO. It was, however, found in trace quantities in almost every province. Ta-rich rutile was detected in the Kibara Belt and at Marropino (Mozambique). Nb-rich rutile is present in Sierra Leone and at Jos (Nigeria). Ta–Nb–Fe-poor rutile occurs in placer deposits of the Congo Craton and at Kenticha (Ethiopia). In Nb-rich rutile from Sierra Leone, REE are enriched up to 500 times chondritic. Normalised REE patterns are commonly flat (unfractionated) and sometimes exhibit weak negative Eu anomalies; La_N/Yb_N ranges from 0.1 to 23. Similar patterns are observed in the associated columbite.

7. Discussion

7.1. Formation of TNO in granites and pegmatites: processes and sources

Rare-metal granites represent the latest, most fractionated end-members of layered sequences in upwardly differentiated plutons (Černý et al., 2005; Linnen and Cuney, 2005). Crystal fractionation leads to rare-metal enrichment from a large variety of source materials, explaining the highly dissimilar enrichment of HFSE and large-ion-lithophile elements (LILE) observed in rare-metal granites. High concentrations of fluxing agents (F, Li, Be, P, H_2O) reduce the viscosity and solidus temperature of the magma, thus facilitating crystal-melt fractionation and concentration of rare metals in residual melts. Additional processes, such as liquid–liquid separation and fluid separation at the magmatic–hydrothermal transition may have contributed to the development of some rare-metal granites (for references, see Černý et al., 2005).

Granitic pegmatites form by late-stage crystallisation of fractionated melts produced from partial melting of crustal or mantle rocks (Černý et al., 2005; London, 2008). Pegmatites separate from their host ("parental") granites by filter pressing and compaction of vertically zoned melt conduits, thus expelling residual melt into the country rocks (London, 2005). The models and conditions of crystallisation and internal evolution of pegmatites are elaborated and summarised in Černý et al. (2005) and London (2008). Alternative models for the formation of rare-element granites by anatexis or fluid-induced overprinting of barren pegmatites have largely remained untested and speculative (Černý, 1992; Černý et al., 2005).

LILE and HFSE become progressively enriched in rare-metal granite and pegmatite melts, and eventually form separate mineral phases, such as spodumene, petalite, amblygonite (Li), pollucite (Cs), beryl (Be), cassiterite (Sn) and TNO. Based on solubility experiments, the lower solubility of columbite-(Mn) compared to tantalite-(Mn) explains crystallisation of columbite before tantalite (Bartels et al., 2010; Linnen and Cuney, 2005; Linnen and Keppler, 1997). Fluorine does not have much influence on the solubility products of $MnTa_2O_6$ and $MnNb_2O_6$ in a melt of given composition; however, changes in melt structure and alumina saturation index due to the presence of F do have an impact (Fiege et al., 2011). Although little is known about the crystallisation temperatures of TNO, it appears that they form from magmas at temperatures well below their equilibrium solidus, because the solubilities of HFSE in felsic melts decrease with decreasing temperature (e.g., Linnen and Cuney, 2005). The high to extreme concentrations of HFSE in specific zones of pegmatite bodies are explained by the process of constitutional zone refining in boundary layers along crystallisation fronts, a process that efficiently concentrates incompatible elements in small volumes of melt during cooling and crystallisation (Černý, 2005; London, 2005, 2008).

Major- and trace-element compositions of TNO are controlled by a combination of the following processes (Černý and Ercit, 1985): (a) regional source protolith (e.g., metapelitic vs. igneous rocks); (b) the conditions of anatexis (e.g., pressure, temperature, fluid composition) of the source rock; (c) the degree and way of fractionation of the pegmatite or granite melt, including the role of volatiles; (d) the role of associated minerals (e.g., Fe–Mg–Mn-minerals such as garnet, and various accessory minerals such as REE- and U-bearing phases); (e) contamination of the pegmatite melt or contamination during subsolidus interaction with the host rocks (Černý, 2005; Černý and Němec, 1995); and (f) other types of potential subsolidus overprint (e.g., metamorphism, tectonic processes).

In addition, the structural state (i.e., order–disorder in CGM, tapiolite and wodginite–ixiolite) will also influence trace element compositions, allowing for more extensive heterovalent substitutions with increasing cation disorder. CGMs tend to develop from early disordered towards late ordered phases with a decreasing rate of cooling (Černý et al., 1986, 2004; Ercit et al., 1995).

CGM form solid solutions with structurally similar minerals such as cassiterite, rutile and wolframite-group minerals that eventually lead to the formation of monoclinic wodginite-group minerals (ixiolite structure; Černý et al., 2007). Trace elements enter the CGM structure via simple or heterovalent substitutions. The incorporation of minor elements (Ti, Fe^{3+}, Sn) in the cation sites of the columbite structure has been well established (e.g. Ercit, 1994). A rutile-type substitution is responsible for Ti in the columbite structure ($A^{2+}B^{5+}{}_2Ti^{4+}{}_{-3}$). Hexavalent cations such as W may enter the structure via a wolframite-type substitution ($B^{5+}{}_4Fe^{2+}{}_{-1}W^{6+}{}_{-3}$). An alternative is the substitution of W^{6+} into the B site ($B^{5+}{}_3M^{3+}{}_{-1}W^{6+}{}_{-2}$, where M = metal, e.g., Fe^{3+}; Ercit, 1994). Ercit (1994) described the effects of Fe–Mn and Nb–Ta fractionation on the concentrations of Mg, Ca, Sc, REE, tetravalent cations and W in NYF-family pegmatites (Ercit, 1994). For Zr and Hf, heterovalent substitutions in both A and B sites such as $(Nb,Ta)^{5+}{}_2(Fe,Mn)^{2+}{}_1(Zr,Hf)^{4+}{}_{-3}$ have been discussed (Černý et al., 2007), implying the existence of a solid solution towards srilankite (ixiolite-structured ZrO_2). Scandium incorporation is favoured in highly disordered structures via the euxenite-type substitution $A^{2+}B^{5+}M^{3+}{}_{-1}Ti^{4+}{}_{-1}$ (Wise et al., 1998); the same substitution scheme may apply to REE + Y. REE can also enter the structure via the coupled substitution $A^{2+}{}_2B^{5+}(REE + Fe)^{3+}{}_{-3}$, eventually leading to samarskite ABO_4, where A = REE + Y, Ca, U and Fe; B = Ta, Nb and Ti (Warner and Ewing, 1993).

The provenance of pegmatite magmas remains poorly understood. Based on a study of fertile granites and their rare-element pegmatite aureoles, Černý (1991b) concluded that there is "no clear-cut correlation between the tectonic affiliation and rare-element signature of the granite–pegmatite systems". Peraluminous granites and associated LCT-family pegmatites are largely syn- to late-orogenic, but can also be post-orogenic, whereas metaluminous granites and associated NYF-family pegmatites tend to be present in post- to anorogenic settings; peralkaline intrusions are commonly anorogenic. However, it was also pointed out that most geologically comparable pegmatite fields and provinces are internally homogeneous (Černý, 1991b). From the investigation of compositional variations in TNO, we propose that trace element compositions, particularly HFSE distributions in Nb–Ta minerals, provide important insights on these issues. By summarising data on the tectonic setting of pegmatites, Martin and De Vito (2005) concluded that orogenic or calc-alkaline magmatism often produces LCT-family pegmatites, which are enriched in Li, Cs, Ta, Rb, Be, Sn, B, P and F and commonly are of peraluminous bulk composition. The enrichment in B and Li is attributed to authigenic minerals in the source sediments, such as clay minerals and chlorite. The elements are mobilised in subduction-zone settings and rise through the mantle wedge, along with Sn, Ta, Nb and P. Using Sm–Nd isotopes, Tomascak et al. (1998) demonstrated the existence of distinctly different and identifiable sources of different granitic pegmatites in Maine. Černý et al. (2012) postulated that most LCT-family pegmatites are products of melting of metamorphosed juvenile sediments, from which S-type granites arise. I-type granites are rare hosts to significant pegmatite fields because they are largely devoid of fluxing components such as B and P.

In contrast to orogenic suites, anorogenic plutons including A-type granites are often associated with NYF-family granitic pegmatites, as well as with silica-undersaturated rocks. Such anorogenic

magmatic suites may form in response to sudden changes from extension to compression or in transtensional settings several hundred million years after the last orogenic event in the area. NYF pegmatites are enriched in Nb over Ta, with appreciable levels of Ti, REE + Y, Zr, Th, U, Sc and F. Some interpretations of source rocks claim a second melting event of middle to lower crustal high-pressure lithologies (e.g., granulites) that have been dehydrated and depleted during a preceding anatectic episode (Černý, 1991b), with heat supplied by basaltic, mantle-derived melts. Granulites may become enriched in Ti, Zr, Nb, Ta and F after the initial melting episode and these elements may be mobilised during later anatexis. Thorium and U are problematic because they are not expected to survive the first melting event; nevertheless, they are significantly enriched in many NYF pegmatites. Other authors favour a model where NYF magmas originate by direct differentiation from mantle-derived mafic magmas (see references in Černý et al., 2005). Černý (1991b) stated that the anatectic model involving a granulite source appears most probable, followed by the model involving anatexis of juvenile lithologies, whereas direct differentiation of NYF magmas from mantle-derived melts is not likely. A good example of mineralisation associated with anorogenic A-type granitic magmatism is the Younger Granites of Nigeria.

Martin and De Vito (2005) found evidence that NYF-family pegmatites may also occur in orogenic suites. According to Novák and Filip (2010), Novák et al. (1999, 2000, 2011, 2012) and Škoda and Novák, (2007), fractionation in NYF- and LCT-family pegmatites may converge producing mineralogically similar dikes showing combined NYF and LCT signatures. In fact, similar cases were observed in some African Ta pegmatites, e.g., at Marropino (Mozambique), where CGM in LCT-family pegmatites of the complex spodumene-type (Fig. 7i) are accompanied by abundant primary microlite, Y–REE–Th–U–Ta-rich phases such as euxenite and samarskite, monazite, bismutotantalite and native bismuth, which are typical of NYF pegmatites. The Marropino pegmatite is of late-Pan-African age (ca. 460–480 Ma) and post-orogenic, but certainly not anorogenic. Other pegmatites in this region are clearly of the LCT family (Morrua), some have a strong NYF character (Somipe). According to Černý (1991b), such mixed types may form from pristine NYF magmas undergoing partial contamination by undepleted supracrustal rocks (metasediments).

LILE are expected to be enriched in melts derived from eutectic melting of pelitic rocks containing abundant muscovite, which can supply Li, Cs, B and F to the liquid phase. Melting of biotite-rich host rocks may result in elevated Sn, whereas pyroxenes and other mafic minerals may serve as a source of Sc and REE. The behaviour of Sc in TNO has been investigated by Wise et al. (1998). They observed extreme variability of Sc concentrations in CGM and ixiolite from moderately to highly fractionated rare-element granitic pegmatites. Significant Sc enrichment was only found in "Sc-rich provinces", such as at Tordal (Norway), Antsirabe (Madagascar), Muiane (Mozambique) and the Ilmen Mountains (Russia). Such elevated Sc contents have tentatively been attributed to either (i) contamination of granitic melts by mafic country rocks, or (ii) destabilisation of Sc complexes in the granitic melt. The behaviour of Sc during fractionation of discrete pegmatites and within individual pegmatite provinces was also found to be erratic and enigmatic.

7.2. Compositional variation of columbite–tantalite, tapiolite and wodginite–ixiolite

CGMs are the most abundant TNO in all Ta provinces investigated. Their composition varies over a large range for major and trace element concentrations, with Ti, W, Zr, Sn, Hf and Sc being the most abundant trace elements (Fig. 8). The extensive dataset used in the present study demonstrates variations over two to four orders of magnitude for most trace elements. The structure of the CGM is derivative from the α-PbO_2 structure with two distinct octahedral sites; the valence and ionic radii (Shannon, 1976) of the major elements in the structure are: Fe^{2+} (0.78 Å), Mn^{2+} (0.83 Å), Nb^{5+} (0.64 Å), and Ta^{5+} (0.64 Å). The following trace elements were investigated, grouped according to their preferred or assumed valence, with their ionic radii in sixfold coordination (in Å): M^{1+} (Li 0.76; Rb 1.52); M^{2+} (Be 0.45; Mg 0.72; Ca 1.0; Sr 1.18; Pb 1.19; Ba 1.35); M^{3+} (Al 0.54; As 0.58; Sc 0.745; Sb 0.76; Y 0.9; REE 0.86–1.03; Bi 1.03); M^{4+} (Ti 0.605; Sn 0.69; Hf 0.71; Zr 0.72; U 0.89; Th 0.94); M^{5+} (As 0.46, Sb 0.6, Bi 0.76) and M^{6+} (Mo 0.59; W 0.6). The concentration ranges for some of these elements are presented in Fig. 8, grouped according to their preferred valence and ordered according to their ionic radii.

The most important findings on the minor and trace elements based on 5138 analyses of single grains from all African Ta provinces examined in this study are discussed below (for multiple analyses from the same grain an average was used).

Lithium varies from <1 to 1300 ppm, showing a broadly positive correlation with #Mn and a weak negative one with #Ta. The median of 8 ppm and the fact that less than 5% of the grains have concentrations >100 ppm indicate that Li is a very minor trace element in CGM. Maximum values rarely exceed 500 ppm in Mn-rich columbite and tantalite, and such grains were only found in some spodumene pegmatites of the Kibara Belt (Katanga, Maniema, Kivu and Rwanda) and at Lema, Nigeria. The LCT-family pegmatites of Bikita (Zimbabwe Craton) have the highest median values, followed by Kokobin (Birimian), Tantalite Valley (Orange River Belt), Kamativi, the Older Granites of Nigeria, the Damara Belt and the Kibara Belt (Table 5). Lithium contents are low in pegmatites from the Archean Man Shield, the Congo Craton, and the rare-metal granites of Nigeria and Egypt. The incorporation of Li into CGM has not yet been investigated; however, in wodginite, the coupled heterovalent substitution $Mn^{2+}Sn^{4+}Li^{+}_{-1}Ta^{5+}_{-1}$ is responsible for Li in the structure (Ercit et al., 1992b).

Beryllium concentrations in CGM are very low; only 15% of the analyses show detectable Be (i.e., >0.1 ppm). Only one grain of columbite-(Mn) from the Ruhanga pegmatite in Rwanda gave a high Be value (604 ppm, probably due to sub-μm sized micro-inclusions of beryl). Elevated values from 1 to 20 ppm are found in several pegmatites of the Kibara Belt, at Bikita, Tantalite Valley, Kenticha, Marropino and Liha (Congo Craton). Beryllium concentrations do not show any correlation with #Mn and #Ta values.

Magnesium shows a maximum content of 2 wt.% in columbite-(Mn) from Ruhanga (Gatumba district, Kibara Belt, Rwanda). The median (30 ppm), P25 (5 ppm), P75 (170 ppm) and P90 (536 ppm) values for the entire dataset indicate that Mg is a common trace element in CGM, albeit typically present at low levels. High concentrations exceeding 3000 ppm are found in some pegmatites in the Kibara Belt (mainly in Rwanda), at Mocuba (Mozambique), at Jos (Nigeria) and on the Congo Craton. Although elevated values occur in both columbite-(Fe) and columbite-(Mn), Mg shows an overall negative correlation with Mn, but none with Nb or Ta. This indicates substitution of Fe by Mg as the dominant substitution mechanism. Among the African Ta provinces, Mg enrichment is most prominent in pegmatites of the Man Shield (Md, 741 ppm) and the Congo Craton (403 ppm), but is also observed in the Older Granites of Nigeria (116 ppm). In individual pegmatites, Mg, along with Ti and Fe^{3+}, may indicate contamination (e.g., during metamorphic reactions, Černý and Němec, 1995). The Mg end-member, columbite-(Mg), was encountered only in one concentrate from Rwanda, where the geological context is unknown (sample 041, Muhanga; Appendix 2). Galliski and Černý (2006) have shown that Mg in CGM from Argentinian localities decreases from beryl-columbite to albite and petalite-subtype pegmatites.

Aluminium contents in CGM are homogeneously distributed around a median value of 52 ppm (P25 = 25 ppm; P75 = 118 ppm). The highest concentrations of up to 1.7 wt.% are likely caused by contribution from associated Al-silicates, because Si in these analyses is also >1 wt.%. Regionally, pegmatites from the Tantalite Valley (Namibia) have the highest median value (196 ppm; Table 5), followed by the

Man Shield, Bikita and the Congo Craton. Low Al contents are measured in CGM from the Younger Granites of Nigeria.

Calcium concentrations measured by LA-ICP-MS are often affected by alteration to pyrochlore-supergroup minerals and thus are difficult to interpret. In addition, Ca contents are above their detection limit only in 30% of the measurements. Ercit (1994) already noted that CGMs have extremely low Ca concentrations, but also mentioned some exceptions.

Scandium contents vary over four to five orders of magnitude, e.g., from 0.05 (P5) to 410 ppm (P95), at a median of 6.7 ppm. The highest concentrations exceeding 1 wt.% (up to 1.8 wt.%) are found at Marropino and Somipe (Mozambique), Ruhanga (Rwanda), the Man Shield (Sierra Leone), the Older Granites of Nigeria and in Madagascar. Such extreme Sc values are restricted to Nb-rich columbite (#Ta <20). Thus, Sc shows a negative correlation with #Ta and a weaker one with #Mn. This is opposite to Sc behaviour reported from NYF pegmatites in North America (Ercit, 1994), where the Sc content increases during Nb–Ta fractionation. The African Ta provinces can be subdivided into Sc-rich provinces (Congo Craton: Md, 238 ppm; Man Shield: 211 ppm; Eastern Desert: 173 ppm), intermediate-Sc provinces (Bikita: 56 ppm; Younger Granites: 46 ppm; Alto Ligonha: 17 ppm) and Sc-poor provinces (<10 ppm; Kibara Belt, Kamativi Belt, Damara Belt, Birimian, Older Granites of Nigeria, Tantalite Valley); the latter are all LCT-family pegmatites. The high and intermediate-Sc provinces comprise both NYF and LCT-types. Scandium shows a weak positive correlation with Y ($R^2 = 0.06$) and the REE (Y–Yb: +0.07) in many provinces.

Titanium is the most important substituent element in CGM (Md = 0.35 wt.%; P5 = 0.05, P95 = 2 wt.% TiO_2). The highest concentrations (10–15 wt.% TiO_2) are encountered in the Man Shield (Sierra Leone), where they are often associated with the presence of Nb–Ta rutile (Md, 2.63 wt.% TiO_2; Table 5), and in Alto Ligonha (Mozambique). Other occurrences of Ti-rich CGM are Bikita (Zimbabwe), the Congo Craton, and Older Granites of Nigeria. In the granitic pegmatites of the Pampean Ranges (Argentina), the highest Ti contents are found in the most primitive late-orogenic beryl-type pegmatites, followed by post-orogenic beryl-columbite-phosphate and petalite subtypes; CGM from spodumene and albite subtypes are Ti-poor (Galliski and Černý, 2006). Titanium exhibits weak negative correlations with both the Fe–Mn ($R^2 = 0.04$) and Nb–Ta fractionation indices ($R^2 = 0.03$), in line with the proposed rutile-type substitution mechanism and the "normal" behaviour of Ti during fractionation. However, the opposite behaviour has been described as well (Ercit, 1994); other Ti-bearing minerals such as rutile, wodginite and tapiolite will have an influence on the behaviour of Ti in CGM. Along with Mg and Fe^{3+}, Ti is thought to be susceptible to late-stage alteration processes and may indicate contamination.

Arsenic contents in CGM are low (Md = 0.27 ppm; P95 =12.6 ppm); only 55% of the values are above the detection limit. The highest concentrations reaching 575 ppm occur in columbite-(Mn) and tantalite-(Mn) from the Manono deposit (Kibara Belt, DRC). Values >50 ppm are also recorded from other deposits in the Kibara Belt (Kabambare, Pangi, Rutsiro, Kabera), and from placer deposits on the Congo Craton (Liha). Among the African Ta provinces, Bikita (Zimbabwe) has the highest median (9.4 ppm), followed by the Congo Craton and the Man Shield. Although several pegmatites in the Kibara Belt are As-rich, the median value is only 0.2 ppm. Arsenic contents tend to increase during Nb–Ta fractionation. Arsenic, Sb and Bi correlate positively with one another.

Rubidium concentrations are very low (P95 = 3.8 ppm; P75 = 0.15 ppm), with only 30% of the values above detection limit. Maximum concentrations reaching 500 ppm are measured in pegmatites of the Kibara Belt (Rutsiro district, Gatumba district). Given the structure of CGM (Rb^+ is ~2 times larger than Mn^{2+}), the detected Rb is probably from inclusions in the sub-micrometre scale.

Strontium contents are similarly low (Md = 0.19 ppm; P95 = 15 ppm), with 55% of the values above detection limit. The Tantalite Valley pegmatite (Namibia) has the highest median Sr (15 ppm), followed by the granite-hosted CGM of the Eastern Desert, the Congo Craton and the Man Shield. Strontium values increase with Nb–Ta fractionation, whereas Fe–Mn fractionation has no significant effect. However, the fact that Sr^{2+} is 50% larger than Mn^{2+} makes it likely that the detected Sr is also from inclusions in the sub-micrometre scale.

Yttrium abundances, similar to Sc and the REE, vary over four to five orders of magnitude (P5 = 0.06 ppm; P95 = 2454 ppm; Md =4 ppm). The highest concentrations exceeding 1 wt.% (at a maximum of 2 wt.%) are recorded for columbite-(Mn) and tantalite-(Mn) from the Marropino pegmatite, Mozambique. Two trends are visible in Y versus #Ta and #Mn plots, both showing Y decrease with fractionation, but at different concentration levels. The highest median value of 547 ppm (Table 5) corresponds to samples from Alto Ligonha (although not all pegmatites investigated are Y-rich). CGM from the Congo Craton, Bikita, Eastern Desert, Mozambique, the Younger Granites of Nigeria and the Man Shield are also characterised by high Y. Typical LCT-family pegmatite provinces such as the Kibara, Adola and Damara Belts are low in Y. Significant positive correlations exist with Ti (R^2 =0.18) and Th (0.05). In the Pampean pegmatites (Argentina), the late-orogenic pegmatites have low Y, whereas the post-orogenic beryl-columbite-phosphate pegmatites contain CGM that are comparatively enriched in Y; there, Y correlates with W, Nb, Ti and Th (Galliski and Černý, 2006).

Zirconium is a significant trace element in CGM, with a median of 815 ppm and a moderate range (P5 = 140 ppm; P95 = 4400 ppm). The highest contents (up to 1.8 wt.% ZrO_2) were measured in several pegmatites from South Kivu (Kibara Belt). However, values exceeding 1 wt.% are rare and mostly related to Ta-rich columbite–tantalite. There is no obvious correlation between Zr and the Fe–Mn or Nb–Ta fractionation indices, but Zr is positively correlated with Hf ($R^2 = 0.62$), and Zr/Hf ratios correlate well with Nb/Ta. The most Zr-enriched African Ta province is the Tantalite Valley pegmatite field, followed by the Congo Craton, Eastern Desert, Man Shield and Bikita (all Md values >2000 ppm). The other provinces, including the Kibara Belt, have median values close to or below 1000 ppm Zr.

Molybdenum concentrations in CGM have not yet been reported in the literature. However, this element is present in most CGM grains at low concentrations, and shows little variation (Md = 1.7 ppm; P10 = 0.6 ppm, P95 = 18.7 ppm). However, columbite-(Fe) from the Jos Plateau often contains >100 ppm Mo (up to 537 ppm). These data form a separate cluster in Mo vs. #Mn and #Ta diagrams. The remaining data show a clear positive correlation with #Mn and a negative one with #Ta. High Mo concentrations correlate with elevated W. Among the African Ta provinces, high Mo contents are recorded for the samples from the rare-metal granites of Nigeria and Egypt (Md > 50 ppm) and from placer CGM of the Man Shield (Md = 16 ppm). The remaining provinces, including typical LCT-family provinces, have low Mo concentrations (Md < 10 ppm).

Tin is third in average abundance among the tetravalent metals in CGM, after Ti and Zr (Fig. 8). The median value is 0.13 wt.% SnO_2 and the variation is moderate (P5 = 0.013 wt.%, P95 = 0.64 wt.% SnO_2). Highest concentrations exceeding 3 wt.% (up to 4.4 wt.%) were measured in CGM from the Kibara Belt; these high values are independent of #Mn and #Ta values. Tin correlates with Zr ($R^2 = 0.12$) and Hf. While there is no dependence on Fe–Mn fractionation, a positive correlation with the Nb–Ta fractionation index is visible to #Ta = 60, followed by a steep decline to higher #Ta values. The LCT-pegmatite from Bikita (Zimbabwe) has the highest median Sn value (0.64 wt.% SnO_2) followed by the granite-hosted mineralisation in the Eastern Desert (0.49 wt.%), and the Birimian Province. Pegmatites from the Kibara and Kamativi Belts and the Nigerian Older Granites have intermediate median Sn values (ca. 0.15 wt.%). Some provinces are characterised by low Sn concentrations in CGM (<0.05 wt.%; Man Shield, NE Congo Craton; Namaqualand; Damara and Mozambique Belts), and some of these occurrences do not contain any cassiterite associated with CGM.

The low Sn contents in these cases may be due to a contribution from Sn-depleted crustal sources (e.g., Archean or juvenile crust), whereas elevated Sn in the Kibara, Kamativi and Nigerian provinces may be due to underlying thick continental crust with abundant metapelite. Nevertheless, additional factors must be taken into account to explain the high variations in Sn concentrations among the different provinces. In the Pampean Pegmatite Province (Argentina), Sn contents are elevated in CGM from lepidolite- and spodumene-subtype pegmatites, whereas CGM from the albite type have low Sn (Galliski and Černý, 2006).

Antimony contents in CGM are generally low (P95 = 3.3 ppm); only 40% of the measurements are above the detection limit. Elevated concentrations (>50 ppm) are found exclusively in columbite-(Mn) and tantalite-(Mn) from pegmatites at Lema (Older Granites, Nigeria), Alto Ligonha, and Bikita; some of these occurrences also contain stibiotantalite as a discrete phase. With a median Sb content of 25 ppm, the samples analysed from the Bikita pegmatite are most enriched. Among the studied provinces, Sb is slightly enriched only in the pegmatites from Namaqualand, Mozambique, in the granite-hosted mineralisation in the Eastern Desert (Egypt), and locally in pegmatites related to the Older Granites (Nigeria). Antimony contents show an overall positive correlation with both, the Fe–Mn and Nb–Ta fractionation indices.

Barium contents are low (50% below detection limit) and display a narrow range (P75 = 2.3 ppm; P95 = 33 ppm). Elevated concentrations (>200 ppm) are detected in all chemical members of the CGM group, mainly in grains analysed from the Kibara Belt (e.g., Kabambare, Manono, Pangi; all DRC), but also erratically from Kenticha, Mozambique, Sierra Leone and Nigeria. In these cases, elevated Ba contents may be explained by alteration minerals; e.g. pyrochlore-supergroup minerals may carry Ba substituting for Ca. The Tantalite Valley and Bikita pegmatites have elevated Ba, similar to the samples from the Man Shield and Congo Craton (Md values of 5–10 ppm), whereas the median values of most Ta provinces are below 1 ppm. Barium correlates well with other divalent cations of large ionic radius ($R^2_{Ba–Sr}$ = 0.24; $R^2_{Ba–Pb}$ = 0.13), but not with the #Mn and #Ta values, indicating that most of the Ba is present in small inclusions within the CGM.

Hafnium is an abundant trace element in CGM, giving a median value of 110 ppm and a moderate variation (P5 = 20 ppm; P95 = 767 ppm). High concentrations (>2500 ppm, to a maximum value of 4308 ppm) are recorded in the samples from pegmatites in the Kibara Belt, but also from Kenticha and Marropino. Hafnium concentrations are closely correlated with Zr, and therefore also progressively increase with Ta fractionation (R^2 = 0.09). The highest median values are recorded from the Eastern Desert samples (719 ppm), followed by those from the Tantalite Valley, Congo Craton, Bikita and Kokobin (Ghana). The Kibara and Kamativi Belts, and the anorogenic granite-hosted CGM from the Younger Granites of Nigeria, have low Hf concentrations.

Tungsten is the second most abundant trace element in CGM, attaining a median value of 0.16 wt.% WO_3 and a moderate range of values (P5 = 0.02 wt.%, P95 = 0.87 wt.% oxide). A maximum concentration of 4.7 wt.% is reported for a columbite-(Fe) from North Kivu, followed by samples from the Man Shield with 1.8–4.5 wt.% WO_3. The highest W values are restricted to columbite-(Fe), and to a lesser extent, columbite-(Mn). This indicates a strong dependence on the fractionation vector #Ta (R^2 = 0.11); a negative correlation with #Mn is also observed, as well as a significant positive correlation with Ti (R^2 = 0.25). Tungsten is enriched in CGM from pegmatites in the Man Shield (Md = 1.27 wt.%), Bikita, Congo Craton and granite-hosted CGM in the Eastern Desert. Low median values (<0.1 wt.%) are calculated for pegmatites of the Birimian (Ghana), Adola Belt (Ethiopia) and Older Granites (Nigeria); this depletion may indicate a contribution from mafic/ultramafic source materials. Tungsten is concentrated in CGM from post-orogenic beryl-columbite-phosphate pegmatites and less common in late-orogenic dikes of the same subtype in the Pampean Pegmatite Province; the other pegmatite types are W-poor (Galliski and Černý, 2006). The W content also decreases with progressive Nb–Ta fractionation. In individual pegmatites of the Grenville NYF Pegmatite Province, W correlates positively with Ta and occasionally with Mn, but negatively with Ti, opposite to what is observed in the African Ta provinces.

Lead concentrations range from <0.1 ppm to 2 wt.% (Md = 38 ppm; P5 = 2.5 ppm, P95 = 525 ppm) and correlate with U, Th and Ba. Exceptionally high Pb values exceeding 2000 ppm are encountered spuriously in most provinces, and are partly attributed to secondary alteration (e.g., formation of Pb-bearing microlite). Most of the high-Pb analyses have disturbed U/Pb ratios. The highest median Pb concentrations are encountered in the oldest (Archean) pegmatites, e.g., Bikita (1743 ppm), Man Shield (362 ppm) and Congo Craton (338 ppm; Table 5). CGM associated with the anorogenic Younger Granites of Nigeria have the lowest Pb concentrations (Md = 3 ppm).

Bismuth is a trace element in CGM with a median value of 0.15 ppm and a wide range (P25 = 0.04 ppm, P95 = 40 ppm). The data show a weak positive correlation with #Mn. Concentrations exceeding 1000 ppm (up to 1 wt.%) are recorded for tantalite-(Mn) and columbite-(Mn) at Marropino, Moneia and Muiane (Alto Ligonha), Kenticha (Ethiopia) and a few pegmatites in the Kibara Belt (e.g., Manono, DRC; Nyarigamba, Rwanda). On a province scale, Bi is enriched in CGM from the Adola Belt (Ethiopia, Md = 2.7 ppm), Alto Ligonha (Mozambique, Md = 3.4 ppm) and the Older Granites (Nigeria, Md = 0.9 ppm), all of Pan-African age, and from the Tantalite Valley (Namibia). Bismuth averages 0.02 wt.% and peaks at 0.27 wt.% in CGM from the Pampean Province (Galliski and Černý, 2006), where late-orogenic pegmatites are slightly enriched in Bi. The presence of bismutotantalite or native bismuth inclusions in CGM does not necessarily imply elevated Bi contents in CGM.

Thorium is typically detected in trace amounts in CGM (Md = 3.8 ppm; P5 = 0.2 ppm, P95 = 78 ppm). Exceptionally high concentrations (>300 ppm, up to 2000 ppm) occur in granite-hosted CGM from Nigeria and the Eastern Desert (giving the highest median value of 312 ppm among all Ta provinces), and in pegmatite-hosted CGM from Mozambique, Sierra Leone, Congo Craton, and several deposits in the Kibara Belt. High values of Th are commonly associated with high U concentrations. Columbite-(Mn) from the Bikita pegmatite averages 247 ppm Th, and tantalite-(Mn) from the U-rich Tantalite Valley pegmatites to 136 ppm. The LCT-family pegmatites from the Kibara, Kamativi and Damara Belts, and the Older Granites, have low Th contents (Md values <5 ppm). Thorium concentrations tend to increase with progressive Fe–Mn and Nb–Ta fractionation.

Uranium concentrations in CGM vary over a wide range with a median value of 240 ppm (P5 = 24 ppm, P95 = 1965 ppm). The highest values, close to or exceeding 1 wt.%, were measured in CGM from pegmatites in the Kibara Belt (e.g., Buranga and Kiyanja in Rwanda), from Marropino (Mozambique) and Tantalite Valley (Namibia). In most cases, these CGMs are intergrown with U-rich microlite or contain exsolved uraninite, euxenite, samarskite, or fergusonite. Nevertheless, concentrations exceeding 0.5 wt.% were also measured in homogeneous areas by high-resolution electron microprobe techniques indicating that uranium may reach significant concentration levels in CGM. Tantalite-(Mn) from the Tantalite Valley pegmatite attains the highest median U content (4779 ppm), followed by samples from Bikita (2852 ppm), the granite-hosted CGM from Egypt (1537 ppm) and the Congo Craton (1036 ppm; Table 5). The columbite-(Fe) from the Younger Granites have the lowest median U content (83 ppm), followed by those from the Kamativi Belt (94 ppm). Typical LCT-family pegmatite provinces have median U values of 200–300 ppm. Considering the complete dataset, U contents tend to increase with both, Fe–Mn and Nb–Ta fractionation. Uranium is correlated to Pb (mainly due to the production of radiogenic Pb by decay), Th (R^2 = 0.21), Ti (0.13), Zr (0.34) and Hf (0.16). In NYF pegmatites of the Grenville Province, U correlates with other tetravalent cations (Zr, Ti, Sn) and attains values up to 9000 ppm

(Ercit, 1994). Exsolution of a samarskite phase occurs at high Y and U contents.

Rare-earth elements are present in highly variable amounts in CGM. Their concentrations may reach 1.2 wt.% REE_2O_3, but are commonly in the 2–50 ppm range (Md = 5 ppm; P75 = 40 ppm, P90 = 471 ppm, P95 = 1413 ppm). The major findings concerning the incorporation of REE in the columbite structure, the different types of REE_N patterns and the parameters controlling REE concentrations and patterns have already been discussed by Graupner et al. (2010). Chondrite-normalised REE patterns show much variation (Fig. 11). However, within a zoned crystal, a pegmatite or a Ta province, these patterns are often subparallel to each other. Most REE_N patterns are characterised by large negative Eu anomalies, probably due to earlier fractionation of potassium feldspar. On the other hand, Eu anomalies are small or absent in the Kibara and Kamativi Belts and at Kokobin, Ghana. In addition to negative Eu anomalies, the rare-metal granite-hosted CGMs are characterised by prominent negative Y anomalies. Y-rich phases such as xenotime commonly do not fractionate Y from Ho significantly (e.g. Wall et al., 2008); however, Förster (1998) found increased Y/Ho ratios (ratios up to 60; chondritic Y/Ho ratio is 28) in xenotime from late stages of crystallisation of evolved granites from Germany. Positive Ce anomalies were detected in several deposits, and their origin remains speculative. The shape of the REE_N patterns, especially with regard to their $MREE_N$ and $HREE_N$ sections, is an important distinguishing feature for many provinces. In several examples, the "normal" fractionation pattern (progressively increasing concentrations from $LREE_N$ to $HREE_N$) is modified, resulting in low $HREE_N/MREE_N$ ratios (e.g., Tantalite Valley, Alto Ligonha).

In 11 out of the 13 provinces studied, the majority of CGM show negative Eu anomalies, which are most pronounced in the samples from the Zimbabwe Craton, Tantalite Valley, Alto Ligonha, and the granite-hosted mineralisation in the Eastern Desert and Nigeria. The CGMs from the Kibara and Kamativi Belts have weak or no Eu anomalies. The only CGM displaying positive Eu anomalies are documented from the Birimian in Ghana (Fig. 11c). The presence of negative Eu anomalies may reflect precipitation of CGM from melts crystallising potassium feldspar. The lack of Eu anomalies is not easy to interpret; Graupner et al. (2010) discussed that the degree of contamination of pegmatitic rare metal-enriched melts by clastic metasedimentary and mafic rocks increases with distance from presumed parental granites (cf. Fig. 8c in the above paper). Both recrystallisation and/or replacement of early potassium feldspar by secondary minerals may result in redistribution of Eu between the silicates and a melt/fluid. No indication of a significant increase in oxygen fugacity (maintaining Eu in its trivalent state) or the existence of compositionally different melts in the Kibaran rare-element pegmatitic systems is currently available. Therefore, there is no reason to expect that magmatic differentiation was responsible for the formation of Eu-undepleted REE distribution patterns (type 3) in CGM from the Kibaran pegmatites.

The rutile structure of *tapiolite* allows accommodation of minor tetravalent cations, such as Sn, Ti, Zr and Hf (Fig. 8) (Ercit, 2010). Compared to CGM, tapiolite has a rather restricted major element composition close to $FeTa_2O_6$. A dataset containing more than 640 analyses (including 174 by LA-ICP-MS) was used to characterise the chemical variation (Table 6). The major elements range from 9.8 to 16.5 wt.% for FeO, <3.8 wt.% for MnO, <14 wt.% for Nb_2O_5 and 61 to 88 wt.% for Ta_2O_5. The maximum #Mn value is close to 25, and the lowest #Ta is close to 74 (see Fig. 7d, e, h, j, k, l). Maximum and median concentrations of the minor elements are: TiO_2 (12.7 wt.%, 0.63 wt.%); SnO_2 (4.4 wt.%, 0.45 wt.%); and WO_3 (1.1 wt.%, 0.01 wt.%) (Table 6). Trace elements that are commonly detected by LA-ICP-MS include (in ppm; minimum–maximum; Md): Li (<1–60; 6); Mg (<1–1732; 30); Sc (<1–1100; 2.8); Y (<1–48; 0.03); Zr (23–16,673; 1016); Hf (12–3978; 417); U (1–1887; 116); and Pb (1–833; 20). In agreement with Novák et al. (2004), tapiolite does not accommodate trivalent cations (As, Sb, Bi, and REE) in significant amounts. The concentrations of individual REE are below their respective detection limits in >75% of the measured values. Where detectable, REE give chondrite-normalised patterns that resemble those of the coexisting CGM in shape, but are at lower levels of REE enrichment (Fig. 12a).

Ta-rich phases accommodating high levels of Sn, Ti or W (Fig. 8) commonly occur as inclusions in CGM, cassiterite and Ta–Nb-rich rutile, occasionally as exsolution lamellae, or form discrete grains that may be intergrown with other CGM or cassiterite (Fig. 6f, j). About 470 analyses (including 122 by LA-ICP-MS) of Sn-rich Ta–Nb oxides were acquired. In African pegmatite provinces, wodginite–ixiolite is common in Zimbabwe (Benson mine and Sutswe), in many deposits of the Kibara Belt, in some of the pegmatites in the Older Granites of Nigeria and in the Damara Province (e.g., Uis) (Table 1). In Sn–Nb–Ta concentrates from the Younger Granites of Nigeria, W-rich ixiolite ("wolframixiolite"; Mücke and Neumann, 2006) was encountered. In the present study, lithiowodginite was confirmed only in samples from the Mumba area of North Kivu. Wodginite–ixiolite is very rare in the Ethiopian pegmatites and absent in Mozambique, the Tantalite Valley, Man Shield and Congo Craton. In the Kibara Province, wodginite–ixiolite was identified at more than 20 different locations (Fig. 6f; Table 1).

The chemical composition of wodginite–ixiolite is highly variable (Figs. 7, 8 and Table 6). Mn–Fe substitution is complete, whereas #Ta commonly ranges from 60 to 100. Lower #Ta is only encountered in grains from the Jos Plateau (Fig. 7l) and in the Kibara Province in Rwanda and the DRC (Fig. 7e). These Fe- and Nb-rich grains are most probably disordered ixiolite. The SnO_2 concentrations detected in phases classified as wodginite–ixiolite range from 0.5 to 33 wt.%, with an average and median of 12 wt.%. Significant concentrations of TiO_2 (up to 21 wt.%; Md, 1.2 wt.%), WO_3 (up to 50 wt.% in "wolframixiolite"; Md, 0.17 wt.%), ZrO_2 (up to 10 wt.%; Md, 0.95 wt.%) and Hf (up to 8500 ppm; Md, 1813 ppm) may occur, with concentration levels generally higher than in CGM and tapiolite. Černý et al. (2007) found up to 9.59 wt.% ZrO_2 and 1.15 wt.% HfO_2 in wodginite from pegmatites and observed that Zr/Hf ratios in wodginite are lower (1 to 4) than in coexisting columbite–tantalite (6 to 13). Scandian ixiolite containing between 4 and 19 wt.% Sc_2O_3 has been reported from Madagascar, Mozambique, Norway, Maine and the Czech Republic (Wise et al., 1998).

Trace elements that are present in higher concentrations in the African localities include U (up to 6743 ppm; Md, 676 ppm), Sc (up to 2363 ppm; Md, 39 ppm), Li (up to 0.9 wt.% in lithiowodginite, up to 520 ppm in ordinary wodginite–ixiolite; Md, 29 ppm), Mg (up to 981 ppm; Md, 12 ppm), Th (up to 825 ppm; Md, 14 ppm), As (up to 54 ppm), Sb (up to 135 ppm) and Bi (up to 3200 ppm) (Table 6). The concentration levels and chondrite-normalised patterns of the REE (including Y) are similar to those in coexisting CGM, and REE concentrations are higher than in tapiolite (Figs. 10, 12b, c).

7.3. Chemical variability of Ta–Nb oxides on different scales

Pegmatites are extremely variable magmatic rocks in terms of textures and trace element geochemistry. This variability is reflected by complex zoning patterns within single pegmatites, a wide variety of rare element minerals and, among them, different compositions of individual minerals. These variations develop through fractional crystallisation, contamination, postmagmatic overprint and other processes. Large mineralogical and chemical variations may exist between pegmatites in spatially, timely and genetically related pegmatite fields or provinces. In many Li-rich pegmatites, for example, a general sequence of columbite-(Fe) → columbite-(Mn) → tantalite-(Mn) → microlite → (tapiolite) is observed (e.g., Černý and Ercit, 1985; Spilde and Shearer, 1992). However, the data presented in this paper suggests that rare element minerals within pegmatite fields and provinces are frequently chemically related. To illustrate this, we discuss the following points: (1) chemical variation within individual crystals, (2) chemical variation within single pegmatite bodies and (3) the behaviour of trace elements during fractionation in single pegmatites.

(1) Crystals of CGM and wodginite–ixiolite are commonly zoned, which is best visible in BSE images that usually record a Ta vs. Nb variation (Figs. 6 and 7). The variation in #Mn and #Ta may be as high as 30 mol%, but is typically on the order of 10–20 mol% or less. The concentration levels of trace elements in zoned crystals usually vary over one order of magnitude (e.g., 2–20 ppm Li) and such variations are similar for most elements, except for REE that may vary over two orders of magnitude within a single crystal. Fig. 15 illustrates variations in trace elements for three crystals. The analyses of an oscillatory zoned columbite-(Fe) crystal from Muika (Katanga, DRC; Fig. 15a) define two populations differing in #Mn. The REE and trace element patterns are subparallel, but show a spread that is attributable to these variations in #Mn (e.g., low abundance of trace elements in the Fe-rich phase that forms patchy overgrowths on an earlier zoned crystal). A Nb–Ta zoned columbite-(Fe) crystal from Buranga (Rwanda) shows a large variation in LREE, Bi, Ti, Zr, Hf and Sn contents, with the low values found in the more Mn-rich phase (Fig. 15b). A large columbite-(Mn) crystal from Mbuye (Rwanda) displays only minor compositional variations, mainly

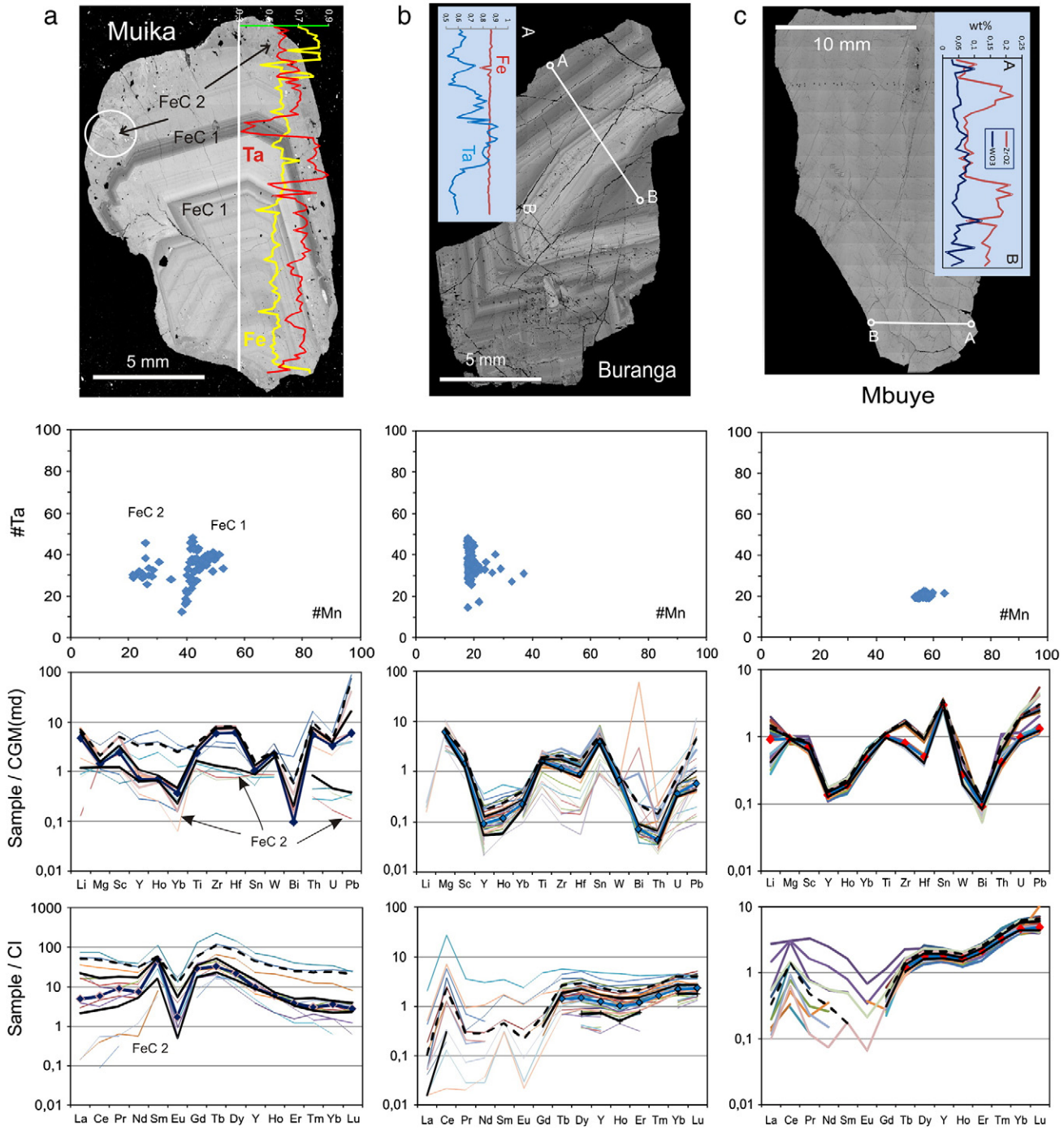

Fig. 15. BSE images and chemical composition of zoned (a, b) and unzoned (c) CGM crystals from the Kibara Belt (sample 116 Muika, DRC; sample 152 Buranga, Rwanda; sample 154 Mbuye, Rwanda). In the normalised diagrams, individual analyses as well as median (blue line with diamond symbols), P25, P75 (solid black lines) and P90 (broken black line) values are plotted. Element profiles in Fig. 15a and b give cation distributions in atoms per formula unit, calculated to six oxygens; element profile in Fig. 15c is in wt.%.

in LREE, Li, Zr, Hf, U and Pb (Fig. 15c). Although line scans show that the major element composition of this sample is uniform, some trace elements (such as Zr and W) indicate internal zoning.

(2) Trace element concentrations (P75–P25 around the Md and mean ± standard deviation) in a single pegmatite deposit can vary within one order of magnitude or less, as shown by the Manono deposit on the basis of 290 measurements (Figs. 9f, 13a). In the Marropino pegmatite (400 measurements), P75–P25 values of trace elements in CGM vary less than one order of magnitude for Y, HREE, Ti, Zr, Hf, W, Th, U and Pb; around one order of magnitude for Sb, Mg and Sc; and more than two orders of magnitude for Bi, and probably also Li and Sn (Fig. 13b). The difference between the P10 and P90 values is slightly larger, i.e. between one and two orders of magnitude for most elements. These examples support the suggestion that trace element concentrations in single pegmatite deposits form parallel "bands" in normalised trace element diagrams.

(3) Some minor and trace elements show correlations with fractionation indices in CGM and wodginite–ixiolite, i.e. with #Mn and/or #Ta. The most obvious ones are negative correlations between TiO_2 and #Mn as well as between WO_3 and #Ta, and positive correlations between #Mn and Zr, or Hf and U. These are visible in many datasets acquired for individual pegmatites. As an example, major and trace element variations of single grains from the Manono pegmatite are illustrated in Appendix 3. However, there are only a few statistically consistent correlations that apply to all pegmatite- and granite-related deposits in the complete dataset. Therefore, such correlations appear to be governed by factors other than simple substitution mechanisms based on valence and ionic radius; these factors appear to be operating on the regional to local scale.

In order to illustrate the variation of major and trace elements in pegmatite provinces, and to highlight the differences, cumulative distribution functions were constructed for CGM populations from the African Ta provinces. The #Mn and #Ta ratios for 11 provinces are summarised in Fig. 16. Significant differences are observed for #Mn, whereas #Ta distributions are similar in many provinces. Only the Kibara Belt shows a normal distribution of #Mn values (Fig. 16a); all other provinces have skewed distributions, being dominated by Fe (Congo Craton/Ubenidan; Kamativi; Man Shield; Jos Plateau) or Mn (Eastern Desert; Birimian) (Fig. 16a, b). The #Mn ratios of the samples from Ethiopia–Somalia, the Damara Belt, the Older Granites of Nigeria and Alto Ligonha follow almost normal distributions, but start off at #Mn values of 30 to 40. The #Ta distributions differ from the #Mn distribution curves; most are skewed towards Nb (Fig. 17a, b), with the Jos and Man Shield samples having the most extreme Nb enrichments (Fig. 17b). The samples from Alto Ligonha and Adola Belt approach normal distributions.

In Fig. 17a and b, log-normalised cumulative distribution curves for Sn, Ti, Y, Sc and Zr display nearly log-normal distributions for the Kibara Belt, as do Sn, Ti and Zr curves for the Alto Ligonha Province. However, Sc and Y in the Alto Ligonha samples are polymodally distributed, as illustrated by kinks in the cumulative frequency curve. Clearly, the concentration levels differ for Sn, Y and Sc between the two provinces; Y and Sc are more enriched in CGM from Mozambique, whereas Sn is more enriched in those from the Kibara Belt (see also Fig. 9e and k). Cumulative frequency curves for Sn, Ti, W, Sc, Y, Th and Zr reveal consistent log-normal distributions for the Kibara Belt only (Fig. 17c–i); this is probably due to the large number of analyses (almost 5000). The data set for the remaining provinces comprises between <100 and 1000 measurements, resulting in bimodal, polymodal and occasionally multistage distributions. Comparison of the data for six African Ta provinces reveals some characteristic differences. The Kibara Belt samples have low levels of Ti, Sc, Y, Th and Zr, but high levels of Sn. The Congo Craton/Ubendian and Man Shield populations are characterised by high Ti, W, Sc, Y and Zr; however, the Man Shield material is low in Sn. The data from Ethiopia (Adola Belt) are distinguished from the other groups by their low W and Y concentrations. CGMs from the Jos Plateau have steep (low variability) curves at high Y concentrations and low Th.

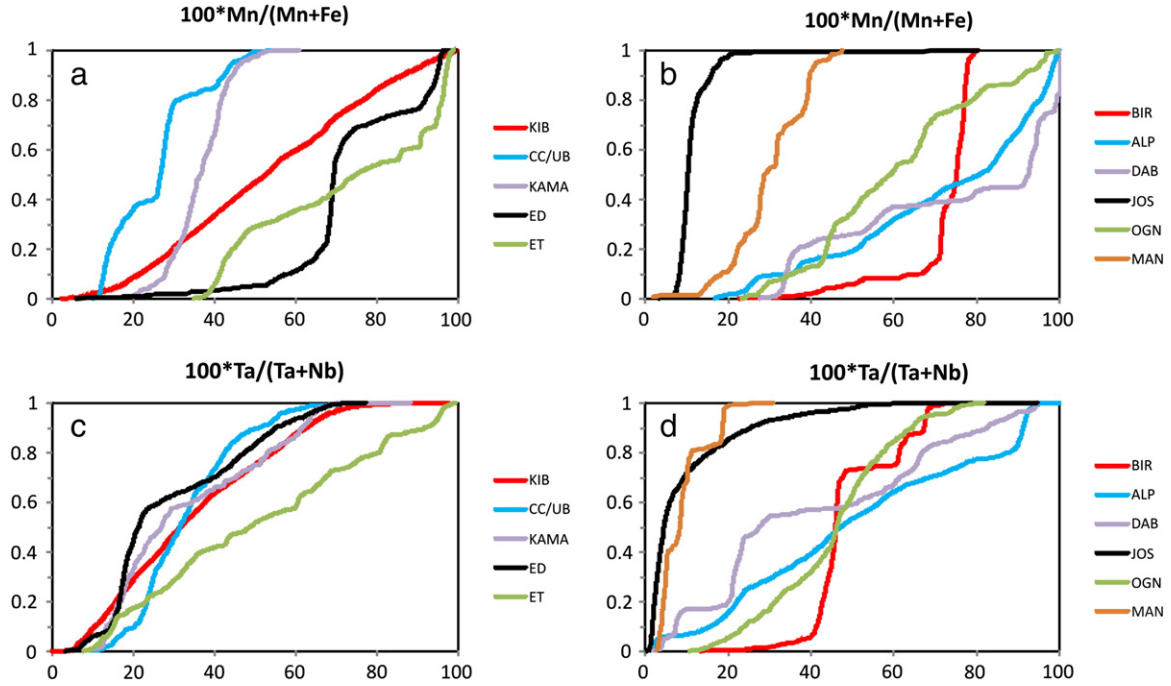

Fig. 16. Cumulative probability curves for #Mn and #Ta in CGM from 11 provinces; combined EPMA and LA-ICP-MS data; number of analyses: KIB, Kibara Belt = 10,238; CC/UB = NE Congo Craton/Ubendian = 491; KAMA, Kamativi Belt = 197; ED, Eastern Desert, Egypt = 598; ET, Adola Belt, Ethiopia = 1423; BIR, Birimian, Ghana = 359; ALP, Alto Ligonha Province = 1659, DAB, Damara Belt = 621; JOS, Younger Granites, Nigeria = 877; OGN, Older Granites, Nigeria = 381; MAN, Man Shield = 261.

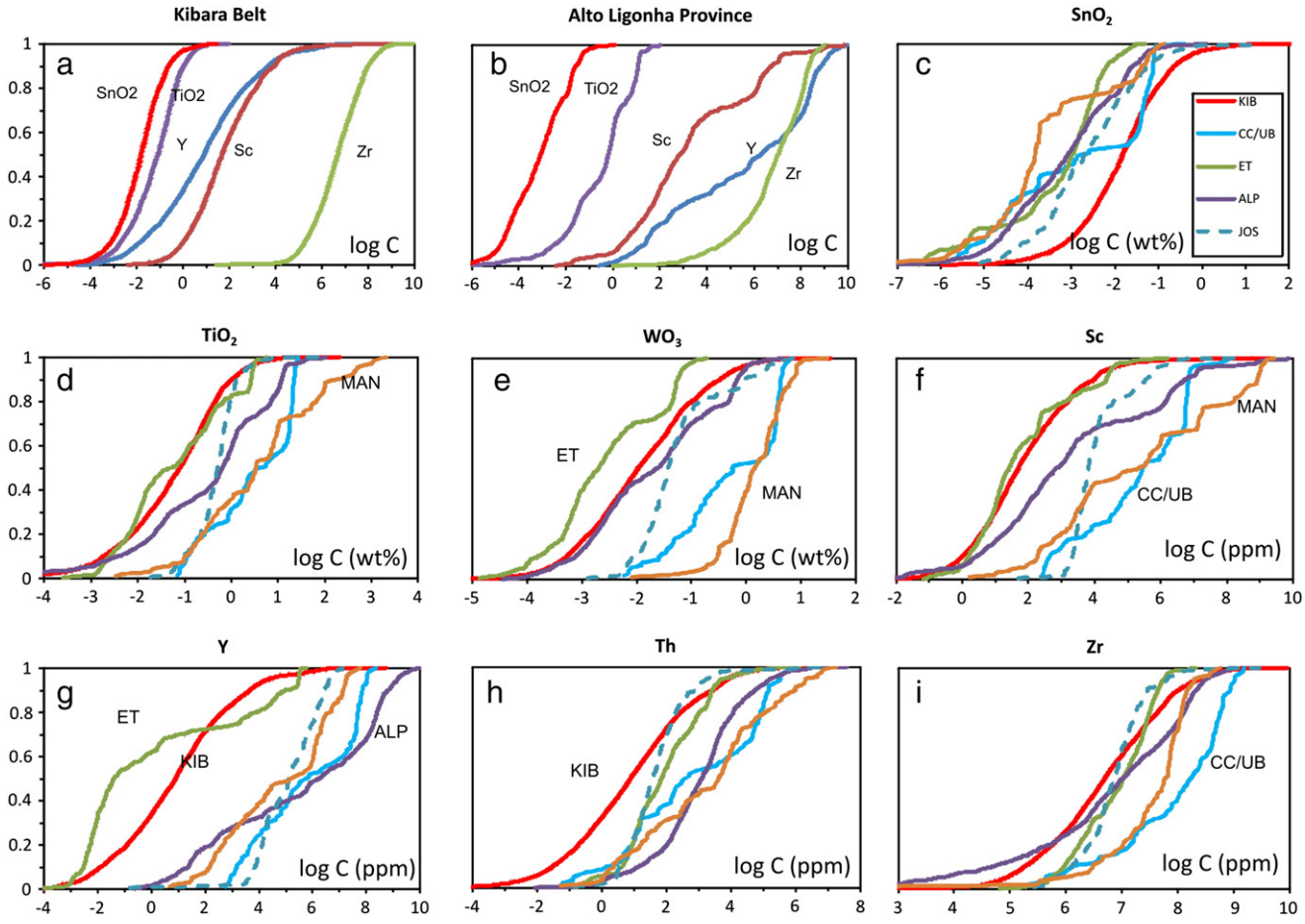

Fig. 17. Cumulative probability curves for log-normalised WO_3 (%), TiO_2 (%), SnO_2 (%), Sc (ppm), Y (ppm) and Zr (ppm) in CGM. LA-ICP-MS data; number of analyses: KIB, Kibara Belt = 4967; CC/UB = NE Congo Craton/Ubendian = 84; ET, Adola Belt, Ethiopia = 535; ALP, Alto Ligonha Province = 979, JOS, Younger Granites, Nigeria = 195; MAN, Man Shield = 112.

7.4. Chemical evolution of Ta provinces in Africa

Von Knorring (1970), in his review on pegmatites from orogenic belts of Africa (Kibara Belt, Damara Belt, Alto Ligonha Province/Mozambique Belt, Madagascar), expressed an opinion that regional geochemical patterns observed in these pegmatites probably reflect fundamental crustal variations. He pointed out high levels of tin in the Kibara and Damara Belts, associated with Nb, Ta, Zr, Hf and W, and variable Li and Be. In pegmatites of the Mozambique Belt and Madagascar, Sn is virtually absent, but pegmatites in these regions are characterised by Ti, Th, U, REE and Sc enrichment. Based on the data available at that time, von Knorring (1970) deduced the presence of a western "tin belt" (Kibara, Damara) and an eastern "rare-earth belt" (Mozambique, Madagascar).

Evaluation of the data from African Ta provinces strongly supports the hypothesis that the trace element compositions of TNO in pegmatite provinces are similar, irrespective of fractionation processes. Both median and P75 values of CGM populations, wodginite–ixiolite and tapiolite frequently show parallel trends in normalised trace element diagrams (Fig. 10). This implies that these features are related to the source of the pegmatites. Furthermore, mineralogical compositions of individual pegmatites and mineralised granites both in rare metal pegmatite and granite provinces are similar. Regional characteristics discriminate Ta–Nb–(Sn) ore provinces in Africa, as summarised in Table 7.

For the purpose of a better comparison, we decided to treat both pegmatites and rare-metal granites using the pegmatite classification (Černý and Ercit, 2005); ore-forming processes are very similar between both groups (see Section 7.1). In Table 7, the examined African rare-element pegmatite and rare-metal granite provinces are grouped according to their intrusion age, type (granite or pegmatite prevailing) and geochemical affinity, by using the LCT/NYF family classification. Deposits hosting Ta–Nb mineralisation dominated by Fe-rich columbite that is characterised by high concentrations of REE and Sc were attributed to the NYF family. This mainly applies to Archean and Proterozoic provinces in West and Central Africa (Man Shield, Congo Craton), Pan-African pegmatites of Madagascar and the anorogenic Sn–Nb-rich granites of central Nigeria. The remaining African Ta–Nb provinces are attributed to the LCT family, with the exception of Alto Ligonha that shows mixed LCT–NYF-type characteristics. LCT family pegmatites are characterised by CGM following Fe–Mn and Nb–Ta fractionation trends and typical trace element associations, including Li, Zr and Hf, at commonly low REE concentrations. Some minor and trace elements in TNO, such as Sn, Sb, Bi, Mg and U, show consistent patterns within the provinces.

Trends of compositional evolution, commonly regarded as fractionation trends, are clearly seen in CGM in many African Ta provinces (Fig. 7). Fe–Mn fractionation, and to a lesser degree Nb–Ta fractionation, have been explained by the increasing influence of F (Černý, 1989; Černý et al., 1986); however, experiments demonstrate that the content of volatile species such as F does not control Nb–Ta fractionation (Bartels et al., 2010; Fiege et al., 2011). Whereas fractionation trends of TNO in LCT-family pegmatites are well documented and understood, those in NYF pegmatites are not as clear. Ercit (1994) showed that CGM from Grenvillian (1.0 Ga) pegmatites in Canada comprise a broad range of Fe/Mn ratios but a limited variation in Ta/Nb. However, on the scale of single pegmatite bodies, Ta–Nb fractionation was also observed. In the Nine Mile pluton,

Table 7
African Ta provinces: age, type, mineralogy and geochemistry of Ta–Nb oxide minerals.

Section	Province/belt	Countries[a]	Deposits (examples)	Age (Ga)	REG/ REP+	LCT/NYF[b]	Mineralogy		Geochemistry REE type[c]	Trace element specialisation	Setting with respect to		Source rocks	
							TNO	Cassiterite			Intrusion of granite (type)	Deformation	Type	Age
4.1.1.	Man Shield	SL	Maburagwa	2.8–2.6	REP	NYF ?	Rt, FeC	x	1c, 2c, 5	Mg, Sc, REE, Ti, Zr, Th, W; (–Li, U, Sn)	?	?	Granite–greenstone terrane	Archean
4.1.2./4.2.2.	Congo Craton	CD	Enehe, Lubero	2.5–1.8	REP	NYF ?	FeC–FeT, Tap	x	1a, 1b	Mg, Sc, Y, REE, Ti, Hf, U, Th; (–Li, Sn)	?	Post?	Granite–greenstone terrane	Archean to Paleoproterozoic
4.1.3.	Zimbabwe Craton	ZW	Bikita, Benson, Sutswe	2.6	REP	LCT	MnC, Wdg	x	2a	Li, Be, Y, REE, Sb; Ti, Zr, Sn, Hf, Th, U, W; (–Mg)	Syn	Syn?	Greenstone belt	Archean
4.2.1.	Birimian Province	GH	Kokobin	2.1	REP	LCT	MnC–MnT		5b	Li, Sn, Hf, U; (–Sc, Y, REE, W, Bi)	Syn (S)	Post	Juvenile crust (granite–greenstone)	Paleoproterozoic
4.3.1.	Kibara Belt	CD, RW, BI, UG	Manono, Ruhanga, Nemba, Ndora	0.93–0.99	REP	LCT	CGM, Tap, Wdg, Mc, Rt	x	3a, 3b, 3c, 4a	Li, Mg, Sn, Hf; (–Sc, Y, REE, Sb, Bi, Th)	Syn (S, "G4")	Syn/post	heterogeneous continental crust, mafic intrusions	Paleo- to Neoproterozoic
4.3.2.	Orange River Belt	NA, ZA	Tantalite Valley	0.98	REP	LCT	MnC–MnT, Mc		2c	Li, Be, Sb, Bi, Zr, Hf, U; (–Mg, Sc, Sn)	Syn (S, I)	Post	heterogeneous continental crust, mafic intrusions	Paleo- to Neoproterozoic
4.3.3.	Kamativi Belt	ZW	Kamativi	1.0	REP	LCT	FeC–FeT, Tap	x	2a	Li, Sn, W; (–Sc, Y, Sb, Bi, Zr, Hf, Th, U)	Syn	Post	.Heterogeneous continental crust	Paleo- to Neoproterozoic
4.4.1.	ANS, granites (Eastern Desert)	EG	Nuweibi, Abu Dabbab	0.63	REG	NYF	MnC–MnT, Wdg, Mc	x	1d	Sc, Y, HREE, Mo, Zr, Hf, Sn, Th, U, W; (–Li, Mg)	Syn (A)	Post	Juvenile crust (oceanic, granites)	Neoproterozoic
4.4.2.	ANS, pegmatites	ET, SO	Kenticha, Bupo, Shuni Hill	0.53	REP	LCT	FeC–MnC–MnT		2a, 2b, 2c, 4, 5	Be, Ba, Bi, Zr, Hf; (–Sc, Y, REE, Sn, W)	Syn (I)	Post	Juvenile crust (oceanic, granites)	Neoproterozoic
4.4.3.	Alto Ligonha Province	MZ	Marropino, Moneia, Morrua, Somipe	0.4–0.5	REP	LCT + NYF	FeC–MnC–MnT, Mc, BiT, Eux		1a, 2a, 2b	Mg, Sc, Y, REE, Sb, Bi, Ti, Hf, Th, U; (–Sn)	Syn to post (A)	Post	Heterogeneous continental crust	Paleo- to Neoproterozoic
4.4.4.	Damara Belt	NA	Uis, Rubikon, Donkerhoek	0.5	REP	LCT	CGM, Tap, Wdg	x	2a, 3a	Li, Zr, Hf, W; (–Sc, Y, REE,Zr, Sn, Th)	Syn to post (S, A)	Post	Heterogeneous continental crust	Neoproterozoic
4.4.5.	Older Granites	NG	Lema, Maru, Olode, Sepeteri, Komu	0.5	REP	LCT	CGM, Tap, Wdg, SbT	x	1d, 5a	Li, Mg, Sb, Bi, Ti; (–Sc, Y, REE, Th, W)	Syn to post (S, A)	Post	Heterogeneous continental crust	Archean to Neoproterozoic
4.5.1.	Jos, Nigeria	NG	Jantar	0.2	REG	NYF	FeC–FeT, Tap, Ix, Fg, Eux	x	1d	Sc, Y, HREE, Mo, Sn, Th; (–Li, Hf, Sb, Bi, U)	Syn (A)	Anorogenic	Heterogeneous continental crust	Archean to Neoproterozoic

ANS: Arabian–Nubian Shield REG/REP + Rare-element granite; rare-element pegmatite.
[a] ISO 3166.
[b] LCT: Li, Cs, Ta-family; NYF: Nb, Y, F-family.
[c] Types according to Graupner et al. (2010).

Wausau syenite complex (Wisconsin, U.S.), constituting a Proterozoic anorogenic complex, CGM display prominent Nb–Ta fractionation with late enrichment of Ta in miarolitic NYF-family pegmatites at low Mn/Fe ratios (Falster et al., 1999). Thus, CGM from NYF-family pegmatites show similar fractionation trends to those observed in LCT-family pegmatites and their granitic equivalents. Using the "columbite–tantalite quadrilateral" diagram, the following pegmatite types can be identified in the African Ta provinces:

- Types characterised by vertical or subvertical Nb–Ta dominated fractionation patterns (virtually no Fe–Mn fractionation) typical of primitive potassic pegmatite phases and less fractionated pegmatites (Černý et al., 1986), such as those found in the Man Shield (Fig. 7a), the Congo Craton (Fig. 7b) and in rare-metal granites of the Jos Plateau (Fig. 7l). Such trends are common in beryl and spodumene-bearing pegmatites.
- The complex spodumene type (concomitant Fe–Mn and Nb–Ta fractionation) in the Birimian (Fig. 7d), Kamativi (Fig. 7f), Kenticha (Fig. 7h), Marropino, Morrua (Fig. 7i), Uis (Fig. 7j) and some of the pegmatites related to the Older Granites of Nigeria (Fig. 7k).
- The complex lepidolite type (initial horizontal Fe–Mn fractionation, followed by subvertical Nb–Ta fractionation), represented by the Muiane (Fig. 7i) and Maru pegmatites (Fig. 7k).
- The most evolved complex petalite, spodumene, lepidolite and pollucite-bearing types are found at Homestead (Fig. 7f), Kenticha (Fig. 7h), Moneia (Fig. 7i) and in some of the Damara Belt pegmatites (Fig. 7j).
- Abu Dabbab and Nuweibi, representing rare-metal granites, follow prominent Nb–Ta fractionation trends with little Fe–Mn fractionation starting off at high #Mn (>50). For a similar case in the pegmatites of the Mongolian Altai, possible contribution from Mn-enriched protoliths was discussed (Černý et al., 1986)
- CGM from pegmatites of the Kibara Belt do not adhere to one particular fractionation trend. All of the above-mentioned types were observed in these samples, with the complex lepidolite type (two-step fractionation: initial Mn and then Ta) observed most commonly (Fig. 7e) and the complex petalite types being the rarest.

Deviations from simple fractionation trends can often be observed, e.g. at Homestead or Kenticha (Küster et al., 2009), as well as at Manono and others, where trends from very Mn-rich to more Fe-rich compositions are detected at more or less constant Nb–Ta ratios. This is attributed to "contamination" with host rock material (e.g., Černý and Němec, 1995) or to late-stage metasomatic-hydrothermal overprint.

7.5. Temporal evolution of Ta provinces in Africa

The present study added further age constraints from radiometric dating of columbite–tantalite to the understanding of Ta mineralisation in Africa. The data obtained for individual provinces agree within the uncertainties of the methods (see Section 3 and Table 2; Gäbler et al., 2011). The U–Pb method for CGM has been introduced by Romer and Wright (1992) and was widely used in subsequent publications (e.g., Baumgartner et al., 2006; Dewaele et al., 2011; Küster et al., 2009; Sweetapple and Collins, 2002). Recoil effects in U-rich columbite–tantalite may severely affect the results, necessitating additional leaching steps (Romer, 2003). In the past, TIMS dating has been more commonly applied, whereas LA-ICP-MS methods were developed later (Smith et al., 2004). In the meantime, a large dataset has emerged indicating that results of U–Pb dating of CGM are comparable to those produced by independent methods, such as U–Pb geochronology of zircon and monazite, and Rb–Sr or Ar–Ar dating of mica (e.g., Baumgartner et al., 2006; Glodny et al., 1998). Although data points are not always concordant in the U–Pb concordia diagram, it is evident that the discordant ages produced by all methods have geological significance. From more than 70 TIMS and LA-ICP-MS CGM age determinations carried out in this project (Table 2), there is no evidence that the U–Pb system in CGM is susceptible to complete resetting or homogenisation during postmagmatic evolution (Melcher et al., 2008b, 2009). Only in one case, two age populations within a single crystal were identified; their explanation requires further work. In a few mineral concentrates, we encountered two or more age populations that imply contribution from different sources.

On a global scale, formation of granitic pegmatites peaked at 2.65–2.60, 1.9–1.85, 1.0–0.95 and 0.30–0.25 Ga within Laurasian crustal blocks, whereas Gondwana-derived blocks give less defined peaks of pegmatite activity at 2.85–2.80, 2.10–2.05, 1.20–1.15 and a major one at 0.55–0.50 Ga (Tkachev, 2011). In Africa, Ta–(Nb–Sn) mineralisation formed over a time period spanning from the Archean to the Cenozoic. In this chapter, we provide a summary of these events, while taking into consideration the major orogenic phases, granite intrusions, and timing of pegmatite formation with respect to orogeny (syn-, late-, post-orogenic; Fig. 18). Equivalent periods in other parts of the world will be briefly mentioned. Some Ta provinces in Africa that are not covered in the present work will be discussed.

7.5.1. Archean (2.8 and 2.5–2.6 Ga)

The 3.1 Ga old cassiterite-mineralised pegmatites in the Barberton Belt, Kaapvaal Craton, are Africa's oldest known pegmatites (Maphalala and Trumbull, 1998; Trumbull, 1993, 1995). The oldest CGM encountered in African Ta provinces, however, are from Sierra Leone (ca. 2.85 Ga), and appear to be coeval with a granite-forming event in the Man Shield (also termed the Kenema–Man domain of the Leo Rise, or the West African Craton; Thiéblemont et al., 2004). Such ages are also reported from pegmatites in the Murchison Belt on the Kaapvaal Craton (Poujol and Robb, 1999) and from the world's largest Ta pegmatites at Wodgina, Pilbara Craton, Western Australia (for references see Tkachev, 2011). A second period of Ta mineralisation is documented by the ca. 2.6 Ga age estimates of CGM from placer deposits in Sierra Leone. At about the same time, pegmatitic Ta mineralisation formed in the Zimbabwe Craton (Bikita, Fig. 3a; Benson mine; Table 2) in relation to late- to post-tectonic granite intrusions (e.g., Wedza and Chilimanzi suites, 2634–2517 Ma; Jelsma and Dirks, 2002; Jelsma et al., 1996) that have been interpreted as crustal melts formed due to loading following accretion.

The Archean pegmatites correspond to the Jequié orogeny (2.8 to 2.6 Ga) in South America, and to abundant pegmatite formation on the Yilgarn (Western Australia), Dharwar (India), Kola (Russia) and Superior Cratons (North America). An even younger age (2487 Ma; Table 2) at the Archean/Paleoproterozoic boundary has been reported for Ta mineralisation in the NE Congo Craton. It is coeval with a period of granitic magmatism in the late Archean (Milési et al., 2006).

7.5.2. Paleoproterozoic (2.2–2.0 Ga)

U–Pb ages obtained for CGM from southern Ghana indicate pegmatite formation at 2073–2085 Ma (Table 2; Melcher et al., 2008a) in the Birimian. The Birimian Supergroup is part of the Paleoproterozoic Baoulé–Mossi domain of the West African Craton and is composed of greenstone belts, volcano-sedimentary sequences and voluminous granitoids (Leube et al., 1990). The Birimian was a major juvenile crust-forming event, terminated by the Eburnean orogeny. Geochronological studies indicate formation of these rocks between ~2250 and 2050 Ma (Abouchami et al., 1990; Boher et al., 1992; Egal et al., 2002; Gasquet et al., 2003; Hirdes et al., 1992; Tapsoba et al., 2013; Taylor et al., 1992). Emplacement, deformation and metamorphism of most Paleoproterozoic rocks in Ghana occurred between 2190 and 2080 Ma (Oberthür et al., 1998). Volcanic belts and belt-type plutons represent the oldest rocks, followed by sediments of the Tarkwaian Group consisting of conglomerates, sandstones and minor argillites metamorphosed at low grades; Davis et al. (1994) constrained Tarkwaian sedimentation to 2132–2116 Ma. The youngest rocks are basin-type plutons (ca. 2100 Ma) coeval with the pegmatites. CGMs dated from

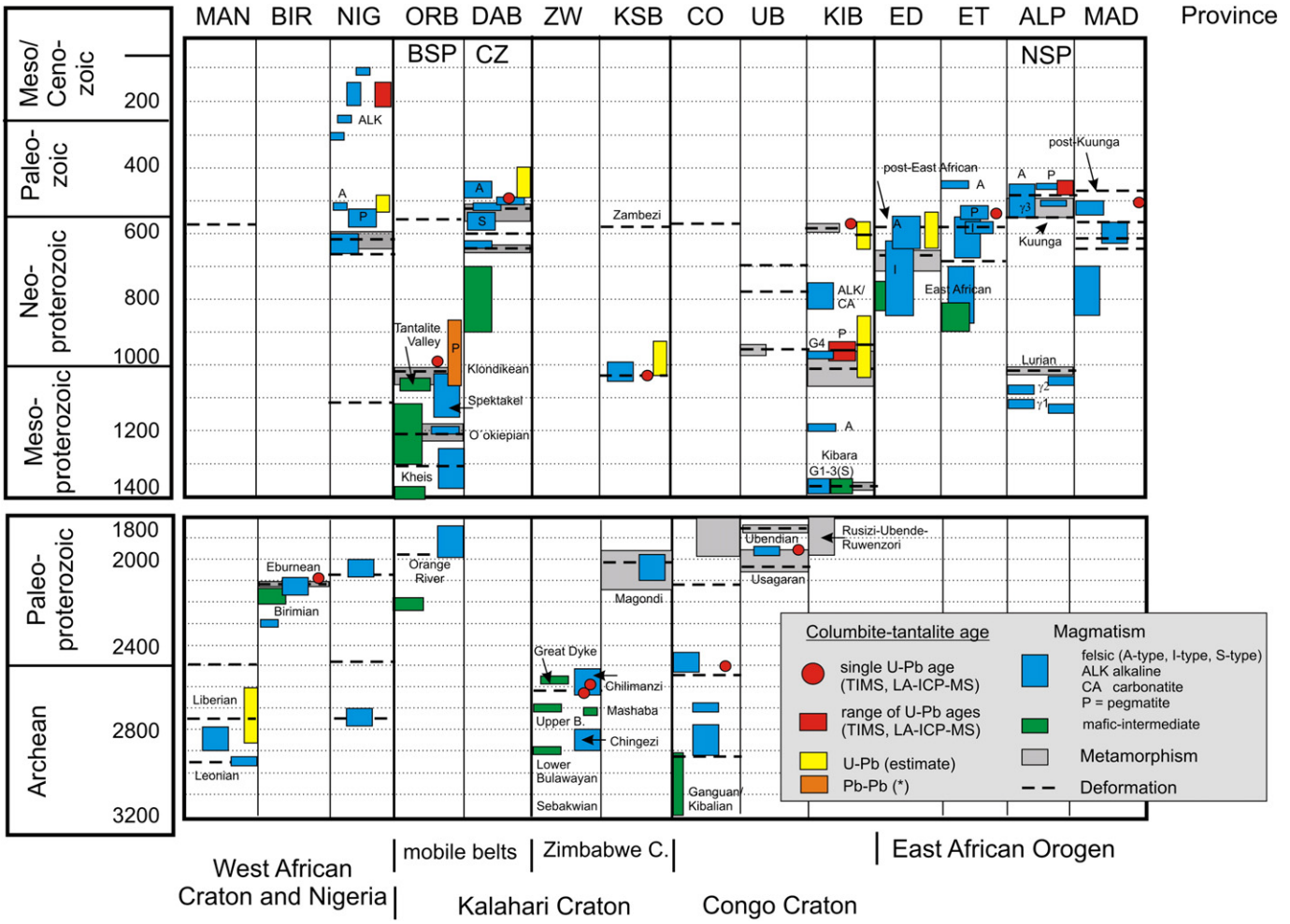

Fig. 18. Compilation of U–Pb ages determined for CGM from African Ta provinces, grouped to their tectonic position, and their relation to pegmatite and granite formation, deformation and orogenic events; in addition to our results, this summary includes data from Cahen and Snelling (1966), Matheis and Caen-Vachette (1983), Petters (1991), Hirdes et al. (1992), Lenoir et al. (1994a,b), Kröner et al. (1997), Jung et al. (1998, 2000, 2003), Woolley (2001), Cronwright (2005), Milési et al. (2006), Becker et al. (2006), Bingen et al. (2009), Küster et al. (2009), Goodenough et al. (2010), Tack et al. (2010), Ali et al. (2012), Fritz et al. (2013). Abbreviations: MAN, Man Shield; BIR, Birimian; NIG, Nigeria; ORB, Orange River Pegmatite Belt, BSP, Bushmanland sub-province; DAB, Damara Belt, CZ, Central Zone; ZW, Zimbabwe Craton; KSB, Kamativi Schist Belt; CO, NE Congo Craton; UB, Ubendian; KIB, Kibara Belt; ED, Eastern Desert, Egypt; ET, Adola Belt, Ethiopia; ALP, Alto Ligonha Province, NSP, Nampula sub-province; MAD, Madagascar. *Pb–Pb ages of U–REE-rich minerals in the Namaqualand Complex (Burger et al., 1965).

southern Ghana thus slightly postdate the Eburnean deformation and metamorphism.

Paleoproterozoic U–Pb ages (1876–2051 Ma) were documented for CGM from the transition zone between the NE Congo Craton and the Ubendian Belt, which is a linear, NW–SE trending orogenic belt that extends from northern Mozambique through Tanzania to the eastern part of the DRC (Cahen et al., 1984). It forms part of a larger Paleoproterozoic orogen developed around the western and south-western margins of the Archean Tanzanian Craton. The Ubendian Belt is characterised by an early deformation and granulite-facies metamorphism, isotopically dated at 2040–1950 Ma (Usagaran orogenic phase; De Waele et al., 2006). A second phase of deformation at 1880–1850 Ma (Ubendian orogenic phase) is characterised by large, NW–SE trending, dextral shear zones. Late- to post-kinematic granitoids occur principally along both the eastern and western marginal zones of the Ubendian Belt (Lenoir et al., 1994a). Since the Paleoproterozoic, the Ubendian Belt acted as a zone of displacement during successive orogenic and rift-forming events (Lenoir et al., 1994a). Around Uvira in the DRC, deformed metasediments and gneisses with N–S oriented structural trends are probable products of these events. These rocks are cut by poorly mineralised pegmatites dated at 2030 Ma (Rb–Sr age from microcline: Cahen and Snelling, 1966; Petters, 1991; Villeneuve, 1980).

The Paleoproterozoic event is also manifested by pegmatites and quartz veins with mica, beryl, CGM, topaz, tourmaline, cassiterite and wolframite from the 2150–2000 Ma Magondi Belt in Zimbabwe and from the Kasai–NE Angola Shield. In the latter, 2230 ± 48 Ma old pegmatites transect both Archean metasediments and metabasites, and Eburnean-age Lukoshi metasedimentary formations (Petters, 1991; e.g., Giraul pegmatite field: Gonçalves et al., 2008, 2009).

The Eburnean, Usagaran and Ubendian phases are correlatable with the Transamazonian orogeny in South America, between 2.1 and 1.8 Ga, Ta-bearing pegmatites occur in the Sao Francisco Craton, Brazil (e.g., Volta Grande pegmatite, 2121 Ma) and the North Guiana Pegmatite Belt (2083 Ma) on the Guiana Shield (Alkmim and Marshak, 1998; Tkachev, 2011).

7.5.3. Mesoproterozoic (ca. 1.0 Ga)

The Mesoproterozoic corresponds to a major episode of Ta mineralisation in Africa. Rare-metal pegmatites are found in the Kibara, Kamativi and Orange River Belts. The 1500 km long, NE trending Kibara Belt of central and eastern Africa is subdivided into the Karagwe–Ankole

Belt in the NE, and the Kibara Belt sensu stricto in the SW. Sedimentation started as early as 1.78 Ga ago, and was terminated by the Kibaran event, a major bimodal intracratonic magmatic and structural event (at 1375 Ma), accompanied by the emplacement of voluminous S-type granitoids, mafic rocks and layered mafic–ultramafic complexes (Tack et al., 2010). Later magmatic events included intrusion of A-type granitoids (1205 Ma) and tin-granites (986 Ma). Only the latter are associated with Ta–Sn–W–(Li–Be–P) mineralisation. U–Pb data for CGM range from 930 to 1030 Ma (Fig. 4c–f; Table 2) and peak at ca. 970 Ma (Dewaele et al., 2011; Melcher et al., 2008a, 2008b, 2009; Romer and Lehmann, 1995), i.e. overlap with a regional metamorphic event at 1079–966 Ma (determined from low Th/U overgrowths on zircon; Kokonyangi et al., 2006). Deformation and granite–pegmatite formation are interpreted as far-field effects of a global orogenic event manifested by the Irumide and Southern Irumide Belts (Fernandez-Alonso et al., 2012). A second compressional event affected the Kibara Belt as a far-field effect of the East African (Pan-African) orogeny at ca. 550–570 Ma; this compression is manifested by N–S-trending thrust sheets, isotopic resetting (Dewaele et al., 2011) and post-compressional (ca. 530 Ma) development of gold mineralisation (Brinckmann et al., 2001). Pan-African formation of CGM (Fig. 4f), cassiterite and zircon attest to a period of Ta–Sn mineralisation in the central rift area. Post-Kibaran deformation within the Kibara Belt is manifested by the N–S-trending Itombwe Basin west of Kivu Lake and northern Tanganyika Lake (Villeneuve, 1987); sedimentation in the basin started around 710 Ma ago, and deformation to a steeply folded synclinal structure postdates intrusion of alkaline complexes, which have been dated at 648 Ma (Numbi; Cahen et al., 1979).

U–Pb ages of 1030 Ma (Table 2) determined for CGM from the Paleoproterozoic Kamativi Schist Belt are slightly older than those for the Kibara Belt. The associated pegmatites have been dated at 990 ± 15 Ma (Rijks and van der Veen, 1972). The paleogeographic location of the Magondi Belt NW of the Zimbabwe Craton is close to the major compressional zone in the Irumide Belt (Fernandez-Alonso et al., 2012), where deformation and metamorphism occurred at 1050–950 Ma (De Waele et al., 2006).

CGM in pegmatites emplaced into the Tantalite Valley Complex of the Namaqua mobile belt crystallised at ca. 985 Ma ago (Fig. 4h, Table 2). The Namaqua Metamorphic Complex in western South Africa and southern Namibia is host to the Orange River Pegmatite Belt of the Aggeneys terrane in the Bushmanland sub-province. Crustal evolution here is characterised by two principal periods of juvenile crust formation (~2.2 and ~1.4 Ga), followed by the "Kheisian orogeny" at ~1.3 Ga and abundant mafic to intermediate igneous activity from ~1.3 to ~1.08 Ga (Becker et al., 2006; Eglington, 2006). Granitoids, locally showing an A-type geochemical signature (e.g., Spektakel suite, Little Namaqualand suite, Concordia granite) intruded during the Namaqua orogeny, from 1.21 (O'okiepian episode) to 1.02 Ga (e.g., Rietberg granite; Klondikean episode). Granite intrusion was accompanied by mafic plutons (Tantalite Valley Complex) and the anorthosite–charnockite-type Koperberg suite in the O'okiep terrane (Clifford and Barton, 2012). The Klondikean episode occurred prior to metamorphism and pegmatite formation at 1.02–1.04 Ga. The pegmatites were dated at 920–1040 Ma (Burger et al., 1965) and these data agree with the U–Pb ages of tantalite-(Mn) obtained in the present study.

The 1.0 Ga belts in Africa (Irumide, Natal, Namaqua) are, among others, correlatable to the Grenville Belt in North America, the Sveconorwegian Belt in Scandinavia and the Aravalli Belt in India, all of which host pegmatites (Tkachev, 2011).

7.5.4. Pan-African (0.6–0.4 Ga)

The rare-metal granites in the Eastern Desert of Egypt (e.g., Abu Dabbab and Nuweibi) represent the oldest of their kinds in orogenic belts (Tkachev, 2011) and were emplaced along late-orogenic structures into juvenile Neoproterozoic rocks including an early Pan-African subduction complex, which was deformed and metamorphosed under greenschist facies conditions between 715 and 640 Ma. There is considerable debate as to the timing of emplacement of the post-collisional A-type "younger granites". Single-crystal evaporation analyses of 10 zircon grains from Nuweibi yielded Pan-African apparent ages ranging from 610 ± 34 to 425 ± 24 Ma (Helba et al., 1997); however, these zircons are small, irregular and partly metamict. While previous studies gave Rb–Sr whole-rock isochron ages of 490 ±27 Ma (Nuweibi), 527 ± 26 Ma (Homr Akarem) and 541 ± 4 Ma (Homrit Mukbid) and Nd model ages of 0.96–1.7 Ga (Hassanen and Harraz, 1996), recent U–Pb zircon measurements gave an age of 620–630 Ma for the Homr Akarem and Homrit Mukbid plutons (Ali et al., 2012). The former authors assumed mixing of lower crust- or mantle-derived magmas and pre-Pan-African, LREE-enriched continental crust. In contrast, the Sm–Nd and U–Pb zircon data of Ali et al. (2012) indicate a juvenile Neoproterozoic magma source with no involvement of older crust. There is ample evidence that zircons in A-type granites are affected by late corrosive (F-rich) fluids; Ali et al. (2012) present arguments in favour of a late magmatic origin of such fluids, producing greisen mineralisation at the roof of the plutons. Younger U–Pb age estimates for tantalite from Abu Dabbab (ca. 550 Ma) may either be attributed to crystallisation from such fluids, or from interaction of late magmatic CGM with these fluids.

The rare-element pegmatites of the Kenticha field in the Adola Belt (Ethiopia) are related to the 550–520 Ma post-collisional phase of peraluminous I-type granitic magmatism (Küster et al., 2009). Tantalite-(Mn) from the Kenticha and Bupo pegmatites revealed U–Pb ages of ca. 530 ± 4 Ma (Küster et al., 2009), within error of the post-orogenic Robelie (554 ± 23 Ma) and Lega Dima (550 ± 18 Ma) biotite granite plutons that cut across 610 to 554 Ma old thrust shear zones. A coeval genetic relationship between the post-orogenic biotite granites and rare-element pegmatites remains poorly understood but the pegmatites are certainly not related to the anorogenic A-type granite magmatism, which is dated between 470 and 450 Ma in southwestern Ethiopia.

U–Pb ages of CGM from several pegmatites in the Nampula Complex, Alto Ligonha Province, range from 480 to 440 Ma (Table 2, Fig. 4i, j). They are in line with Pan-African granites in Alto Ligonha that yielded Rb–Sr and U–Pb ages close to 490 Ma and a SHRIMP zircon age of 453 ± 17 Ma (Cronwright, 2005). Monazites from the Somipe pegmatite were dated between 336 ± 25 and 557 ± 31 Ma using the electron microprobe (Cronwright, 2005), with a peak between 430 and 449 Ma. The Nampula Complex consists of amphibolite to granulite-facies felsic gneisses (1123–1042 Ma; Kröner et al., 1997) intruded by Pan-African syn- to post-kinematic high-K granitoid plutons that were emplaced between 533 and 495 Ma (Grantham et al., 2008); Bingen et al. (2009) reported U–Pb zircon and monazite ages of 511 ± 12 and 508 ± 3 Ma for granites in the northern part of the Nampula Complex. Metamorphism lasted from 520 to 493 Ma. Thus, most pegmatites postdate intrusion of the voluminous syntectonic Pan-African granites by about 30 to 60 Ma.

In Madagascar, which forms the southern extension of the Mozambique Belt, syntectonic (750–600 Ma) and post-tectonic pegmatites are distinguished (Petters, 1991).

Post-collisional granitoids gave a range of ages between 537 and 522 Ma (Maevarano suite of northern Madagascar; Goodenough et al., 2010). A U–Pb age of 506 Ma (Table 2), determined for columbite-(Fe) from an unknown location in Madagascar, appears to postdate the post-tectonic granite intrusions.

In the Damara Belt, pre-Damara basement gneisses with ages between 2.0 and 1.1 Ga are overlain by metasedimentary sequences that were metamorphosed under amphibolite to lower-granulite facies conditions from 665 to 645 Ma during an early Pan-African metamorphic event, and from 559 to 546 Ma (Northern Damara Belt), respectively, as well as from 527 to 515 Ma (Central Belt) during a late Pan-African

event. Five phases of granitoids intruding both basement and cover sequences are distinguished (Seth, 1999): (1) syn-tectonic granites emplaced at ca. 640 Ma, and (2) as the Salem granite suite, from 590 to 540 Ma, (3) syn-tectonic granites at 530–525 Ma, (4) post-tectonic granites from 510 to 505 Ma, and (5) post-collisional granites between 495 and 458 Ma (alaskites). Both syn- to post-tectonic granites were derived from lower crustal sources (Jung et al., 1998, 2003). Ta-bearing pegmatites are related to group (4), late- to post-tectonic granites, such as the Donkerhoek granite (dated at 505 ± 4 Ma using magmatic monazite; Kukla et al., 1991) which intruded into the Okahandja Lineament, a zone of crustal weakness in the Central Zone. This age is close to a U–Pb age of 505 Ma determined for columbite-(Mn) from the Rubikon pegmatite (Table 2). Rb–Sr whole-rock analyses and Ar–Ar dating of biotite and hornblende yielded ages between 448 and 465 Ma and indicate late orogenic rapid cooling ascribed to late-stage regional hydrothermal alteration. This phase is probably also manifested by some U–Pb age estimates for CGM from pegmatites in the Damara Belt (500 to 400 Ma).

U–Pb age estimates for CGM from various pegmatites in SW Nigeria (Oyo and Kwara States) and NW Nigeria (Maru Belt), which are associated with the Older Granites, range from 450 to 560 Ma (this work). The tonalitic to granitic plutons of Pan-African age formed in at least three episodes from 700 to 480 Ma (Matheis, 1987; Matheis and Caen-Vachette, 1983). They intruded a polyphase, heterogeneous migmatite–gneiss complex (2.0–3.0 Ga) and overlying schist belts which were derived from Paleoproterozoic volcanic-sedimentary sequences (Okunlola and Jimba, 2006). In central and SW Nigeria, foliated granites and charnockites have been dated between 632 and 605 Ma, whereas unfoliated post-kinematic plutons were emplaced from 590 to 535 Ma (Küster, 1990). The massive intrusion of the Nigerian crust by Older Granites is a product of collisional processes related to subduction at the eastern margin of the West African Craton. Rb–Sr dating of pegmatites in the central Nigerian pegmatite field (Gwon-Gwon and Nassarawa Eggon near Wamba) indicates emplacement ages of 555 and 535 Ma, respectively, whereas Rb–Sr model ages of muscovite scatter from 594 to 482 Ma (Matheis, 1987). Peralkaline A-type granitoids (syenites) were emplaced in the Maru Schist Belt in NW Nigeria around 510 Ma (Egbuniwe et al., 1985). Matheis (1987) pointed out that the mineralised rare-element pegmatites are not the final fractionation products of the Older Granites, because some are about 100 Ma younger than their host granites (Matheis and Caen-Vachette, 1983). Rather, the mineralised pegmatites are products of high-grade metamorphism enhanced by high heat flow along deep-seated continental lineaments.

Pan-African ages were also obtained for detrital Ta-mineral phases (mostly tapiolite, Fig. 10a) identified in a diamond–(gold–platinum) placer deposit west of the Great Dyke in Zimbabwe (Somabula; Oberthür et al., 2002) (Table 2). There are no Ta provinces of Pan-African age west of the Great Dyke. These grains, therefore, must derive from Pan-African pegmatites that occur somewhere east in the Mozambique Belt.

Rare-element pegmatites of Pan-African age are found in the Anti-Atlas area of Morocco (Angarf, Tazenakht; Schneiderhöhn, 1961) and in the Hoggar Mountains of Algeria (Cheilletz et al., 1992).

The Pan-African orogeny is equivalent to the Brasiliano orogeny that produced numerous rare-element pegmatite provinces in Brazil (e.g., Borborema, Araçuai). Pegmatites of similar age are also known from the Highland Complex Belt (Sri Lanka) and the Kerala Khondalite Belt (India) (Tkachev, 2011).

7.5.5. Mesozoic (<0.2 Ga)

Columbite-(Fe) from placer deposits mined on the Jos Plateau in central Nigeria yields U–Pb ages from 150 to 210 Ma (Fig. 4l, Table 2). This range coincides with intrusion ages of mineralised alkaline anorogenic ring complexes, i.e. 153–183 Ma (Woolley, 2001). Mineralisation (Sn, Zn, W, Nb, –Ta, Cu, Fe, Bi, U, REE) is confined to biotite granites affected by hydrothermal processes, which produced metasomatic disseminated pyrochlore/columbite–cassiterite mineralisation, pegmatites (columbite, thorite, uraninite), quartz veins (wolframite, scheelite, Bi minerals, cassiterite), replacement bodies and mineralised ring-dykes (Kinnaird, 1985). The alkaline rock suite, starting with volcanoes that were intruded by high-level granites and syenites, formed from melts generated along N–S oriented deep shear zones during the opening of the Benue Trough, producing >50 complexes that show progressively younger southward due to plate motion. The primary mantle origin of syenitic magmas parental to intraplate alkaline granites is well established. Substantial crustal contribution from Neoproterozoic and Pan-African basement sources is evident from Sr and Pb isotope work (Bowden, 1985).

The Cretaceous Chilwa Alkaline Province (southern Malawi) has an exceptional variety of lithologies ranging from carbonatite to granite (Eby et al., 1995; Woolley, 1987). Some of the peralkaline granites of the last period of igneous activity (ca. 113 Ma) host NYF-family pegmatites, e.g. at Mount Malosa with exceptional Ba–Be–REE mineralisation and pyrochlore as the major Nb carrier (Guastoni et al., 2003; Martin and De Vito, 2005).

The Tertiary (15.3 Ma) rare-metal granites carrying Ta [columbite-(Fe), Ta-rich rutile, wodginite] and W (ferberite) in the Internal Maghrebides of Algeria are part of the youngest episode of Ta mineralisation in Africa (Bouabsa et al., 2010).

8. Summary and conclusions

Rare-element pegmatites and rare-metal granites are complex and heterogeneous geological bodies. The investigation of heavy mineral fractions and especially of Ta–Nb phases in such rocks enables the definition of Ta ore provinces that share common mineralogical and geochemical features. Within an ore province, mineral compositions are characterised by specific trace element patterns that form under the influence of dominating fractionation-related and subordinate metasomatic-hydrothermal processes. Although the chemical variability is extensive on the grain scale (as manifested by abundant chemical zoning), as well as on the deposit scale (chemical and mineralogical zonation of many pegmatites), specific chemical and mineralogical features are typical of ore districts and provinces. The reason behind this phenomenon is currently unknown. However, the source rocks, degree, depth and conditions of melting, heat flow and tectonic regime all play their role on the regional scale of ore provinces. These large-scale effects will overlap with parameters intrinsic to migrating, fractionating and crystallising volatile rare metal-bearing residual melts, such as the concentration of volatile species and oxygen fugacity.

In Africa, five major periods of Ta mineralisation emerge from the data presented in this work:

- Archean (2.9–2.5 Ga), with numerous pegmatite deposits in the Zimbabwe, Kaapvaal, West African and Congo Cratons;
- Paleoproterozoic, with examples from the Birimian terrane (2.2–2.0 Ga) and the Ubendian Belt of northern Congo (2.4–1.9 Ga);
- early Neoproterozoic, which corresponds to a major pegmatite-forming event at ~1 Ga in central, eastern and southwestern Africa (Kibara Belt, Kamativi Belt, Orange River Belt);
- late Neoproterozoic to Paleozoic (0.6–0.4 Ga), with abundant mineralised granites and pegmatites along the Pan-African mobile belts surrounding the cratons;
- Mesozoic alkaline complexes of Jos, Nigeria.

Each period is characterised by peculiar mineralogical and geochemical features. In representative examples from these provinces, the major and trace element compositions of Ta–Nb-bearing oxides were studied in detail.

(1) Minerals of the columbite–tantalite group are the most abundant Ta–Nb minerals in all provinces. However, their compositions are extremely variable. Fe-rich types predominate in the Man Shield, Congo Craton and Jos Plateau. Mn-rich columbite–tantalite is typical of the pegmatites in the Alto Ligonha Province, Arabian–Nubian Shield and Tantalite Valley. Large compositional variations involving Fe–Mn fractionation, followed by Nb–Ta fractionation are common in pegmatites in the Kibara Belt, those associated with the Older Granites of Nigeria and some pegmatites in the Damara Belt of Namibia.
(2) Tapiolite is abundant only in the Kibara Belt and the Congo Craton and is of minor importance in the Kamativi and Damara Belts and in Nigeria.
(3) Wodginite and ixiolite are generally less abundant Sn-, Ti-, W- and Li-rich minerals, but are quite common constituents in pegmatites of Zimbabwe and are locally abundant in the Kibara Belt, Older Granites of Nigeria, Damara Belt and in rare-metal granites in the Eastern Desert.
(4) All provinces carry microlite and other pyrochlore-supergroup minerals. However, "primary" microlite is mainly restricted to Alto Ligonha and Eastern Desert of Egypt.
(5) Accumulations of rare Ta–Nb phases occur in some provinces (e.g., bismutotantalite at Alto Ligonha; stibiotantalite at Lema, Nigeria; foordite at Kubitaka, Kibara Belt; and an extremely unusual assemblage of simpsonite, cesplumtantite, lithiowodginite and Ba-rich microlite at Mumba, Kibara Belt).
(6) U–Y–REE-rich Ta–Nb minerals are abundant only in NYF-family pegmatites and, thus, are rare in the studied African deposits. However, variable proportions of these minerals were encountered in the Alto Ligonha Province, Jos Plateau and at Lutenga in the Kibara Belt.
(7) Nb–Ta-rich rutile is the major Ta–Nb phase in placer deposits of the Man Shield, whereas Ta-rich rutile occurs in some areas within the Kibara Belt.
(8) Cassiterite is present in large quantities in pegmatites of the Kibara Belt, Kamativi Belt, Congo Craton, Damara Belt, Older Granites of Nigeria and in mineralised granites in the Eastern Desert and Jos Plateau. Its occurrence coincides partly with Sn-rich TNO (wodginite, ixiolite, foordite) and with elevated Sn concentrations in CGM. On the other hand, some provinces (e.g., Alto Ligonha) and deposits like Kenticha in Ethiopia and Tantalite Valley are virtually cassiterite-free.

CGM, tapiolite, wodginite and ixiolite accommodate a multitude of trace elements. Most abundant are Ti, Zr, Sn, Hf, Th, U and W (commonly in the 100 to 10,000 ppm range). Other trace elements are less common. Major element fractionation trends and trace element abundances allow a general classification of the studied African Ta provinces into two groups and several subgroups. The groups largely correspond to the LCT/NYF-family classification.

The first group (LCT) comprises provinces with CGM showing large variations in Fe–Mn and Nb–Ta ratios and containing Li, with Sn as the dominant tetravalent cation, and W as a minor or trace element. A subgroup with low-W CGM includes the Birimian, Adola Belt and Older Granites of Nigeria. A second subgroup is characterised by low Sn levels (Tantalite Valley and Damara Belt). The Tantalite Valley and Bikita pegmatites are unusual in that they contain CGM with appreciable concentrations of Be, Sb, Bi, and high levels of Hf, Zr, U and Th, despite the LCT character of their host pegmatites.

The vast dataset collected from numerous pegmatites in the Kibara Belt of Central Africa illustrates several key features of pegmatite provinces: (1) trace elements show log-normal distributions; (2) extreme values for any trace element may occur within the same province — even mixed LCT–NYF or pure NYF pegmatites might be present in small amounts; (3) the median values for all data from a given province define a robust province average; and (4) U–Pb mineral formation ages are scattered over a significant period of time (ca. 60–80 Ma in the Kibara case).

The second group has affinities to the NYF family with CGM characterised by Fe > Mn and Nb > Ta, and Mg as an important substituent cation. The concentrations of Sc, W and REE + Y are high, and Ti, Th and Mo are important additional constituents. Within this group, a subgroup is identified with low Sn levels (Man Shield, Congo Craton, Mozambique), and another subgroup with high Ta levels (mixed LCT/NYF) and sometimes Li (Mozambique, Congo Craton, Eastern Desert). The anorogenic granite-hosted mineralisation associated with the Younger Granites of Nigeria has typical NYF features, indicated by low Li, Pb, Al and U, and high Fe, Nb, Mg, Sc, REE + Y, Mo, Hf, Th and W contents.

Most LCT-family pegmatites are post-orogenic and post-tectonic with respect to a regional metamorphic event. The characteristic trace element associations found in TNO from the LCT pegmatites may stem from the presence of a thick package of metasedimentary rocks underlying the intrusion. Some of the observed variations may be explained by contributions from felsic and mafic igneous rocks, old continental or oceanic crust, or from the upper mantle.

The origin of the trace element distributions observed in the NYF and mixed LCT/NYF groups is more difficult to explain. The rare-metal granites of the Central Eastern Desert of Egypt were emplaced along late-orogenic structures into juvenile Neoproterozoic rocks including an early Pan-African subduction complex. The numerous pegmatites of the Alto Ligonha Province, Mozambique, were emplaced during the Paleozoic into a metamorphosed basement, as revealed by the U–Pb ages of CGM (440–480 Ma). Their complex geochemical and mineralogical character points to a heterogeneous source and a long-lived magma-generation process postdating typical post-collisional A-type magmatism. Similar observations, including CGM U–Pb ages younger than post-orogenic granite plutons, were also made in some LCT-dominated provinces, such as the Damara Belt and for some of the pegmatites associated to the Younger Granites of Nigeria.

Despite textural complexities, such as complex zoning patterns and multiple mineralisation stages, the chemical compositions of CGM, tapiolite and wodginite–ixiolite from rare-metal granite and rare-element pegmatite provinces indicate that they are cogenetic and reflect specific source characteristics that may be used to determine their origin.

Acknowledgements

The project "Analytical Fingerprint of Coltan" was partly funded by the Federal Ministry for Economic Cooperation and Development (BMZ). Thanks to numerous individuals, companies and institutions that contributed samples from African pegmatite deposits: Naturhistorisches Museum Wien, Mineralogisch-Petrographische Abteilung (sample K1208); Mineralogisches Museum der TU Bergakademie Freiberg (samples 04/42/001/40015 and 40016); Museum für Naturkunde, Berlin; Royal Museum for Central Africa, Tervuren; Geology Department, University of Zimbabwe, Harare; Fernando Lastra, CANMET, Ottawa, Canada; Arno Mücke, Göttingen; Ulrich Vetter, Hannover; Hermann Wotruba, Aachen; Dirk Küster, BGR; Steffen Jahn, Hannover; A.O. Olugbenda, Nigeria; A.M.H. Asran, Sohag, Egypt; Reiner Ellmies, Geological Survey of Namibia. Field work was supported by the Geological Surveys of Ethiopia, Mozambique, Namibia and Rwanda, and by local mining companies. We greatly acknowledge the invaluable and continuous analytical support of our BGR technicians Peter Rendschmidt, Don Henry, Gina Ehlers, Simone Sturm, Jerzy Lodziak, Monika Bockrath, Peter Macaj, Detlef Klosa and Frank Korte. Helene Brätz, University of Erlangen, is acknowledged for conducting LA-ICP-MS measurements. Numerous TIMS analyses were carried out by Don Davis, Jack Satterly Geochronology Laboratory, University of Toronto, Canada. The valuable suggestions by Milan Novák, K.M. Goodenough, two anonymous reviewers, and of editor Anton Chakhmouradian are gratefully acknowledged.

Appendix A. Supplementary data

Supplementary data to this article can be found online at http://dx.doi.org/10.1016/j.oregeorev.2013.09.003.

References

Abdalla, H.M., Helba, H.A., Mohamed, F.H., 1998. Chemistry of columbite–tantalite minerals in rare metal granitoids, Eastern Desert, Egypt. Mineral. Mag. 62, 821–836.

Abouchami, W., Boher, M., Michard, A., Albarede, F., 1990. A major 2.1 Ga event of mafic magmatism in West Africa: an early stage of crustal accretion. J. Geophys. Res. 95 (B11), 17605–17629.

Akintola, O.F., Adekeye, J.I.D., 2008. Mineralization potentials of pegmatites in the Nasarawa area of central Nigeria. Earth Sci. Res. J. 12, 213–234.

Ali, K.A., Moghazi, A.-K.M., Maurice, A.E., Omar, S.A., Wang, Q., Wilde, S.A., Moussa, E.M., Manton, W.I., Stern, R.J., 2012. Composition, age, and origin of the 620 Ma Humr Akarim and Humrat Mukbid A-type granites: no evidence for pre-Neoproterozoic basement in the Eastern Desert, Egypt. Int. J. Earth Sci. 101, 1705–1722.

Alkmim, F.F., Marshak, S., 1998. Transamazonian Orogeny in the Southern Sao Francisco Craton Region, Minas Gerais, Brazil: evidence for Paleoproterozoic collision and collapse in the Quadrila'tero Ferrífero. Precambrian Res. 90, 2–58.

Allou, B.A., Lu, H.-Z.H., Guha, J., Carignan, J., Naho, J., Pothin, K., Yobou, R., 2005. Une corrélation génétique entre les roches granitiques, et les dépots éluvionnaires, colluvironnaires et alluvionnaires de colombo-tantalite d'Issia, Centre-Ouest de la Cote d'Ivoire. Explor. Min. Geol. 14, 61–77.

Anders, E., Grevesse, N., 1989. Abundances of the elements: meteoritic and solar. Geochim. Cosmochim. Acta 53, 197–214.

Angermeier, H.O., Krauss, U., Kruszona, M., Schmidt, H., 1974. Zaïre. Rohstoffwirtschaftliche Länderberichte. Bundesanstalt für Bodenforschung, Hannover (120 pp.).

Anonymous, 2009. Geological Map of Ghana 1:1 000 000. Geological Survey Department (GSD), Accra, Republic of Ghana in cooperation with Bundesanstalt für Geowissenschaften und Rohstoffe (BGR), Hannover, Federal Republic of Germany.

Anthony, J.W., Bideaux, R.A., Bladh, K.W., Nichols, M.C., 1997. Handbook of mineralogy. Halides, Hydroxides, Oxides, vol. III. Mineral Data Publishing, Tucson, Arizona.

Atencio, D., de Andrade, M.B., Christy, A.G., Giere, R., Kartashev, P.M., 2010. The pyrochlore supergroup of minerals: nomenclature. Can. Mineral. 48, 673–698.

Atencio, D., Filho, R.R.C., Mills, S.J., Coutinho, J.M.V., Honorato, S.B., Ayala, A.P., Ellena, J., de Andrade, M.B., 2011. Rankamaite from the Urubu pegmatite, Itinga, Minas Gerais, Brazil: crystal chemistry and Rietveld refinement. Am. Mineral. 96, 1455–1460.

Baldwin, J.R., Hill, P.G., Finch, A.A., von Knorring, O., Oliver, G.J.H., 2005. Microlite–manganotantalite exsolution lamellae: evidence from rare-metal pegmatite, Karibib, Namibia. Min. Mag. 69, 917–935.

Barros, R.M., Vicente, C.A.M., 1963. Estudo dos campos pegmatiticos da Zambezia relatorio da mossão de estudos em Moçambique campanha de 1963. Junta de Energia Nuclear, 1 (133 pp.).

Bartels, A., Holtz, F., Linnen, R.L., 2010. Solubility of manganotantalite and manganocolumbite in pegmatite melts. Am. Mineral. 95, 537–544.

Bassot, J.-P., Morio, M., 1989. Morphologie et mise en place de la pegmatite kibarienne à Sn, Nb, Ta, Li de Manono (Zaire). Chron. Rech. Min., 496 41–56.

Baumgartner, R., Romer, R.L., Moritz, R., Sallet, R., Chiaradia, M., 2006. Columbite–tantalite-bearing granitic pegmatites from the Seridó Belt, northeastern Brazil: genetic constraints from U–Pb dating and Pb isotopes. Can. Mineral. 44, 69–86.

Becker, T., Schreiber, U., Kampunzu, A.B., Armstrong, R., 2006. Mesoproterozoic rocks of Namibia and their plate tectonic setting. J. Afr. Earth Sci. 46, 112–140.

Belkasmi, M., Cuney, M., Pollard, P.J., Bastoul, A., 2000. Chemistry of the Ta–Nb–Sn–W oxide minerals from the Yichun rare metal granite (SE China): genetic implications and comparison with Moroccan and French Hercynian examples. Min. Mag. 64, 507–523.

Berger, A., Gnos, E., Schreurs, G., Fernandez, A., Rakotondrazafy, M., 2006. Late Neoproterozoic, Ordovician and Carboniferous events recorded in monazites from southern-central Madagascar. Precambrian Res. 144, 278–296.

Bering, D., 1976. Bericht über eine Vorbereisung der Tantalit-Vorkommen im Raume Akim-Oda in Ghana. Unpublished report, Bundesanstalt für Geowissenschaften und Rohstoffe, Archive-Nr. 75077, 16 p.

Bermanec, V., Tomasic, N., Kniewald, G., Back, M.E., Zagler, G., 2008. Nioboaeschynite-(Y), a new member of the aeschynite group from the Bear Lake diggings, Haliburton County, Ontario, Canada. Can. Mineral. 46, 395–402.

BGS World Mineral Production, 2012. World Mineral Production 2006–2010. British Geological Survey, Natural Environment Research Council, Keyworth, Nottingham (78 pp.).

Bingen, B., Jacobs, J., Viola, G., Henderson, I.H.C., Skar, O., Boyd, R., Thomas, R.J., Solli, A., Key, R.M., Daudi, E.X.F., 2009. Geochronology of the Precambrian crust in the Mozambique belt in NE Mozambique, and implications for Gondwana assembly. Precambrian Res. 170, 231–255.

Boelema, R., Hira, H., 1998. Pegmatite deposits. The mineral resources of South Africa. In: Wilson, M.G.C., Anhaeusser, C.R. (Eds.), Council for Geoscience. Handbook, 16, pp. 509–521.

Boher, M., Abouchami, W., Michard, A., Albarede, F., Arndt, N., 1992. Crustal growth in West Africa at 2.1 Ga. J. Geophys. Res. 97 (B1), 345–369.

Bouabsa, L., Marignac, C., Chabbi, R., Cuney, M., 2010. The Filfila (NE Algeria) topaz-bearing granites and their rare metal minerals: petrologic and metallogenic implications. J. Afr. Earth Sci. 56, 107–113.

Bowden, P., 1985. The geochemistry and mineralization of alkaline ring complexes in Africa (a review). J. Afr. Earth Sci. 3, 17–39.

BRGM, 1987. Plan Minéral du Rwanda (437 pp.).

Brinckmann, J., Lehmann, B., Hein, U., Höhndorf, A., Mussallam, K., Weiser, T., Timm, F., 2001. La géologie et la minéralisation primaire de l'or de la chaîne Kibarienne, nord-ouest du Brunudi, Afrique orientale. Geol. Jahrb. D101, 3–195.

Burger, A.J., Hugo, P.J., Strelow, F.W.E., 1965. Radiometric dating of certain pegmatites in the Kenhardt and Gorgonia Districts, Cape Province. Ann. Geol. Surv. S. Afr., 4 87–98.

Buttgenbach, H., 1933. Minéraux du Congo belge. Bull. Soc. Géol. Belg. 56, 327–328.

Cahen, L., Snelling, N.J., 1966. The Geochronology of Equatorial Africa. North Holland, Amsterdam.

Cahen, L., Ledent, D., Villeneuve, M., 1979. Existence d'une chaîne plissée protérozoïque supérieur au Kivu oriental (Zaïre): données géochronologiques relatives au Supergroupe de l'Itombwe. Bull. Soc. Belg. Géol. 88, 71–83.

Cahen, L., Snelling, N.J., Delhal, J., Vail, J.R., Bonhomme, M., Ledent, D., 1984. The Geochronology and Evolution of Africa. Clarendon Press, Oxford (512 pp.).

Černý, P., 1989. Characteristics of pegmatite deposits of tantalum. In: Möller, P., Černý, P., Saupé, F. (Eds.), Lanthanides, Tantalum and Niobium. Springer, Berlin, Heidelberg, New York, pp. 195–239.

Černý, P., 1990. Distribution, affiliation and derivation of rare-element granitic pegmatites in the Canadian Shield. Geol. Rundsch. 79, 183–226.

Černý, P., 1991a. Rare-element granite pegmatites. I. Anatomy and internal evolution of pegmatite deposits. Geosci. Can. 18, 49–67.

Černý, P., 1991b. Fertile granites of Precambrian rare-element pegmatite fields: is geochemistry controlled by tectonic setting or source lithologies? Precambrian Res. 51, 429–468.

Černý, P., 1992. Geochemical and petrogenetic features of mineralization in rare-element granitic pegmatites in the light of current research. Appl. Geochem. 7, 393–416.

Černý, P., 2005. The Tanco rare-element pegmatite deposit, Manitoba: Regional context, internal anatomy, and global comparisons. In: Linnen, R.L., Samson, I.M. (Eds.), Rare-Element Geochemistry and Mineral Deposits. Geological Association of Canada, Short Course Notes, 17, pp. 127–158.

Černý, P., Chapman, R., 2001. Exsolution and breakdown of scandium and tungstenian Nb–Ta–Ti–Fe–Mn phases in niobian rutile. Can. Mineral. 39, 93–101.

Černý, P., Ercit, T.S., 1985. Some recent advances in the mineralogy and geochemistry of Nb and Ta in rare-element granitic pegmatites. Bull. Mineral. 108, 499–532.

Černý, P., Ercit, T.S., 1989. Mineralogy of niobium and tantalum: crystal chemical relationships, paragenetic aspects and their economic implications. In: Möller, P., et al. (Ed.), Lanthanides. Tantalum and Niobium. Springer Verlag, Berlin, Germany, pp. 27–79.

Černý, P., Ercit, T.S., 2005. The classification of granitic pegmatites revisited. Can. Mineral. 43, 2005–2026.

Černý, P., Němec, D., 1995. Pristine vs. contaminated trends in Nb, Ta-oxide minerals of the Jihlava pegmatite district, Czech Republic. Miner. Petrol. 55, 117–129.

Černý, P., Goad, B.E., Hawthorne, F.C., Chapman, R., 1986. Fractionation trends of the Nb- and Ta-bearing oxide minerals in the Greer Lake pegmatitic granite and its pegmatite aureole, southeastern Manitoba. Am. Mineral. 71, 501–517.

Černý, P., Fransolet, A.M., Ercit, T.S., Chapman, R., 1988. Foordite $SnNb_2O_6$, a new mineral species, and the foordite–thoreaulite series. Can. Mineral. 26, 889–898.

Černý, P., Ercit, T.S., Wise, M.A., 1992. The tantalite–tapiolite gap; natural assemblages versus experimental data. Can. Mineral. 30, 587–596.

Černý, P., Chapman, R., Ferreira, K., Smeds, S.-A., 2004. Geochemistry of oxide minerals of Nb, Ta, Sn, and Sb in the Varuträsk granitic pegmatite, Sweden: the case of an "anomalous" columbite–tantalite trend. Am. Mineral. 89, 505–518.

Černý, P., Blevin, P.L., Cuney, M., London, D., 2005. Granite-related ore deposits. Econ. Geol. 100th Anniversary Volume. 337–370.

Černý, P., Ercit, T.S., Smeds, S.-A., Groat, L.A., Chapman, R., 2007. Zirconium and hafnium in minerals of the columbite and wodginite groups from granitic pegmatites. Can. Mineral. 45, 185–202.

Černý, P., London, D., Novák, M., 2012. Granitic pegmatites as reflections of their sources. Elements 8, 289–294.

Cheilletz, A., Bertrand, J.M., Charoy, B., Moulahoum, O., Bouabsa, L., Farrar, E., Zimmermann, J.L., Dautel, D., Archibald, D.A., Boullier, A.M., 1992. Géochimie et géochronologie Rb–Sr, K–Ar et $^{40}Ar/^{39}Ar$ des complexes granitiques pan-africains de la région de Tamanrasset (Algerie); relations avec les minéralisations Sn–W associées et l'evolution tectonique du Hoggar central. Bull. Soc. Geol. Fr. 163, 733–750.

Clifford, T.N., Barton, E.S., 2012. The O'okiep copper district, Namaqualand, South Africa: a review of the geology with emphasis on the petrogenesis of the cupriferous Koperberg suite. Miner. Deposita 47, 837–857.

Cronwright, M.S., 2005. A Review of the Rare-element Pegmatites of the Alto Ligonha Pegmatite Province, Northern Mozambique and Exploration Guidelines. MSc thesis (unpublished), Rhodes University, Grahamstown, South Africa.

Davis, D.W., Hirdes, W., Schaltegger, E., Nunoo, E.A., 1994. U/Pb age constraints on deposition and provenance of Birimian and gold-bearing Tarkwaian sediments in Ghana, West Africa. Precambrian Res. 67, 89–107.

De Clercq, F., Muchez, P., Dewaele, S., Boyce, A., 2008. The tungsten mineralisation at Nyakabingo and Gifurwe (Rwanda): preliminary results. Geol. Belg. 11 (3–4), 251–258.

De Kun, N., 1960. Die Zinn-Niob-Tantal-Lagerstätten des Bezirks von Nord-Lugulu in Belgisch Kongo. N. Jb. Mineral. (Abh.) 95, 106–140.

De Vito, C., Pezzota, F., Ferrini, V., Aurisicchio, C., 2006. Nb–Ti–Ta oxides in the gem-mineralized and "hybrid" Anjanabonina granitic pegmatite, central Madagascar: a record of magmatic and postmagmatic processes. Can. Mineral. 44, 87–103.

De Waele, B., Liégeois, J.-P., Nemchin, A.A., Tembo, F., 2006. Isotopic and geochemical evidence of Proterozoic episodic crustal reworking within the Irumide belt of south-central Africa, the southern metacratonic boundary of an Archaean Bangweulu Craton. Precambrian Res. 148, 225–256.

Delbos, L., 1965. Influence du cycle récemt de 500 millions d'années sur les minéralisations de Madagascar. Sci. Terre Tome X (3–4), 521–533 (1964–1965).

Deschamps, Y., Hocquard, C., Pelon, R., Milési, J.P., Ralay, F., 2006. Geology and Ta Ore Deposits (Africa). BRGM, Map 1:10,000,000.
Dewaele, S., Tack, L., Fernandez-Alonso, M., Boyce, A., Muchez, P., Schneider, J., Cooper, G., Wheeler, K., 2008. Geology and mineralization of the Gatumba area, Rwanda (Central Africa): present state of knowledge. Etudes Rwandaises 16, 6–24.
Dewaele, S., De Clerq, F., Muchez, P., Schneider, J., Burgess, R., Boyce, A., Fernandez-Alonso, M., 2010. Geology of the cassiterite mineralisation in the Rutongo area, Rwanda (Central Africa): current state of knowledge. Geol. Belg. 13 (1–2), 91–112.
Dewaele, S., Henjes-Kunst, F., Melcher, F., Sitnikova, M., Burgess, R., Gerdes, A., Fernandez-Alonso, M., De Clerq, F., Muchez, P., Lehmann, B., 2011. Late Neoproterozoic overprinting of the cassiterite and columbite–tantalite bearing pegmatites of the Gatumba area, Rwanda (Central Africa). J. Afr. Earth Sci. 61, 10–26.
Dias, M.B., Wilson, W.E., 2000. The Alto Ligonha pegmatites Mozambique. Mineral. Rec. 31, 459–496.
Diehl, B.J.M., 1992. Niobium and tantalum. The Mineral Resources of Namibia.Ministry of Mines and Energy, Geological Survey, Windhoek 1–15.
Dill, H.G., Melcher, F., Füßl, M., Weber, B., 2007. The origin of rutile–ilmenite aggregates ("nigrine") in alluvial–fluvial placers of the Hagendorf pegmatite province, NE Bavaria, Germany. Miner. Petrol. 89, 133–158.
Eby, G.N., Roden-Tice, M., Krueger, H.L., Ewing, W., Faxon, E.H., Woolley, A.R., 1995. Geochronology and cooling history of the northern part of the Chilwa alkaline province, Malawi. J. Afr. Earth Sci. 20, 275–288.
Egal, E., Thiéblemot, D., Lahondère, D., Guerrot, C., Costea, C.A., Iliescu, D., Delor, C., Goujou, J.-C., Lafon, J.M., Tegyey, M., Diaby, S., Kolié, P., 2002. Late Eburnean granitization and tectonics along the western and northwestern margin of the Archean Kénéma–Man domain (Guinea, West African Craton). Precambrian Res. 117, 57–84.
Egbuniwe, I.G., Fitches, W.R., Bentley, M., Snelling, N.J., 1985. Late Pan-African syenite–granite plutons in NW Nigeria. J. Afr. Earth Sci. 3, 427–435.
Eglington, B.M., 2006. Evolution of the Namaqua–Natal Belt, southern Africa — a geochronological and isotope geochemical review. J. Afr. Earth Sci. 46, 93–111.
El-Sharkawy, M.F., 2001. Nb–Ta bearing minerals in a metasomatized granite, Eastern Desert, Egypt. In: Piestrzynski, et al. (Ed.), Mineral Deposits at the Beginning of the 21st Century. Swets & Zeitlinger Publishers, Krakow, pp. 485–487 (Lisse).
Ercit, T.S., 1986. The Simpsonite Parageneses: The Crystal Chemistry and Geochemistry of Extreme Tantalum Fractionation. (PhD Thesis) Univ Manitoba, Winnipeg.
Ercit, T.S., 1994. The geochemistry and crystal chemistry of columbite-group minerals from granitic pegmatites, southwestern Grenville province, Canadian Shield. Can. Mineral. 32, 421–438.
Ercit, T.S., 2005a. REE-enriched granitic pegmatites. In: Linnen, R.L., Samson, I.M. (Eds.), Rare-element Geochemistry and Mineral Deposits. Geol. Soc. Canada, GAC Course Notes, 17, pp. 175–199.
Ercit, T.S., 2005b. Identification and alteration trends of granitic-pegmatite-hosted (Y, REE, U, Th)–(Nb, Ta, Ti) oxide minerals: a statistial approach. Can. Mineral. 43, 1291–1303.
Ercit, T.S., 2010. Hidden story of tapiolite. Min. Mag. 74, 715–729.
Ercit, T.S., Hawthorne, F.C., Černý, P., 1992a. The wodginite group. I. Structural crystallography. Can. Mineral. 30, 597–611.
Ercit, T.S., Černý, P., Hawthorne, F.C., McCammon, C.A., 1992b. The wodginite group. II. Crystal chemistry. Can. Mineral. 30, 613–631.
Ercit, T.S., Cerny, P., Hawthorne, F.C., 1992c. The wodginite group; III, classification and new species. Can. Mineral. 30, 633–638.
Ercit, T.S., Wise, M.A., Cerny, P., 1995. Compositional and structural systematic of the columbite group. Am. Mineral. 80, 613–619.
Falster, A.U., Simmons, W.B., Webber, K.L., Buchholz, T., 1999. The Wausau syenite complex, Marathon County, Wisconsin: origin, geochemistry, and mineralogy of a mid-Proterozoic anorogenic intrusive complex and its pegmatites. Can. Mineral. 37, 835–836.
Fandrich, R., Gu, Y., Burrows, D., Moeller, K., 2007. Modern SEM-based mineral liberation analysis. Int. J. Miner. Process. 84, 310–320.
Fernandez-Alonso, M., Cutten, H., De Waele, B., Tack, L., Tahon, A., Baudet, D., Barritt, S.D., 2012. The Mesoproterozoic Karagwe–Ankole Belt (formerly the NE Kibara Belt): the result of prolonged extensional intracratonic basin development punctuated by two short-lived far-field compressional events. Precambrian Res. 216–219, 63–86.
Fetherston, J.M., 2004. Tantalum in Western Australia. Mineral Res. Bull., 22. Geological Survey of Western Australia (153 S.).
Fiege, A., Kirchner, C., Holtz, F., Linnen, R.L., Dziony, W., 2011. Influence of fluorine on the solubility of manganotantalite ($MnTa_2O_6$) and manganocolumbite ($MnNb_2O_6$) in granitic melts — an experimental study. Lithos 122, 165–174.
Foord, E.E., 1982. Minerals of tin, titanium, niobium and tantalum in granitic pegmatites. In: Černý, Petr (Ed.), Granitic Pegmatites in Science and Industry. Short Course Handbook, vol. 8. Min. Ass. Canada, pp. 187–238.
Förster, H.-J., 1998. The chemical composition of REE–Y–Th–U-rich accessory minerals in peraluminous granites of the Erzgebirge–Fichtelgebirge region, Germany. Part II: xenotime. Am. Mineral. 83, 1302–1315.
Fransolet, A.M., Keller, P., Fontan, F., 1986. The phosphate mineral associations of the Tsaobismund pegmatite, Namibia. Contrib. Mineral. Petrol. 92, 502–517.
Friese, A., 2010. Development of a Fingerprint of Columbite Group Minerals from the Kenticha Rare-element Pegmatite, Ethiopia on the Basis of Trace Element Geochemistry. (Diploma thesis) Geozentrum Nordbayern, Erlangen.
Frindt, S., Haapala, I., Pakkanen, L., 2004. Anorogenic Gross Spitzkoppe granite stock in central western Namibia: part I. Petrology and geochemistry. Am. Mineral. 89, 841–856.
Fritz, H., Abdelsalam, M., Ali, K.A., Bingen, B., Collins, A.S., Fowler, A.R., Ghebreab, W., Hauzenberger, C.A., Johnson, P., Kusky, T., Macey, P., Muhongo, S., Stern, R.J., Viola, G., 2013. Orogen styles in the East African orogens: a review of the Neoproterozoic to Cambrian tectonic evolution. J. Afr. Earth Sci. 86, 65–106.
Gäbler, H.-E., Melcher, F., Graupner, T., Bahr, A., Sitnikova, M., Henjes-Kunst, F., Oberthür, T., Brätz, H., Gerdes, A., 2011. Speeding up the analytical workflow for coltan fingerprinting by an integrated mineral liberation analysis/LA-ICP-MS approach. Geostand. Geoanal. Res. 35, 431–448.
Galliski, M.A., Černý, P., 2006. Geochemistry and structural state of columbite-group minerals in granitic pegmatites of the Pampean ranges, Argentina. Can. Mineral. 54, 645–655.
Galliski, M.A., Marquez-Zavalia, M.F., Cooper, M.A., Černý, P., Hawthorne, F.C., 2001. Bismutotantalite from northwestern Argentina: description and crystal structure. Can. Mineral. 39, 103–110.
Garrett, N., Mitchell, H., 2009. Trading conflict for development. Utilising the Trade in Minerals from Eastern DR Congo for Development.Resource Consulting Services (50 pp., http://www.crisisstates.com/download/others/Trading%20Conflict%20for%20Development.pdf).
Gasquet, D., Barbey, P., Adou, M., Paquette, J.L., 2003. Structure, Sr–Nd isotope geochemistry and zircon U–Pb geochronology of the granitoids of the Dabakala area (Cote d'Ivoire): evidence for a 2.3 Ga crustal growth event in the Palaeoproterozoic of West Africa? Precambrian Res. 127, 329–354.
Geological Survey and Mines Division, 2008. Industrial Mining Activity in Sierra Leone. Geological Survey and Mines Division. Ministry of Mineral Resources, Sierra Leone.
Gerdes, A., Zeh, A., 2006. Combined U–Pb and Hf isotope LA-(MC)-ICP-MS analyses of detrital zircons: comparison with SHRIMP and new constraints for the provenance and age of an Armorican metasediment in Central Germany. Earth Planet. Sci. Lett. 249, 47–61.
Gevers, T.W., Partridge, F.C., Joubert, G.K., 1937. The pegmatite area south of the Orange River in Namaqualand. Memoir. D. o. M. Union of South Africa, Geological Survey. Pretoria, 31 1–164.
Ginsburg, A.I., Timofeyev, I.N., Feldman, L.G., 1979. Principles of Geology of the Granitic Pegmatites. USSR, Nedra, Moscow (in Russian).
Gippsland Limited, 2013. Abu Dabbab tantalum; Nuweibi tantalum, niobium, feldspar. http://www.gippslandltd.com.
Glodny, J., Grauert, B., Fiala, J., Vejnar, Z., Krohe, A., 1998. Metapegmatites in the western Bohemian massif: ages of crystallization and metamorphic overprint, as constrained by U–Pb zircon, monazite, garnet, columbite and Rb–Sr muscovite data. Geol. Rundsch. 87, 124–134.
Gonçalves, A.O., Melgarejo, J.C., Alfonso, P., Paniagua, A., 2008. Composición de la turmalina de las pegmatitas graníticas de Giraúl, Angola. Rev. Soc. Esp. Mineral. 9, 125–126.
Gonçalves, A.O., Melgarejo, J.C., Abella, P.A., 2009. Sequence of crystallisation of pegmatites: the Angola case. Estud. Geol. 19, 35–39.
Goodenough, K.M., Thomas, R.J., De Waele, B., Key, R.M., Schofield, D.I., Bauer, W., Tucker, R.D., Rafahatelo, J.-M., Rabarimanana, M., Ralison, A.V., Randriamananjara, T., 2010. Post-collisional magmatism in the central East African Orogen: the Maevarano Suite of north Madagascar. Lithos 116, 18–34.
Grantham, G.H., Macey, P.H., Ingram, B.A., Roberts, M.P., Armstrong, R.A., Hokada, T., Shiraishi, K., Jackson, C., Bisnath, A., Manhica, V., 2008. Terrane correlation between Antarctica, Mozambique and Sri Lanka; comparison of geochronology, lithology, structure and metamorphism and possible implications for the geology of southern Africa and Antarctica. In: Satish-Kumar, M., Motoyoshi, Y., Osanai, Y., Hiroi, Y., Shiraishi, K. (Eds.), Geodynamic Evolution of East Antarctica: A Key to the East–West Gondwana Connection. Geological Society of London, Special Publications London, 308, pp. 91–119.
Graupner, T., Melcher, F., Gäbler, H.-E., Sitnikova, M., Brätz, H., Bahr, A., 2010. Rare earth element geochmemistry of columbite-group minerals: LA-ICP-MS data. Min. Mag. 74, 691–713.
Gu, Y., 2003. Automated scanning electron microscope based mineral liberation analysis. An introduction to JKMRC/FEI mineral liberation analyser. J. Miner. Mater. Charact. Eng. 2, 33–41.
Guastoni, A., Pezzotta, F., Demartin, F., 2003. Le pegmatiti di Zomba-Malosa. Riv. Mineral. Ital. 27, 66–77.
Guastoni, A., Camara, F., Nestola, F., 2010. Arsenic-rich fergusonite-beta-(Y) from Mount Cervandone (Western Alps, Italy): crystal structure and genetic implications. Am. Mineral. 95, 487–494.
Hanson, S.L., Simmons, W.B., Falster, A.U., Foord, E.E., Lichte, F.E., 1999. Proposed nomenclature for samarskite-group minerals: new data on ishikawaite and calciosamarskite. Min. Mag. 63, 27–36.
Hassanen, M.A., Harraz, H.Z., 1996. Geochemistry and Sr- and Nd-isotopic study on rare-metal-bearing granitic rocks, central Eastern Desert, Egypt. Precambrian Res. 80, 1–22.
Helba, H., Trumbull, R.B., Morteani, G., Khalil, S.O., Arslan, A., 1997. Geochemical and petrographic studies of Ta mineralization in the Nuweibi albite granite complex, Eastern Desert, Egypt. Miner. Deposita 32, 164–179.
Herzog, L.F., Pinson jr., William H., Hurley, Patrick M., 1960. Rb–Sr analysis and age determinations of certain lepidolites, including an international interlaboratory comparison suite. Am. J. Sci. 258, 191–208.
Hirdes, W., Davis, D.W., Eisenlohr, B.N., 1992. Reassessment of Proterozoic granitoid ages in Ghana on the basis of U/Pb zircon and monazite dating. Precambrian Res. 56, 89–96.
Hogarth, D.D., 1977. Classification and nomenclature of the pyrochlore group. Am. Mineral. 62, 403–410.
Hutchinson, R.W., 1955. Preliminary report on investigations of minerals of columbium and tantalum and of certain associated minerals. Am. Mineral. 40, 432–452.
Hutchinson, R.W., Claus, R.J., 1956. Pegmatite deposits, Alto Ligonha, Portugese East Africa. Econ. Geol. 51, 757–780.
Jahn, S., 1996. Geochemische und mineralogische Untersuchungen zur Metallogenese Seltenmetall-führender Granitoide in der Central Eastern Desert, Ägypten. Unpublished Dissertation, Institut für Geowissenschaften I, Technische Universität Berlin, 271 p.

Jahns, R.H., 1955. The study of pegmatites. Econ. Geol. 50th Anniv., vol. 1955, pp. 1025–1130.
Jelsma, H.A., Dirks, P.H.G.M., 2002. Neoarchaean tectonic evolution of the Zimbabwe Craton. In: Fowler, C.M.R., Ebinger, C.J., Hawkesworth, C.J. (Eds.), The Early Earth: Physical, Chemical and Biological Development. Geological Society, London, Special Publications, 199, pp. 183–211.
Jelsma, H.A., Vinyu, M.L., Valbrach, P.J., Davies, G.R., Wijbrans, J.R., Verdurmen, E.A.T., 1996. Constraints on Archaean crustal evolution of the Zimbabwe craton: a U–Pb zircon, Sm–Nd and Pb–Pb whole-rock isotope study. Contrib. Mineral. Petrol. 124, 55–70.
Jung, S., Mezger, K., Hoernes, S., 1998. Petrology and geochemistry of syn- to post-collisional metaluminous A-type granites — a major and trace element and Nd–Sr–Pb–O-isotope study from the Proterozoic Damara Belt, Namibia. Lithos 45, 147–175.
Jung, S., Hoernes, S., Mezger, K., 2000. Geochronology and petrology of migmatites from the Proterozoic Damara Belt — importance of episodic fluid-present disequilibrium melting and consequences for granite petrology. Lithos 51, 153–179.
Jung, S., Mezger, K., Hoernes, S., 2003. Petrology of basemenet-dominated terranes. II. Contrasting isotopic (Sr, Nd, Pb and O) signatures of basement-derived granites and constraints on the source region of granite (Damara orogen, Namibia). Chem. Geol. 199, 1–28.
Kampunzu, A.B., Kramers, J.D., Makutu, M.N., 1998. Rb–Sr whole rock ages of the Lueshe, Kirumba and Numbi igneous complexes (Kivu, Democratic Republic of Congo) and the break-up of the Rodinia Supercontinent. J. Afr. Earth Sci. 26, 29–36.
Keller, P., 1991. The occurrence of Li–Fe–Mn phosphate minerals in granitic pegmatites of Namibia. Commun. Geol. Surv. Namibia 7, 21–34.
Keller, P., von Knorring, O., 1989. Pegmatites at the Okatjimukuju farm, Karibib, Namibia. Part I: phosphate mineral associations of the Clementine II pegmatite. Eur. J. Mineral. 1, 567–593.
Kinnaird, J.A., 1985. Hydrothermal alteration and mineralization of the alkaline anorogenic ring complexes of Nigeria. J. Afr. Earth Sci. 3, 229–251.
Kokonyangi, J., Kampunzu, A.B., Armstrong, R., Yoshida, M., Okudaira, T., Arima, M., Ngulube, D.A., 2006. The Mesoproterozoic Kibaride belt (Katanga, SE D.R. Congo). J. Afr. Earth Sci. 46, 1–35.
Kröner, A., Sacchi, R., Laeckel, P., Costa, M., 1997. Kibaran magmatism and Pan-African granulite metamorphism in northern Mozambique: single zircon ages and regional implications. J. Afr. Earth Sci. 25, 467–484.
Kukla, C., Kramm, U., Kukla, P.A., Okrusch, M., 1991. U–Pb monazite data relating to metamorphism and granite intrusion in the northwestern Khomas Trough, Damara Orogen, central Namibia. Commun. Geol. Surv. Namibia 7, 49–54.
Küster, D., 1990. Rare-metal pegmatites of Wamba, central Nigeria — their formation in relationship to late Pan-African granites. Miner. Deposita 25, 25–33.
Küster, D., 1995. Rb–Sr isotope systematics of muscovite from Pan-African granitic pegmatites of Western and Northeastern Africa. Mineral. Petrol. 55, 71–83.
Küster, D., 2009. Granitoid-hosted Ta mineralization in the Arabian–Nubian Shield: ore deposit types, tectono-metallogenetic setting and petrogenetic framework. Ore Geol. Rev. 35, 68–86.
Küster, D., Romer, R.L., Tolessa, D., Zerihun, D., Bheemalingsewara, K., Melcher, F., Oberthür, T., 2009. The Kenticha rare-element pegmatite, Ethiopia: internal differentiation, U–Pb age and Ta mineralization. Miner. Deposita 44, 723–750.
Lächelt, S., 2004. The geology and mineral resources of Mozambique. Direcçao Nacional de Geologia, Mozambique.Council for Geoscience (515 pp.).
Landes, K.K., 1935. Age and distribution of pegmatites. Am. Mineral. 20 (81–105), 153–175.
Lehmann, B., Melcher, F., Sitnikova, M.A., Ruzindana Munana, J., 2008. The Gatumba rare-metal pegmatites: chemical signature and environmental impact. Etudes Rwandaises 16, 25–40.
Lenoir, J.L., Liégeois, J.P., Theunissen, K., Klerkx, J., 1994a. The Palaeoproterozoic Ubendian shear belt in Tanzania: geochronology and structure. J. Afr. Earth Sci. 19, 169–184.
Lenoir, J.L., Küster, D., Liégeois, J.P., Utke, A., Haider, A., Matheis, G., 1994b. Origin and regional significance of late Precambrian and early Paleozoic granitoids in the Pan-African belt of Somalia. Geol. Rundsch. 83, 624–641.
Lepersonne, J., 1974. Carte géologique du Zaïre. Département des Mines, République du Zaïre, Musée royal de l'Afrique centrale.
Leube, A., Hirdes, W., Mauer, R., Kesse, G.O., 1990. The Early Proterozoic Birimian supergroup of Ghana and some asepcts of its associated gold mineralization. Precambrian Res. 46, 139–165.
Linnen, R.L., Cuney, M., 2005. Granite-related rare-element deposits and experimental constraints on Ta–Nb–W–Sn–Zr–Hf mineralization. In: Linnen, R.L., Samson, I.M. (Eds.), Rare-Element Geochemistry and Mineral Deposits. Geological Association of Canada, Short Course Notes, 17, pp. 45–68.
Linnen, R.L., Keppler, H., 1997. Columbite solubility in granitic melts: consequences for the enrichment and fractionation of Nb and Ta in the Earth's crust. Contrib. Mineral. Petrol. 128, 213–227.
London, D., 1995. Geochemical features of peraluminous granites, pegmatites, and rhyolites as sources of lithophile metal deposits. In: Thompson, J.F.H. (Ed.), Magmas, Fluids, and Ore Deposits. Mineral. Assoc. Can., Short Course Ser., 23, pp. 175–202.
London, D., 2005. Geochemistry of alkali and alkaline earth elements in ore-forming granites, pegmatites, and rhyolites. In: Linnen, R.L., Samson, I.M. (Eds.), Rare-Element Geochemistry and Mineral Deposits. Geological Association of Canada, Short Course Notes, 17, pp. 17–43.
London, D., 2008. Pegmatites. The Canadian Mineralogist, Special Publication. (347 pp.).
Lumpkin, G.R., Chakoumakos, B.C., Ewing, R.C., 1986. Mineralogy and radiation effects of microlite from the Harding pegmatite, Taos County, New Mexico. Am. Mineral. 71, 569–588.
Maphalala, R.M., Trumbull, R.B., 1998. A geochemical and Rb/Sr isotopic study of Archean pegmatite dykes in the Tin Belt of Swaziland. S. Afr. J. Geol. 101, 53–65.
Martin, H.J., 1964. The Bikita tinfield. South. Rhod. Geol. Surv. Bull. 58, 114–131.
Martin, R.F., de Vito, C., 2005. The patterns of enrichment in felsic pegmatites ultimately depend on tectonic setting. Can. Mineral. 43, 2027–2048.
Matheis, G., 1987. Nigerian rare-metal pegmatites and their lithological framework. Geol. J. 22, 271–291.
Matheis, G., Caen-Vachette, M., 1983. Rb–Sr isotopic study of rare-metal bearing and barren pegmatites in the Pan-African reactivation zone of Nigeria. J. Afr. Earth Sci. 1, 35–40.
Mathias, V.V., Rossovskii, L.N., Shostatskii, A.N., Kumskova, N.M., 1963. Magnocolumbite, a new mineral. Dokl. Akad. Nauk SSSR 148, 420–423 (in Russian).
Melcher, M., Graupner, T., Henjes-Kunst, F., Oberthür, T., Sitnikova, M., Gäbler, E., Gerdes, A., Brätz, H., Davis, D., Dewaele, S., 2008a. Analytical fingerprint of columbite–tantalite (coltan) mineralization in pegmatites: focus on Africa. Proceedings, Ninth International Congress for Applied Mineralogy (ICAM) 2008, Brisbane, Qld. Australasian Institute of Mining and Metallurgy, pp. 615–624.
Melcher, F., Sitnikova, M.A., Graupner, T., Martin, N., Oberthür, T., Henjes-Kunst, F., Gäbler, E., Gerdes, A., Brätz, H., Davis, D.W., Dewaele, S., 2008b. Fingerprinting of conflict minerals: columbite–tantalite ("coltan") ores. SGA News, 23 1–14 (June 2008).
Melcher, F., Graupner, T., Sitnikova, M., Henjes-Kunst, F., Oberthür, T., Gäbler, E., Bahr, A., Gerdes, A., Brätz, H., Rantitsch, G., 2009. Ein Herkunftsnachweis für Niob-Tantalerze am Beispiel afrikanischer Selten-Element-Pegmatite. Mitt. Österr. Mineral. Ges. 155, 231–267.
Milési, P., Toteu, S.F., Deschamps, Y., Feybesse, J.L., Lerouge, C., Cocherie, A., Penaye, J., Tchameni, R., Moloto-A-Kenguemba, G., Kampubzu, H.A.B., Nicol, N., Duguey, E., Leistel, J.M., Saint-Martin, M., Ralay, F., Heinry, C., Bouchot, V., Mbaigane, J.C.D., Kanda Kula, V., Chene, F., Monthel, J., Boutin, P., Cailteux, J., 2006. An overview of the geology and major ore deposits of Central Africa: Explanatory note for the 1:4,000,000 map "Geology and major ore deposits of Central Africa". J. Afr. Earth Sci. 44, 571–595.
Minnaar, H., 2006. The exploitability of pegmatite deposits in the lower Orange River area (Vioolsdrif–Henkries–Steinkopf). Faculty of Natural & Agricultural Science.University of Pretoria, Pretoria (M.Sc.: 64 pp.).
MMSD, 2012. Mineral projects, 2012. Nigeria Mineral Projects, Exploration, Development, and Exploitation.Federal Republic of Nigeria, Ministry of Mines and Steel Development, Abuja, Nigeria (36 pp.).
Mobbs, P.M., 2009. The mineral industry of Nigeria. 2006 Minerals Yearbook, U.S. Geological Survey. U.S. Department of the Interior (5 pp.).
Morel, S.W., 1979. The geology and mineral resources of Sierra Leone. Econ. Geol. 74, 1563–1576.
Mücke, A., Neumann, U., 2006. Die mafischen Mineralien und oxidischen Erze der Alkali-Granite und benachbarter Flusssedimente des Jos Plateaus in Zentralnigeria: Petrografie, Mineralogie und Genese. Aufschluss 57, 275–300.
Mücke, A., Strunz, H., 1978. Petscheckite and liandradite, two new pegmatite minerals from Madagascar. Am. Mineral. 63, 941–946.
Musée Royal de l'Afrique Centrale, 2005. Carte Géologique et Minière de la République Démocratique du Congo, 1/2.500.000. Tervuren, Belgium.
Nekrasov, I.Ya., Chistyakova, N.I., Yevstigneyeva, T.L., 1984. On the relationships of thoreaulite, lithiotantite, rankamaite and cassiterite in rare-element pegmatites of Siberia. Mineral. Zh. 6, 42–55 (in Russian).
Nicolaysen, L.O., Burger, A.J., 1965. Note on an extensive zone of 1000 million-year old metamorphic and igneous rocks in southern Africa. Sci. Terre Tome X (3–4), 497–516 (1964–1965).
Novák, M., Černý, P., 2001. Distinctive compositional trends in columbite–tantalite from two segments of the lepidolite prgmatite at Rozna, western Moravia, Czech Republic. J. Czech Geol. Soc. 46, 1–8.
Novák, M., Filip, J., 2010. Unusual (Na, Mg)-enriched beryl and its breakdown products (beryl II, bazzite, bavenite) from euxenite-type NYF pegmatite related to the orogenic ultrapotassic Třebič Pluton, Czech Republic. Can. Mineral. 48, 615–628.
Novák, M., Černý, P., Selway, J.B., 1999. The zinnwaldite–masutomilite–elbaite granitic pegmatite from the Trebíc durbachite massif at Krakovice: a complex pegmatite related to the NYF family. Can. Mineral. 37, 815–816.
Novák, M., Uher, P., Černý, P., Siman, P., 2000. Compositional variations in ferrotapiolite + tantalite pairs from the beryl-columbite pegmatite at Moravanynad Váhom, Slovakia. Miner. Petrol. 69, 295–306.
Novák, M., Černý, P., Uher, P., 2003. Extreme variation and apparent reversal of Nb–Ta fractionation in columbite-group minerals from the Scheibengraben beryl-columbite granitic pegmatite, Marsíkov, Czech Republic. Eur. J. Mineral. 15, 565–574.
Novák, M., Černý, P., Cempirek, J., Srein, V., Filip, J., 2004. Ferrotapiolite as a pseudomorph of stibiotantalite from the Lastovicky lepidolite pegmatite, Czech republic; an example of hydrothermal alteration at constant Ta/(Ta + Nb). Can. Mineral. 42, 1117–1128.
Novák, M., Škoda, R., Filip, J., Macek, I., Vaculovič, T., 2011. Compositional trends in tourmaline from the intragranitic NYF pegmatites of the Třebič Pluton, Czech Republic; electron microprobe, LA-ICP-MS and Mössbauer study. Can. Mineral. 49, 359–380.
Novák, M., Škoda, R., Gadas, P., Krmíček, L., Černý, P., 2012. Contrasting origins of the mixed (NYF + LCT) signature in granitic pegmatites; examples from the Moldanubian Zone, Czech Republic. Can. Mineral. 50, 1077–1094.
Oberthür, T., Vetter, U., Davis, D.W., Amanor, J.A., 1998. Age constraints on gold mineralization and Paleoproterozoic crustal evolution in the Ashanti belt of southern Ghana. Precambrian Res. 89, 129–143.
Oberthür, T., Weiser, T.W., Gast, L., Schoenberg, R., Davis, D.W., 2002. Platinum-group minerals and other detrital components in the Karoo-age Somabula gravels, Gweru, Zimbabwe. Can. Mineral. 40, 435–456.
Obomhense, S., 2008. Mining in Nigeria — Mekios and tin sheds. T.I.C. Bulletin, 133 5–7.
Okunlola, O.A., 1998. Specialty metal potentials of Nigeria. Proceedings of the First Mining in Nigeria Conference and Workshop, NIMAMOP, Federal Ministry of Solid Minerals, Abuja, pp. 67–90.
Okunlola, O.A., 2005. Metallogeny of tantalum–niobium mineralization of Precambrian pegmatites of Nigeria. Mineral. Wealth 137, 38–50.

Okunlola, O.A., Jimba, S., 2006. Compositional trends in relation to Ta–Nb mineralization in Precambrian pegmatites of Aramako–Ara–Ijero areas, southwestern Nigeria. J. Min. Geol. 42, 113–126.

Okunlola, O.A., Oyedokun, M.O., 2009. Compositional trends and rare metal (Ta–Nb) mineralization potential of pegmatite and associated lithologies of Igbeti area, Southwestern Nigeria. RMZ — Mater. Geoenviron. 56, 38–53.

Partington, G.A., McNaughton, N.J., Williams, I.S., 1995. A review of the geology, mineralization, and geochronology of the Greenbushes pegmatite, Western Australia. Econ. Geol. 90, 616–635.

Patrick, D., Forward, P., 2005. Review of a portfolio of exploration porperties held in Sierra Leone by Sierra Leone Diamond Company Limited. ACA Howe International Limited, Report for Sierra Leone Diamond Company Limited, Berkhamsted, Herts, UK. (117 pp., http://www.african-minerals.com/system/files/uploads/financialdocs/ACAHoweReport.pdf).

Petters, S.W., 1991. Regional geology of Africa. Lecture Notes in Earth Sciences, 40. Springer-Verlag (722 S.).

Pohl, W., 1987. Metallogeny of the northeastern Kibaran belt, Central Africa. Geol. J. 22, 103–119.

Pohl, W., 1994. Metallogeny of the northeastern Kibara belt, Central Africa — recent perspectives. Miner. Deposita 9, 105–130.

Poujol, M., Robb, L.J., 1999. New U–Pb zircon ages on gneisses and pegmatite from the south of the Murchison greenstone belt, South Africa. S. Afr. J. Geol. 102, 93–97.

Prigogine, A., 1956. Concentration des minerais de wolfram et de niobium-tantale au Congo belge et au Ruanda–Urundi. Académie royale des Sciences colonials. (Mémoires in-8°. nouvelle série. Tome IV, fasc. 1, 191 pp.).

Reuning, E., 1923. Pegmatite und Pegmatitmineralien in Südwestafrika. Z. Kristallogr. 58, 448–459.

Rijks, H.R.P., van der Veen, A.H., 1972. The geology of the tin-bearing pegmatites in the eastern part of the Kamativi district, Rhodesia. Miner. Deposita 7, 383–395.

Romer, R.L., 2003. Alpha-recoil in U–Pb geochronology: effective sample size matters. Contrib. Mineral. Petrol. 145, 481–491.

Romer, R.L., 2008. Discussion on Dill et al. (2007) "Cu–Fe–U phosphate mineralization of the Hagendorf–Pleystein pegmatite province, Germany: with special reference to laser-ablation inductively-coupled plasma mass spectrometry (LA-ICP-MS) of limonite-cored torbernite". Mineral. Mag. 71, 371–387.

Romer, R.L., Lehmann, B., 1995. U–Pb columbite age of Neoproterozoic Ta–Nb mineralization in Burundi. Econ. Geol. 90, 2303–2309.

Romer, R.L., Smeds, S.A., 1994. Implications of U–Pb ages of columbite–tantalites from granitic pegmatites for the Paleoproterozoic accretion of 1.90–1.85 Ga magmatic arcs to the Baltic Shield. Precambrian Res. 67, 141–158.

Romer, R.L., Smeds, S.A., 1997. U–Pb columbite chronology of post-kinematic Palaeoproterozoic pegmatites in Sweden. Precambrian Res. 82, 85–99.

Romer, R.L., Wright, J.E., 1992. U–Pb dating of columbites: a geochronological tool to date magmatism and ore deposits. Geochim. Cosmochim. Acta 56, 2137–2142.

Roskill, 2012. Tantalum: Market Outlook to 2016, 11th ed. Roskill Information Services Ltd.978 0 86214 580 4.

Sahama, T.G., 1980. Minerals of the tantalite–niobite series from Mozambique. Bull. Mineral. 103, 190–197.

Savu-Krohn, C., Rantitsch, G., Auer, P., Melcher, F., Graupner, T., 2011. Geochemical fingerprinting of coltan ores by machine learning on uneven data sets. Nat. Resour. Res. 20, 177–191.

Schaetzl, L., 1971. The Nigerian Tin Industry. Report of the Nigerian Institute. Soc. Econ. Res, Ibadan, Nigeria.

Schlüter, T., 2006. Geological Atlas of Africa, With Notes on Stratigraphy, Tectonics, Economic Geology, Geohazards, Geosites and Geoscientific Education of Each Country. Springer Verlag, Berlin, Heidelberg (307 pp.).

Schneiderhöhn, H., 1961. Die Pegmatite. Die Erzlagerstätten der Erde, vol. II. Gustav Fischer Verlag, Stuttgart (720 pp.).

Schutte, I.C., 1972. The main pegmatites of the area between Steinkopf, Vioolsdrif and Goodhouse, Namaqualand. Mem. Geol. Surv. S. Afr. 60, p. 19.

Schwela, U., 2007. Tantalum. Min. J. Suppl. Nov. 2007 (12 pp.).

Seth, B., 1999. Crustal evolution of the Kaoko belt, NW Namibia. Geochemical and Geochronological Study of Archaean to Mesoproterozoic Basement Gneisses and Pan-African Migmatites and Granitoids. (PhD thesis) University of Würzburg (135 pp.).

Shannon, R.D., 1976. Revised effective ionic radii and systematic studies of interatomic distances in halides and chalcogenides. Acta Crystallogr. A32, 751–767.

Sharara, N.A.F., 2000. Geochemistry and genesis of the specialized stanniferous granites of the central Eastern Desert of Egypt. Bulletin of the Faculty of Science. F, Geology, 29, pp. 1–26.

Simmons, W.M.B., Webber, K.L., 2008. Pegmatite genesis: state of the art. Eur. J. Mineral. 20, 421–438.

Škoda, R., Novák, M., 2007. Y, REE, Nb, Ta, Ti-oxide (AB_2O_6) minerals from REL–REE euxenite-subtype pegmatites of the Třebič Pluton, Czech Republic; substitutions and fractionation trends. Lithos 95, 43–57.

Smith, S.R., Foster, G.L., Romer, R.L., Tindle, A.G., Kelley, S.P., Noble, S.R., Horstwood, M., Breaks, F.W., 2004. U–Pb columbite–tantalite chronology of rare-element pegmatites using TIMS and Laser Ablation-Multi collector-ICP-MS. Contrib. Mineral. Petrol. 147, 549–564.

Spilde, M.N., Shearer, C.K., 1992. A comparison of tantalum–niobium oxide assemblages in two mineralogically distinct rare-element granitic pegmatites, Black Hills, South Dakota. Can. Mineral. 30, 719–737.

Spittaels, S., 2010. The Complexity of Resource Governance in a Context of State Fragility: An Analysis of the Mining Sector in the Kivu Hinterlands. IPIS, International Alert (65 pp.; http://www.ipisresearch.be/natural-resources.php).

Stern, R.J., 1994. Arc assembly and contintal collision in the Neoproterozoic East African orogen: implications for the consolidation of Gondwanaland. Ann. Rev. Earth Planet. Sci. 22, 319–351.

Sweetapple, M.T., Collins, P.L.F., 2002. Genetic framework for the classification and distribution of Archean rare metal pegmatites in the North Pilbara craton, Western Australia. Econ. Geol. 97, 873–895.

Tack, L., Wingate, M.T.D., De Waele, B., Meert, J., Belousova, E., Griffin, B., Tahona, A., Fernandez-Alonso, M., 2010. The 1375 Ma "Kibaran event" in Central Africa: prominent emplacement of bimodal magmatism under extensional regime. Precambrian Res. 180, 63–84.

Tadesse, S., Zerihun, D., 1996. Composition, fractionation trend and zoning accretion of the columbite–tantalite group of minerals in the Kenticha rare metal field (Adola, southern Ethiopia). J. Afr. Earth Sci. 23, 411–431.

Tapsoba, B., Lo, C.-H., Jahn, B.-M., Chung, S.-L., Wenmenga, U., Iizuka, Y., 2013. Chemical and Sr–Nd isotopic compositions and zircon U–Pb ages of the Birimian granitoids from NE Burkina Faso, West African Craton: implications on the geodynmaich setting and crustal evolution. Precambrian Res. 224, 364–396.

Taylor, P.N., Moorbath, S., Leube, A., Hirdes, W., 1992. Early Proterozoic crustal evolution in the Birimian of Ghana: constraints from geochronology and isotope geology. Precambrian Res. 56, 97–111.

Thiéblemont, D., Goujou, J.C., Egal, E., Cocherie, A., Delor, C., Lafon, J.M., Fanning, C.M., 2004. Archean evolution of the Leo Rise and its Eburnean reworking. J. Afr. Earth Sci. 39, 97–104.

Tkachev, A.V., 2011. Evolution of metallogeny of granitic pegmatites associated with orogens throughout geological time. In: Sial, A.N., Bettencourt, J.S., de Campos, C.P., Ferreira, V.P. (Eds.), Granite-related Ore Deposits. London, Geol. Soc. Spec. Publ., 350, pp. 7–23.

Tomascak, P.B., Krogstad, E.J., Walker, R.J., 1998. Sm–Nd isotope systematic and the derivation of granitic pegmatites in southwestern Maine. Can. Mineral. 36, 327–337.

Trumbull, R.B., 1993. A petrological and Rb/Sr isotopic study of an early Archean fertile granite–pegmatite system: the Sinceni Pluton in Swaziland. Precambrian Res. 61, 89–116.

Trumbull, R.B., 1995. Tin mineralization in the Archean Sinceni rare element pegmatite field, Kaapvaal Craton, Swaziland. Econ. Geol. 90, 648–657.

Uher, P., Černý, P., Chapman, R., 2008. Foordite–thoreaulite, $Sn^{2+}Nb_2O_6$–$Sn^{2+}Ta_2O_6$: compositional variations and alteration products. Eur. J. Mineral. 20, 501–516.

Van Lichtervelde, M., Salvi, S., Beziat, D., Linnen, R.L., 2007. Textural features and chemical evolution in tantalum oxides: magmatic versus hydrothermal origins for Ta mineralization in the Tanco Lower Pegmatite, Manitoba, Canada. Econ. Geol. 102, 357–374.

Van Lichtervelde, M., Melcher, F., Graupner, T., Linnen, R.L., 2011. Tantalum mineralization in the Homestead pegmatite, Tantalite Valley, Namibia. 23rd Colloquium of African Geology Abstract volume, p. 409.

Varlamoff, N., 1972. Central and West African rare-metal granitic pegmatites, related aplites, quartz veins and mineral deposits. Miner. Deposita 7, 202–216.

Vearncombe, J.R., Barton, J.M., Cheshire, P.E., De Beer, J.H., Stettler, E.H., Brandl, G., 1992. Geology, geophysics and mineralization of the Murchison schist belt, Rooiwater Complex and surrounding granitoids. Geol. Surv. S. Afr. 81 (139 pages).

Villeneuve, M., 1980. Les formations précambriennes antérieures ou rattachées au Supergroupe de l'Itombwe au Kivu oriental et méridional (Zaïre). Bull. Soc. Belg. Géol. 89, 301–308.

Villeneuve, M., 1987. Géologie du synclinal de l'Itombwe (Zaïre oriental) et le problème de l'existence d'un sillon plissé pan-africain. J. Afr. Earth Sci. 6, 869–880.

Von Knorring, O., 1970. Mineralogical and geochemical aspects of pegmatites from orogenic belts of equatorial and southern Africa. In: Clifford, T.N., Gass, I.G. (Eds.), African Magmatism and Tectonics. Oliver & Boyd, Edinburgh, pp. 157–210.

Von Knorring, O., 1985. Some mineralogical, geochemical and economic aspects of lithium pegmatites from the Karibib–Cape Cross pegmatite field in South West Africa/Namibia. Comm. Geol. Surv. Southwest Africa/Namibia, 1 79–84.

Von Knorring, O., Condliffe, E., 1987. Mineralized pegmatites in Africa. Geol. J. 22, 253–270.

Von Knorring, O., Fadipe, A., 1981. Niobium and tantalum minerals. Comm. Geol. Surv. Southwest Africa/Namibia, 1 85–88.

Von Knorring, O., Hornung, G., 1963. Simpsonite and stibiotantalite from Benson pegmatite mine, Mtoko, southern Rhodesia. Min. Mag. 33, 458–466.

Von Knorring, O., Vorma, A., Nixon, P.H., 1969. Rankamaite, a new tantalum mineral from Kivu, Congo. Bull. Geol. Soc. Finl. 41, 47–56.

Wall, F., Niku-Paavola, V.N., Storey, C., Müller, A., Jeffries, T., 2008. Xenotime-(Y) from carbonatite dykes at Lofdal, Namibia: unusually low LREE:HREE ratio in carbonatite, and the first dating of xenotime overgrowths on zircon. Can. Mineral. 46, 861–877.

Warner, J.K., Ewing, R.C., 1993. Crystal chemistry of samarskite. Am. Mineral. 78, 419–424.

Watson, R.L.A., 1962. The geology of the Kamativi and Lubimbi areas. South. Rhod. Geol. Surv. Bull. 57 (39 pp.).

Wayland, E.J., Spencer, L.J., 1929. Bismutotantalite, a new mineral, from Uganda. Min. Mag. 33, 185–192.

Wegorzewski, A., 2009. Kristallisation von $FeTa_2O_6$–$MnTa_2O_6$ in pegmatitischen Schmelzen bei 2 kbar. Unpubl. Diploma thesis, University of Hannover, Germany, 139 p.

Wise, M.A., Černý, P., 1990. Primary compositional range and alteration trends of microlite from the Yellowknife pegmatite field, Northwest Territories, Canada. Miner. Petrol. 43, 83–98.

Wise, M.A., Turnock, A.C., Černý, P., 1985. Improved unit cell dimensions for ordered columbite–tantalite end members. N. Jb. Mineral. Mh. 8, 372–378.

Wise, M.A., Černý, P., Falster, A.U., 1998. Scandium substitution in columbite-group minerals and ixiolite. Can. Mineral. 36, 673–680.

Woolley, A.R., 1987. Lithosphere metasomatism and the petrogenesis of the Chilwa Province of alkaline igneous rocks and carbonatites, Malawi. J. Afr. Earth Sci. 6, 891–898.

Woolley, A.R., 2001. Alkaline rocks and carbonatites of the world. Part 3: Africa. The Geological Society Publishing House, Bath, U.K. (372 pp.).

Wright, J.P., Hastings, D.A., Jones, W.B., Williams, H.R., 1985. Geology and Mineral Resources of West Africa. Georg Allen and Unwin, Boston Sydney 129–137.

Yager, T.R., 2013. The mineral industry of Madagascar. 2011 Minerals Yearbook, U.S. Geological Survey. U.S. Department of the Interior (5 pp.).